2014

Control Based Soft Switching Three-phase Micro-inverter: Efficiency And Power Density Optimization

Ahmadreza Amirahmadi
University of Central Florida

CONTROL BASED SOFT SWITCHING THREE-PHASE MICRO-INVERTER: EFFICIENCY AND POWER DENSITY OPTIMIZATION

by

AHMADREZA AMIRAHMADI
B.S. Shahrood University of Technology, 2007
M.S. Shahrood University of Technology, 2010

A dissertation submitted in partial fulfillment of the requirements
for the degree of Doctor of Philosophy
in the Department of Electrical Engineering and Computer Science
in the College of Engineering and Computer Science
at the University of Central Florida
Orlando, Florida

Spring Term
2014

Major Professor: Issa Batarseh

ABSTRACT

In the field of renewable energy, solar photovoltaic is growing exponentially. Grid-tied PV micro-inverters have become the trend for future PV system development because of their remarkable advantages such as enhanced energy production due to MPPT implementation for each PV panel, high reliability due to redundant and distributed system architecture, and simple design, installation, and management due to its plug-and-play feature. Conventional approaches for the PV micro-inverters are mainly in the form of single-phase grid connected and they aim at the residential and commercial rooftop applications. It would be advantageous to extend the micro-inverter concept to large size PV installations such as MW-class solar farms where three-phase AC connections are used.

The relatively high cost of the three-phase micro-inverter is the biggest barrier to its large scale deployment. Increasing the switching frequency may be the best way to reduce cost by shrinking the size of reactive components and heat-sink. However, this approach could cause conversion efficiency to drop dramatically without employing soft switching techniques or using costly new devices.

This dissertation presents a new zero voltage switching control method that is suitable for low power applications such as three-phase micro-inverters. The proposed hybrid boundary conduction mode (BCM) current control method increases the efficiency and power density of the micro-inverters and features both reduced number of components and easy digital implementation. Zero voltage switching is achieved by controlling the inductor current bi-directional in every switching cycle and results in lower switching losses, higher operating frequency, and reduced size and cost of passive components, especially magnetic cores. Some

practical aspects of hybrid control implementation such as dead-time insertion can degrade the performance of the micro-inverter. A dead-time compensation method that improves the performance of hybrid BCM current control by decreasing the output current THD and reducing the zero crossing distortion is presented.

Different BCM ZVS current control modulation schemes are compared based on power losses breakdown, switching frequency range, and current quality. Compared to continuous conduction mode (CCM) current control, BCM ZVS control decreases MOSFET switching losses and filter inductor conduction losses but increases MOSFET conduction losses and inductor core losses. Based on the loss analysis, a dual-mode current modulation method combining ZVS and zero current switching (ZCS) schemes is proposed to improve the efficiency of the micro-inverter.

Finally, a method of maintaining high power conversion efficiency across the entire load range of the three-phase micro-inverter is proposed. The proposed control method substantially increases the conversion efficiency at light loads by minimizing switching losses of semiconductor devices as well as core losses of magnetic components. This is accomplished by entering a phase skipping operating mode wherein two phases of an inverter are disabled and three inverters are combined to form a new three-phase system with minimal grid imbalance.

A 400W prototype of a three-phase micro-inverter and its hybrid control system have been designed and tested under different conditions to verify the effectiveness of the proposed controller, current modulation scheme, and light load efficiency enhancement method.

To my parents

Mehri Famili and Majid Amirahmadi

ACKNOWLEDGMENTS

I would like to express my sincere gratitude and appreciation to my advisor, Dr. Issa Batarseh, for his tremendous support and continuous inspiration to my research work throughout my studies and research at University of Central Florida. He has been a strong and supportive adviser to me during the development of this work, but he has always given me great freedom to pursue independent work.

I wish to express my sincere gratitude to my professor, Dr. John Shen, for providing me the invaluable opportunity to be part of the Florida Power Electronic Center (FPEC) and introducing me to the wonders and frustrations of scientific research.

I would like to thank Dr. Thomas Xinzhang Wu, Dr. Wasfy Mikhael, Dr. Nasser Kutkut and Dr. Saeed Lotfifard for serving as my committee members, and for their insightful comments and kind suggestions.

I would also like to thank Dr. Nasser Kutkut and Charles Jourdan for their precious and patient guidance on my research.

I would like to express my deep appreciation to Dr. Haibing Hu who introduced me to the area of the soft switching converters and kindly gave me insightful suggestions for my academic research.

I would also like to thank my fellow FPEC colleagues and scholars, Anna Grishina, Dehua Zhang, Xiang Fang, Qian Zhang, Frank Chen, Utsav Somani, Ala Hussein and Jesus Barrios. My study and research life were full of joy with their helpful discussions, great support and

precious friendship. It is a great honor for me to be part of this team at the University of Central Florida.

In the end, I would like to thank my parents, Mehri Famili and Majid Amirahmadi, for all the love and support they have given me throughout my life and believing in me so I could believe in myself. I would also like to thank my brother for all of the advice and wise words he has provided me with over the last several years and all of the incredible strength he has forced me to see in myself.

TABLE OF CONTENTS

LIST OF FIGURES

LIST OF TABLES

CHAPTER 1. INTRODUCTION

1.1 Background and Challenges

Non-renewable energy will become more expensive as supplies dwindle and demand increases while renewable energy is reliable and plentiful and will potentially be very cheap once technology and infrastructure improve [1]. Among the six primary renewable resources (solar, wind, hydro, geothermal, biomass, and ocean), the potential of solar energy is perhaps the most promising. This is because solar energy is low-cost, non-polluting and therefore no threat to the environment, and depends on an available resource – sunshine[2].

Through research and technological advances solar energy could become capable of competing with conventional sources of energy and become a mainstream electricity source within the next few years [3].

The best and most efficient way to use solar energy is to convert it to electricity and inject it into the utility grid. Grid tie solar systems do not need any kind of expensive power storage systems. They are essentially composed of power electronics interfaces to account for the different characteristics between the generated electricity and the utility grid [4]. Solar source is low voltage DC power while the utility grid is high voltage AC power. A grid tie solar system is shown in Figure 1-1.

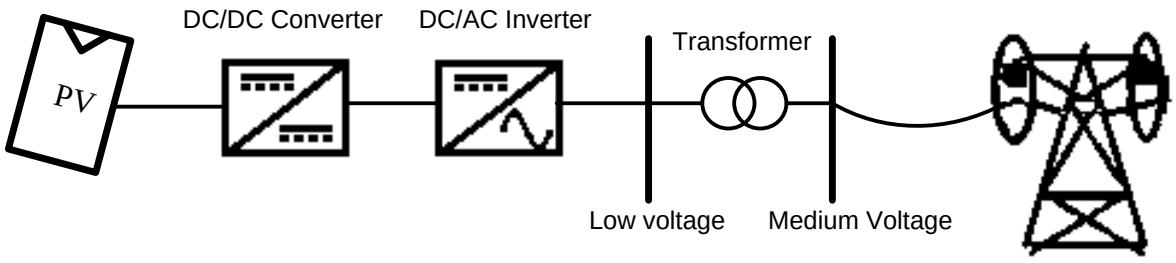

Figure 1-1: Grid-tie solar system

The solar system shown in Figure 1-1 is based on two-stage power conversion architecture. This kind of architecture can better interface with the crystalline PV panels featuring low DC output voltage. The first stage is a DC/DC converter and the second stage is a DC/AC inverter. The front-end DC/DC stage features voltage boosting and maximum energy harvesting, while the inverter stage realizes power conversion from DC to AC and grid connection functions [5].

Various circuit topologies and control methods have been proposed to improve the efficiency, decrease the cost, and enhance the performance and reliability of solar systems. In this dissertation, a new soft switching control based three-phase micro-inverter is proposed for a highly reliable, high-efficiency, high-power density, and low cost solar system. To achieve the targeted power conversion efficiency and power density a comprehensive investigation and research were done on the new topologies and soft switching techniques.

1.2 Centralized, String and Micro-inverters

Three basic architectures for the PV solar systems with respect to the type of the grid-tied inverter are:

- Centralized inverter
- String inverter or multi-string inverter
- Micro-inverter

In centralized inverter architecture, a large number of PV modules are grouped into several series of connections using string diodes or junction boxes [6]. With sufficient high voltage generated by each series group (referred to as a string), PV modules are directly fed to the central inverter. Centralized inverter architecture can operate at high efficiency due to only one power conversion stage [7]. This architecture has become conventional for 100 kilowatt peak solar plants. Some limitations of this architecture shown in Figure 1-2 can be mentioned as:

1- Single point of failure
2- Individual PV panels may not operate in their maximum power tracking due to partial shading or some other kind of coverage
3- Junction boxes or string diodes introduce extra losses
4- It usually needs an additional power stage to convert the wide range input voltage into a stable and compatible voltage to the grid. The normal operation voltage range varies significantly
5- Mismatch of each string or PV panel affects the PV array efficiency significantly

In order to solve the problems of centralized inverter structure, string inverter architecture was proposed. This structure as shown in Figure 1-3 does not need string diodes. In this architecture each string can apply the MPPT, resulting in higher PV efficiency utilization than that of a centralized inverter. The other centralized inverter limitations remain in this structure.

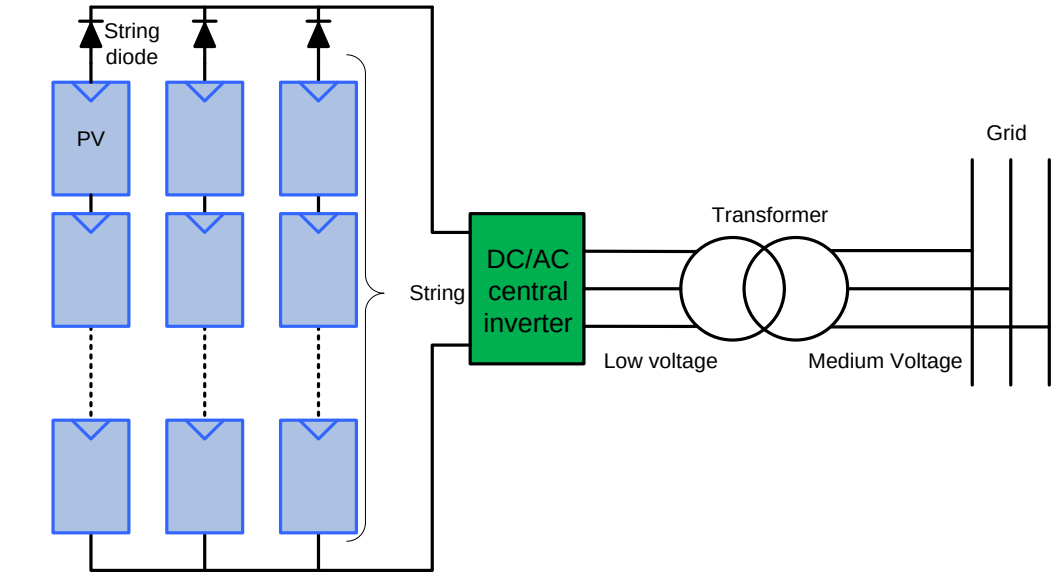

Figure 1-2: Diagram of centralized inverter system architecture

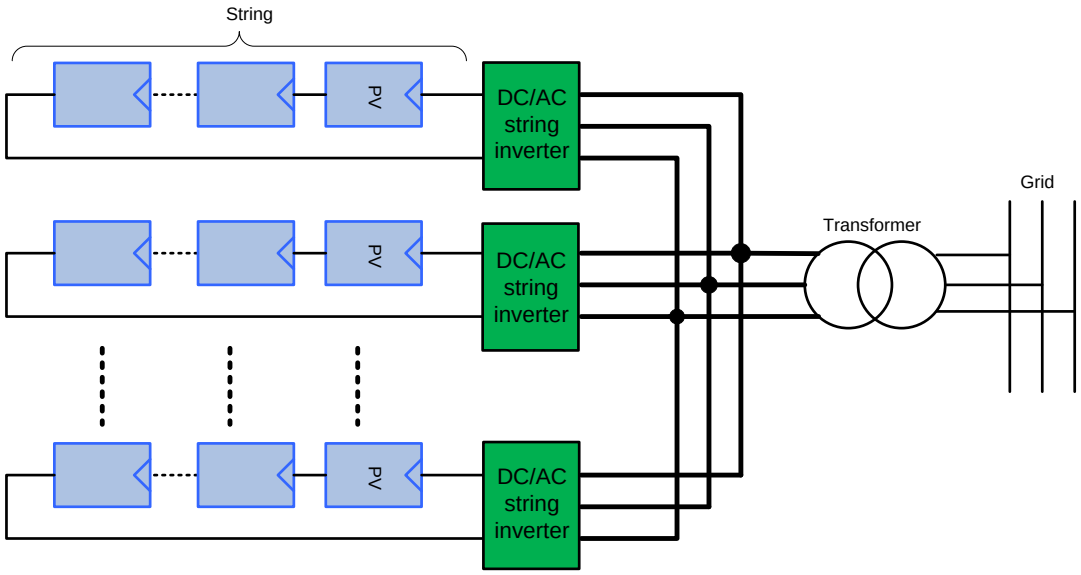

Figure 1-3: Diagram of string inverter system architecture

In order to implement the maximum power tracking for individual panels, a power maximizer consisting of a DC/DC converter can be attached to the PV panels. This new approach can be

applied to either central inverter structure as illustrated in Figure 1-4 or string inverter architecture. Using the power maximizer, there is no mismatch issue between strings or PV panels. At the cost of an additional DC/DC module, central and string inverters can maximize power production from each PV panel, but they still suffer drawbacks such as single point of failure, high DC voltage hazard, and difficulties in maintenance. Various companies are trying to improve the efficiency and reliability of these power maximizers and reduce their costs [8],[9].

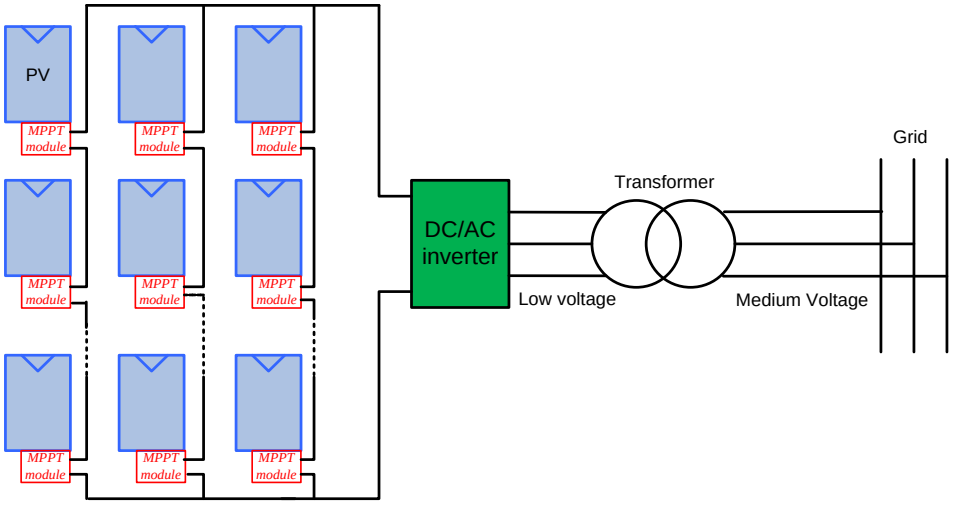

Figure 1-4: Maximum power tracking for individual panels in the centralized inverter structure

Distributed PV electricity generation, which takes granularity of large-scale solar farms down to a single PV panel, will be a tendency for future solar PV deployment. Micro-inverters, one of the typical distributed PV systems, are small grid-tie inverters of 150-400W that convert the output of a single PV panel to AC [10]. Micro-inverters have the potential to be fully integrated into the PV modules to realize a true Plug-and-Play system that can be purchased, installed, and connected by homeowners without the need to engage outside consultants or contractors.

Although micro-inverter and AC PV module products have been very successful in the market, their uses have been limited to small scale, single phase (110VAC & 220VAC) residential and commercial PV installations.

Conventional systems for large size PV installation are based on centralized or string inverters. Considering the merits of solar systems based on micro-inverters, it is advantageous to extend this concept to large size PV installations such as MW-class solar farms where three-phase AC connection is used.

At a solar farm based on three-phase micro-inverters, output of the micro-inverters are connected in parallel and routed to a common AC coupling point. Series or parallel DC connections are not required and all DC wiring is made at a relatively low voltage level of a single panel that is less than 50 volts. AC PV modules with micro-inverters will be a tendency for future solar PV deployment because of the remarkable merits such as:

- Maximum Power Point Tracking (MPPT) for individual panels
- Preventing mismatch losses due to parallel connection of PV modules
- Ease of installation through flexible and modular solar farm architecture
- Lower installation costs
- Possible inverter cost reduction due to mass production
- Lower DC distribution losses
- Distributed and redundant system architecture (Higher reliability)
- Preventing DC high voltage safety hazards

The new architecture for a PV solar farm based on three-phase micro-inverter is shown in Figure 1-5 [11]. The outputs of each micro-inverter are directly connected to a low voltage three-phase utility grid. A medium voltage transformer boosts this three-phase low voltage to high voltage at the power transmission line side. Each micro-inverter operates independently regardless of the other micro-inverters' failure.

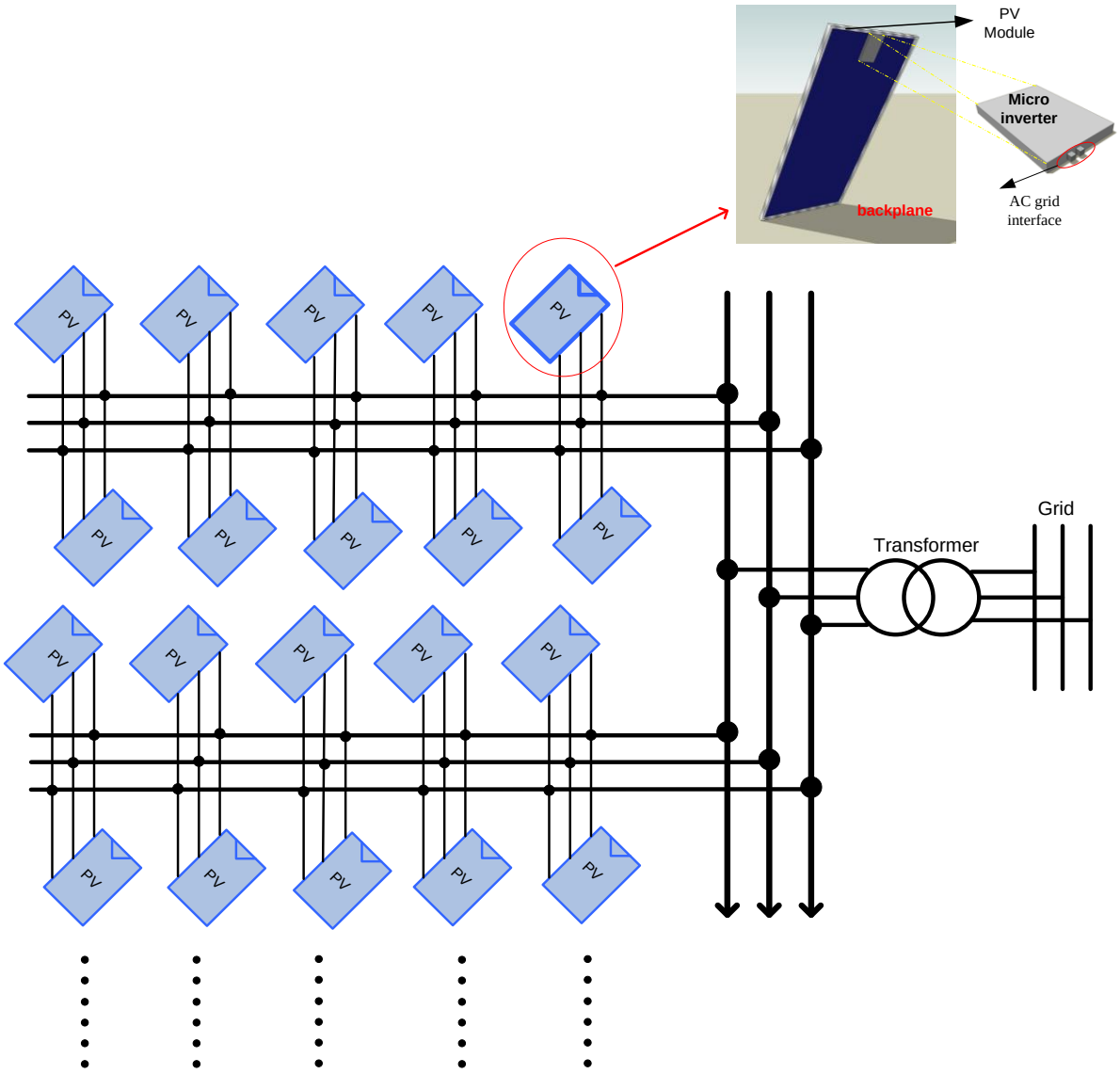

Figure 1-5: Solar farm architecture based on three-phase micro-inverters

1.3 Required Characteristics of Micro-inverters

The relatively high cost of the micro-inverter is the biggest barrier to its large scale deployment. Increasing power converter switching frequency may be the best way to reduce cost by shrinking the size of inductors, capacitors and heat spreaders. However, this approach could cause conversion efficiency to drop dramatically without employing soft switching techniques or using costly new semiconductor devices. In conventional soft switching techniques resonant components and auxiliary devices are employed to create either zero voltage or zero current across the switching device prior to the switching transition. These additional auxiliary switches, passive components, and more gate driving circuits will reduce the reliability and increase the cost and control complexity of the inverter. Conventional soft switching techniques will be referred as topology based soft switching methods in this dissertation.

1.4 Benefits and Limitations of Topology-based Soft Switching Inverters

Topology based soft switching strategies for voltage source inverters are basically classified into two families: passive approach and active approach. Those in the category of passive approach are usually bulky and are not able to completely eliminate the switching loss. The family of active approach, according to the placement of the auxiliary circuitry, can be further classified into two categories: DC-side topologies and AC-side topologies.

DC-side topologies are the Resonant DC-link family and Quasi-Resonant DC-link family in which an auxiliary circuit is inserted between the input DC power supply and main bridges to create a zero-voltage interval of the DC-bus at each switching transition [12].

The Resonant DC link (RDCL) circuit proposed by Divan is composed of an inductor and capacitor that resonate at a certain frequency to provide a soft DC bus at switching transitions [13]. Switching the main devices at zero voltage transitions of the DC bus introduces undesirable harmonic distortion since Discrete Pulse Modulation has to be applied [13]. To reduce these harmonics the DC link has to resonate at higher frequencies, which increases resonant circulating conduction loss. Another limitation of this technique is high voltage stress on the main switches [14].

High voltage stress can be reduced to 1.4 times Vdc by applying a clamped circuit shown in Figure 1-6 which requires one additional switch [15]. Voltage stress is still higher than the source voltage Vdc and the problem of high THD is not solved. Several modified versions of RDCL such as the passive clamped type using the couple inductors [16], and a one switch resonant inverter that need special space vector PWM were proposed to overcome the drawbacks of the RDCL inverters [17],[18]. These improved soft switching inverters still suffer from voltage stress and reliability problems [14].

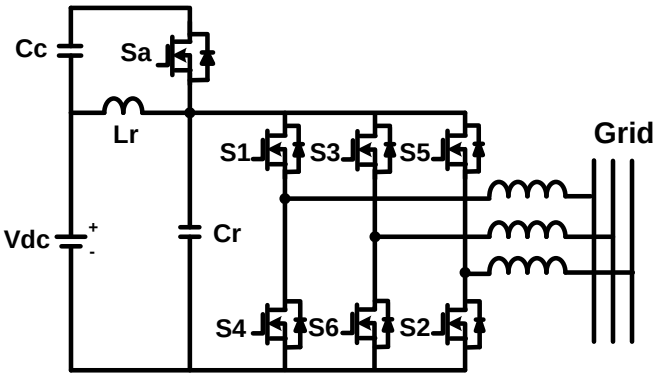

Figure 1-6: Clamped Resonant DC Link inverter

Quasi Resonant DC link (QRDCL) topologies proposed to solve before mentioned problems of RDCL inverters offer lower component stress limited to DC voltage supply. They are also compatible with conventional PWM schemes. QRDCL consists of a controlled resonant branch in parallel with the main power bridge circuit and an auxiliary switch in the DC rail that make the dc link resonate to zero and keep it at zero for the switching transition in the PWM inverter. The common disadvantage of QRDCL topologies is that the DC rail switch has to conduct the full load current of the inverter, and for every switching cycle it is turned off with high current and under hard-switching condition [19],[20],[21].

Parallel Resonant DC link (PRDCL) proposed by He needs large active component counts that must withstand high current or voltage stress [22]. A different version of PRDCL with lower component stress was proposed by Cho, however it needs three auxiliary switches and two additional diodes and this large component count is not affordable for the micro-inverter applications [23]. Auxiliary QRDCL inverter proposed by DeDoncker has a charge balance problem in its capacitors besides the common disadvantages of QRDCL inverters [14]. One

solution to this problem is to increase the resonant frequency, however that increases the peak current and results in higher conduction losses. Soft switching inverter topology shown in Figure 1-7 utilizes only one dc rail switch and one auxiliary switch [24]. The control timing of this topology is complicated and quite challenging to maintain the location and duration of zero voltage for a wide operation range.

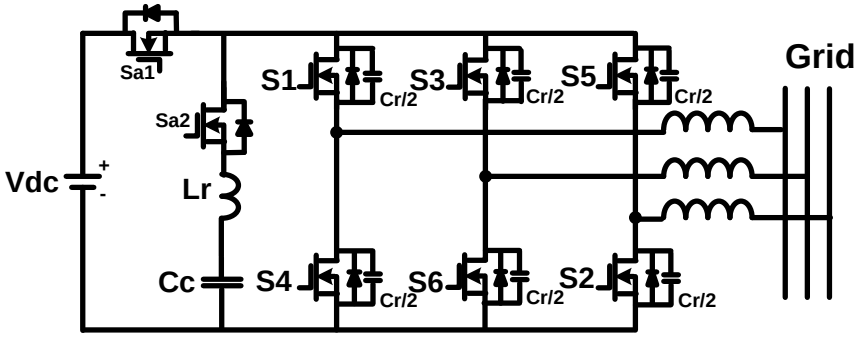

Figure 1-7: Quasi Resonant DC Link inverter

The soft switching topologies proposed in [25], [26] and [27] need magnetically coupled inductors and some modification in the control method. The coupled inductor is bulky which reduces the power density of the micro-inverter, and moreover brings additional magnetic losses. The topology proposed by Mandrek reduces the number of switches at the cost of adding a capacitive voltage divider at the input of the inverter [28].

In the AC side topologies there are basically two techniques, zero voltage switching (ZVS) and zero current switching (ZCS). For these soft switching inverters the auxiliary circuit is placed on the AC side of the main power bridge. Essentially the auxiliary circuit is out of the main power

path therefore reducing the conduction losses. Low conduction loss of AC-side topologies makes them preferable for high power applications.

The Auxiliary Resonant Commutated Pole (ARCP) inverter can completely operate under soft switching condition and achieve high power conversion efficiency. ARCP requires the addition of a resonant inductor and two auxiliary switches per phase that makes the topology and control costly and complicated. The overvoltage protection is required for ARCP since its auxiliary switches are connected back to back and there is no path for the inductor current to return to the source. Furthermore, ARCP has the disadvantage of charge imbalance in the bulky input capacitors [29],[30].

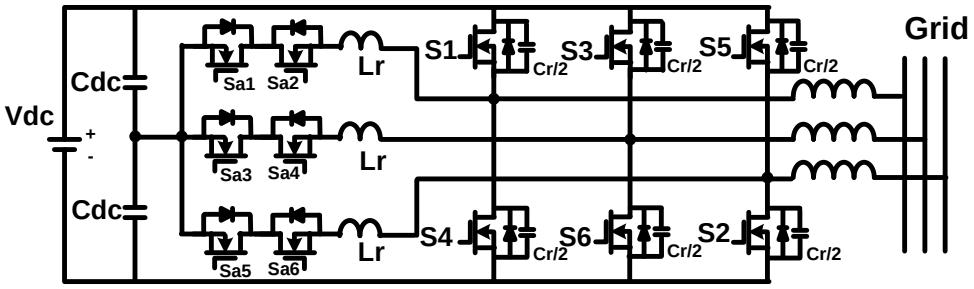

Figure 1-8: Auxiliary Resonant Commutated Pole inverter

ZVS inverter topologies with coupled inductor feedback developed by Frame [31] and Yuan [32] for three-phase inverters offer several advantages over the ARCP. However, the main drawback of these topologies is the use of coupled inductors. They are bulky and moreover they bring additional magnetic losses. Although three-auxiliary-switch topologies reduce the cost of AC side soft switching inverters [33],[34], but their practical implementation is very challenging.

Another family of ZVS inverters with one or two auxiliary switches were proposed in which an evaluation study indicates that although they reduce the cost, their efficiency is actually worse than hard-switching inverters [35] or they introduce very complex control circuitry and limitations on the operation of the inverter [36],[37].

Zero current switching (ZCS) techniques are usually implemented for high-power inverters which are built with minority-carrier devices, such as IGBTs and GTOs. Diode reverse recovery and Turn-off loss are the dominant causes of switching losses in these inverters and they can be minimized using the ZCS techniques. ZCS soft switching approach diverts the current through the main power device to another path prior to the switching transition.

Six and three auxiliary switches ZCS inverters were proposed in [38],[39],[40],[41]. They feature many advantages such as high efficiency, conventional PWM implementation, and low voltage stresses across the switches/diodes. The major disadvantages are the high complexity, cost, and size associated with the large number of auxiliary switches.

Resonant components and auxiliary devices are required to achieve soft switching conditions in all previously reviewed techniques. These additional components reduce the reliability and increase the control complexity and price of the micro-inverter. High efficiency hard switched inverter topologies also require costly silicon carbide devices or additional magnetic components [42].

In order to solve the before mentioned problems and reduce the cost of micro-inverters, a novel control based zero voltage switching technique is proposed and will be discussed in the next chapter of this dissertation. The proposed technique is based on a current control scheme that

creates a soft switching condition for the switches of the conventional half-bridge topology with no additional devices, magnetic components or analog circuits.

1.5 Research Motivation and Objective

The objectives of this dissertation are to develop a low cost, high efficiency, long lifetime, ultra-compact, three-phase micro-inverter. The application of this three-phase micro-inverter can be for residential and commercial rooftops or for MW-class solar farms.

More specifically, the development targets for the three-phase inverter are summarized as follows:

- To employ soft switching without any additional cost or components
- To achieve power conversion efficiency more than 96%
- To increase the life span of the micro-inverter for more than 25 years
- To increase the power density of the micro-inverter for more than 12W/in3
- To implement smart functions such as: Var compensation, Grid support…

With the above development targets, the research objectives of this dissertation can be summarized as:

- To design and build a new three-phase micro-inverter that can achieve soft switching operation without any additional cost or external components
- To design a control method that can be implemented fully using the digital control thereby removing the analog control components and increasing the power density and

reliability and reducing the cost of the inverter

- To explore different current modulations for further improvement of micro-inverter efficiency and output current quality
- To solve current distortion problems caused by dead-time
- To implement a new method for light load efficiency improvement of three-phase micro-inverters

CHAPTER 2. CONTROL BASED SOFT SWITCHING MICRO-INVERTER

2.1 Introduction

The relatively high cost of a micro-inverter is the biggest barrier to its large scale deployment. Increasing the switching frequency may be the best way to reduce cost by shrinking the size of output filter components and heat spreaders [43]. However, this approach could cause conversion efficiency to drop dramatically without employing soft switching techniques or using costly new devices [44],[45]. A good efficiency is achievable if a proper soft-switching technique is employed [46],[47]. In most conventional soft switching techniques resonant components and auxiliary devices are employed to create either zero voltage or zero current across the semiconductor devices prior to the switching transition. These additional auxiliary switches, passive components, and more gate driving circuits will reduce the reliability and increase the cost and control complexity of the inverter [48].

In order to solve the before mentioned problems, this chapter proposes a new control based soft switching method. The proposed control technique is based on a boundary conduction mode (BCM) zero-voltage switching (ZVS) method and features both reduced number of components and easy digital implementation. Since the soft switching condition for the switches of the three-phase inverter topology is created by the proposed control scheme, no additional devices or magnetic components are required. The proposed method also allows for easy implementation in a DSP and thus eliminates the requirement for external analog components, further decreasing

the component count and increasing the power density. The proposed soft switching technique is suitable for low power applications where switching losses are dominant [49],[50].

This chapter first presents the topology and analyzes the operation principle of a control based zero voltage switching inverter. It secondly introduces the new hybrid current control method for three-phase micro-inverter applications. Finally, it shows a 400W hardware prototype along with experimental results under different conditions to demonstrate the feasibility and advantages of the proposed control based soft switching method [51].

2.2 Topology of Half Bridge Three-phase Inverter

A standard half-bridge three-phase inverter topology is shown in Figure 2-1. In this topology the diodes and capacitors paralleled with the MOSFETs are the body diodes and parasitic output capacitors of the MOSFETs. The control based soft switching technique is implemented for this topology. As can be seen the device count is the same as the standard voltage source inverter (VSI) and the new soft switching technique does not add any auxiliary devices or magnetic components to the topology.

2.1 Zero Voltage Switching Boundary Current Control

The ZVS BCM current control is implemented for half-bridge three-phase inverter topology. In the proposed soft switching method ZVS is achieved by allowing the bi-directional current flow

which discharges the MOSFET output capacitor and passes through the body diode prior to each switching transition.

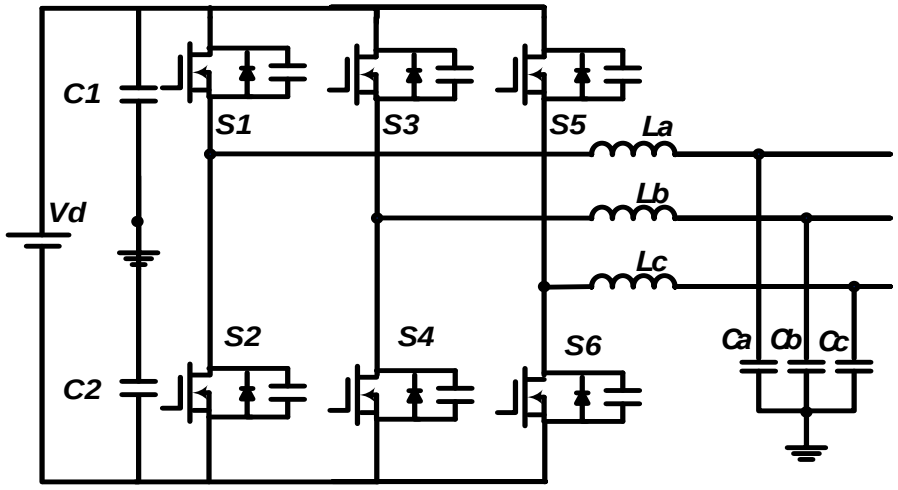

Figure 2-1: Standard half-bridge three-phase DC/AC inverter

Each phase of three-phase half-bridge inverter under ZVS BCM current control operates independently. Therefore to analyze the detailed operation principle, transition from one switch to another one in one phase leg of the three-phase inverter is discussed in this part. This phase leg is shown in Figure 2-2.

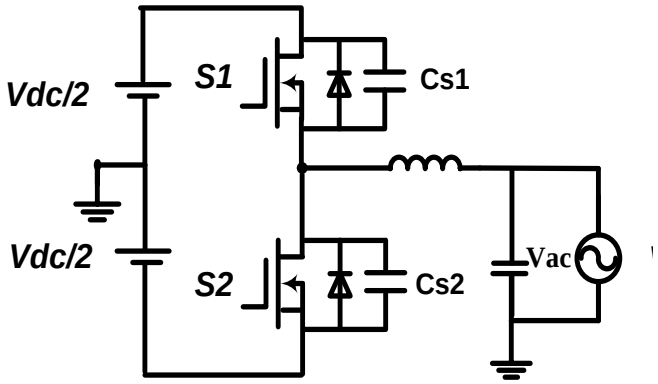

Figure 2-2: One phase leg of half-bridge three-phase micro-inverter

In order to simplify the analysis of the soft switching inverter the following assumptions are made:

1. The whole inverter system operates in steady state.
2. The output voltage (Vo) is considered as the grid voltage.

Since the switching frequency (fs: 20KHz-180KHz) is much higher than the grid voltage frequency (60Hz), the output voltage is assumed to be constant in one switching period (Ts). Figure 2-3 shows the current and voltage waveforms during the transition from the switch S2 to the switch S1.

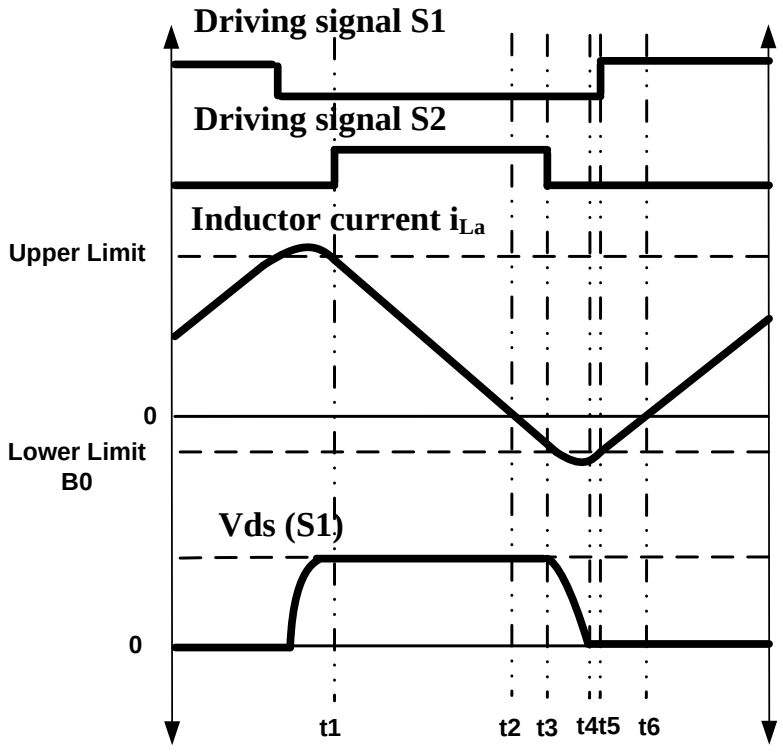

Figure 2-3: Current and voltage waveform for ZVS BCM current control

The detailed operation analysis for different time intervals is presented as follows:

Stage 1 (t1-t2): In this stage as shown in Figure 2-4 the switch S2 is on and the switch S1 is off. The inductor current is linearly decreasing until it crosses the zero point at time t2. The inductor current can be calculated according to equation (2-1).

$$i_{La}(t) = \frac{V_{ac} - V_{dc}/2}{La} t + i_{La}(t_1) \tag{2-1}$$

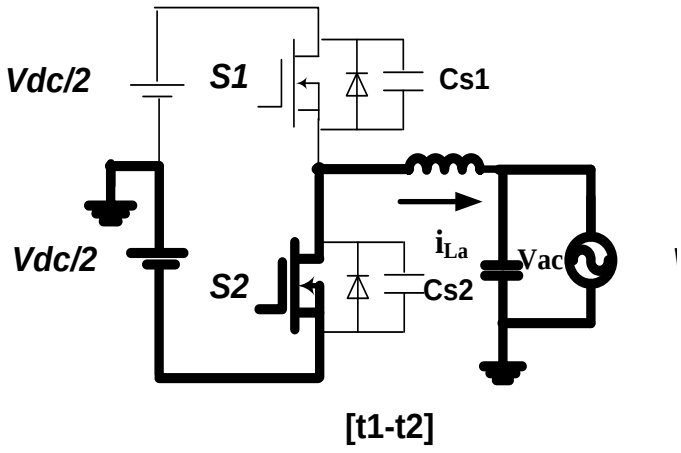

Figure 2-4: Stage one of transition from Switch S2 to Switch S1

Stage 2 (t2-t3): In this stage, same as the previous stage the switch S2 is on and the switch S1 is off. The inductor current is linearly increasing from the zero point in the opposite direction compared to stage 1. The inductor current can be calculated according to equation (2-2). The power circuit can be seen in Figure 2-5.

$$i_{La}(t) = \frac{V_{ac} - V_{dc}/2}{La} t \tag{2-2}$$

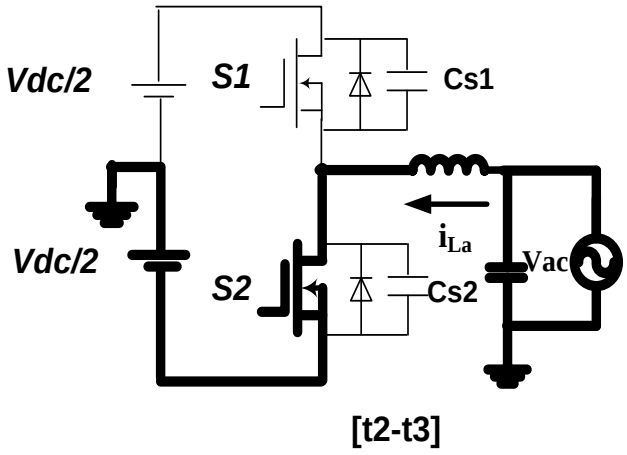

Figure 2-5: Stage two of transition from Switch S2 to Switch S1

Stage 3 (t3-t4): In time t3 the inductor current has reached the expected reverse value and switch S2 is turned off; as switch S2 is turned off, the resonant current of inductor La discharges and charges the parasitic capacitors of the MOSFETs S1 and S2 respectively. Figure 2-6 shows the power circuit. This stage ends when the capacitor of MOSFET S1 is totally discharged and its voltage is zero. The status equation for the inductor current and capacitor voltage can be written as equation (2-3).

$$\begin{cases} i_{La}(t) = -i_{La}(t_3)\cos(\omega_0 t) - \dfrac{V_{ac} + V_{dc}/2}{Z_0}\sin(\omega_0 t) \\ V_{Cs1}(t) = (V_{dc}/2 - V_{ac}) + (V_{dc}/2 + V_{ac})\cos(\omega_0 t) - i_{La}(t_3) Z_0 \sin(\omega_0 t) \end{cases} \tag{2-3}$$

The natural resonant frequency (ω_0) and the characteristic impedance (Z_0) of the resonant tank, composed by La, Cs1, and Cs2 are expressed in equation (2-4) and (2-5) respectively.

$$\omega_0 = 1/\sqrt{2CL_a} \tag{2-4}$$

$$Z_0 = \sqrt{L_a / 2C} \qquad C = C_{s1} = C_{s2} \tag{2-5}$$

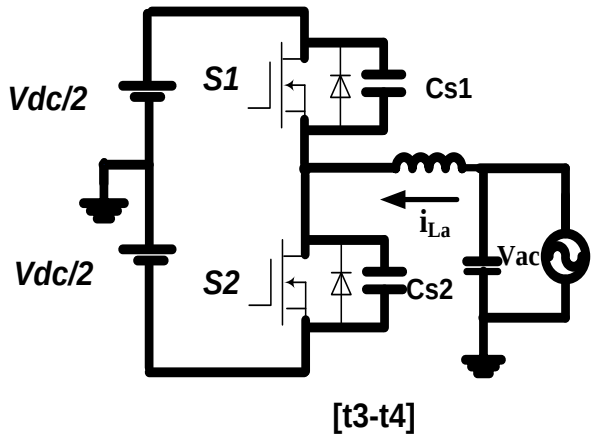

Figure 2-6: Stage three of transition from Switch S2 to Switch S1

Stage 4 (t4-t5): In time t4, the voltage across S1 drops to zero, and the anti-parallel diode of the switch S1 starts to conduct. Switch S1 can be turned on under ZVS condition. During this stage the inductor current starts ramping up according to equation (2-6). This stage is shown in Figure 2-7.

$$i_{La}(t) = \frac{V_{dc}/2 - V_{ac}}{La} t + i_{La}(t_4) \tag{2-6}$$

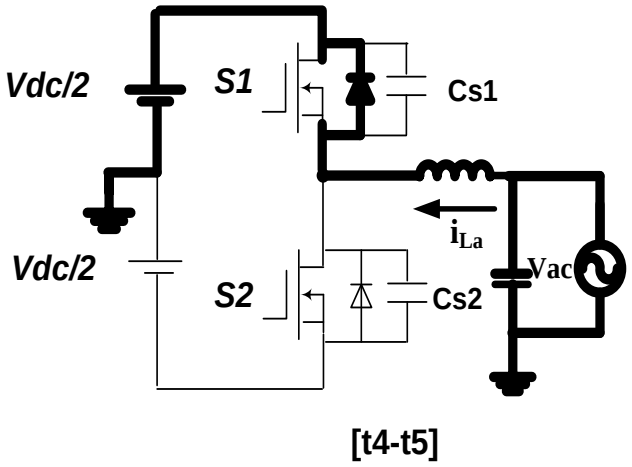

Figure 2-7: Stage four of transition from Switch S2 to Switch S1

Stage 5 (t5-t6): In time t5 the switch S1 turns on at zero voltage. Inductor current transfers from the anti-parallel diode to the switch S1, and keeps decreasing linearly until it reaches a zero value at time t6. Inductor current still follows the equation (2-6). This stage is shown in Figure 2-8.

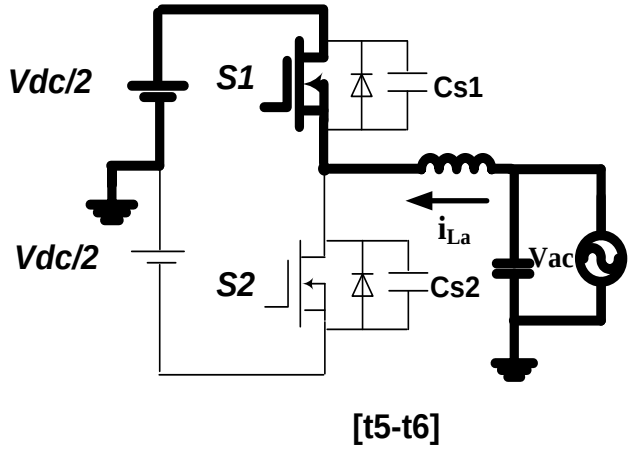

Figure 2-8: Stage five of transition from Switch S2 to Switch S1

Stage 6 (t6-t7): Inductor current is increasing from a zero value at t6 in the opposite direction compared to the previous stage. Inductor current follows equation (2-7) and its direction is shown in Figure 2-9.

$$i_{La}(t) = \frac{V_{dc}/2 - V_{ac}}{La} t \qquad (2\text{-}7)$$

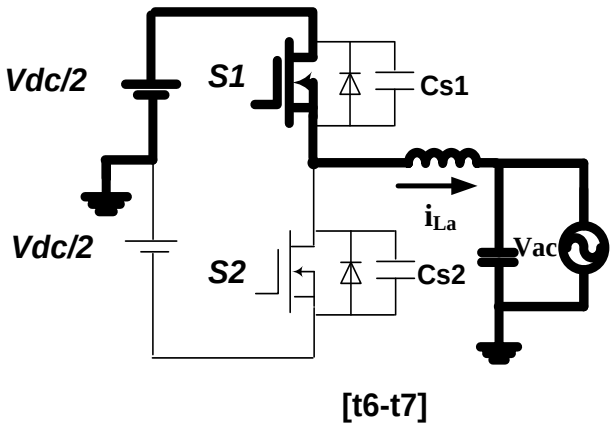

Figure 2-9: Stage six of transition from Switch S2 to Switch S1

Before moving to the next step, one important point about the switches of the half-bridge inverter should clearly be described. The power MOSFETS of ZVS BCM current control operates in their first (Vds> 0 and Ids> 0) and third quadrants (Vds < 0 and Ids< 0). The operation of low voltage power MOSFETs in their third quadrant is widely used in synchronous rectifier buck converters. The use of higher voltage (i.e. 600V in our case) power MOSFET in the third quadrant is less common, but nevertheless follows a similar operation principle.

2.2 BCM ZVS Implementation Requirements

Implementation of the ZVS BCM current control requires setting the upper and lower boundaries (limits) of the inductor current. The value of the reverse current (lower boundary for the positive half cycle and upper boundary for the negative half cycle) during each half line period is determined by the amount of current required to charge the inductor such that the discharging current from that during the dead-time interval is large enough to discharge the parasitic

capacitance and turn on the body diode of the MOSFET which is about to turn on thereby ensuring ZVS operation for the MOSFETs. The other boundary is chosen in a way that it ensures the average of inverter inductor current follows the reference current. Depending on the boundary shape of the current limits there are different current modulations for achieving ZVS operation that will be discussed in more detail in Chapter Four of this dissertation.

Boundaries of BCM ZVS current control are shown in Figure 2-10. As seen in this figure this current modulation scheme has a fixed value reverse current. For the positive half cycle the upper limit is set to ensure that the average current during each switching cycle is equal to the reference current whereas the lower limit is set to ensure that the reverse current is sufficient to discharge the output capacitor of the MOSFETs. During the negative half cycle the situation is opposite and the upper limit ensures the soft switching and the lower boundary is calculated from the current reference. Upper and lower limits for this current modulation scheme can be calculated from equation (2-8), where B_0 is the reverse current required to achieve zero voltage switching and $i_{ref} \sin(\omega t)$ is the reference current.

$$\begin{cases} i_{upper} = 2i_{ref} \sin(\omega t) + B_0 \\ i_{lower} = -B_0 \end{cases} \quad if\ i_{ref} \sin(wt) \geq 0$$
$$\begin{cases} i_{upper} = B_0 \\ i_{lower} = 2i_{ref} \sin(\omega t) - B_0 \end{cases} \quad if\ i_{ref} \sin(wt) < 0 \qquad (2\text{-}8)$$

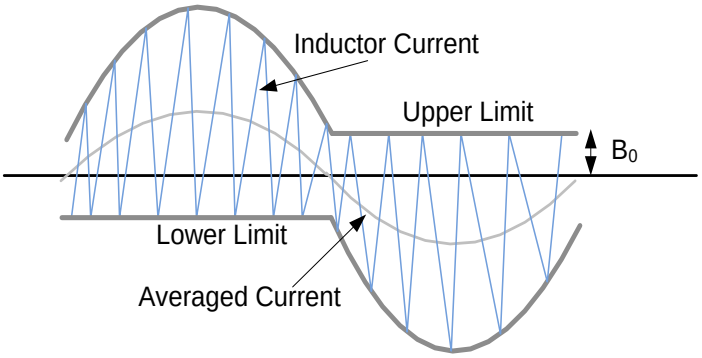

Figure 2-10: Upper and lower boundaries of BCM ZVS current control

2.3 Hybrid BCM Current Control

For power electronics applications, peak current control is usually implemented using the analog circuits to turn on and off the inverter switches. This transition happens when the current reaches the expected boundaries. The analog circuits have the problem of reliability and they also decrease the power density of the micro-inverter. The second method to implement the peak current control is to predict the required switching time using the calculation inside the controller. The required turn on and turn off of the switches can be predicted in order to change the current between the desired boundaries. The problem of this method is accumulated error caused by the change in the inverter parameters.

In this part a new method of ZVS BCM current control is proposed which is a combination of hardware reset and predictive control and is referred to as hybrid current control. Hybrid current control doesn't require external analog components and can be completely implemented using

the advanced features of DSPs designed for power electronics applications. By taking advantage of the internal comparator of these DSPs, PWM period can be reset whenever the inductor current reaches the required boundary. Turn-on or Turn-off duration can be predicted using the calculation inside the DSP. This hybrid current control method is shown in Figure 2-11.

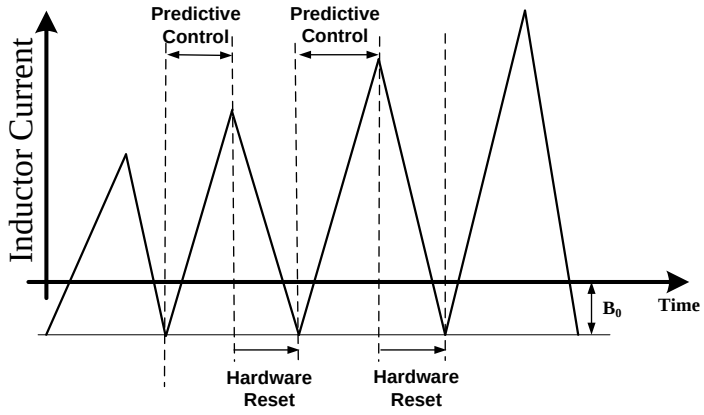

Figure 2-11: Hybrid BCM current control

Figure 2-12 shows the implementation of Hybrid BCM current control using a DSP designed for power electronics application. Basically current control methods for power electronics applications require accurate sensing of the inductor peak current. Since the inductor current for the half-bridge inverter includes both the switching frequency and the line frequency, it is bulky to measure with a single current transformer. However, it can easily be sensed with a high frequency current transformer and a low frequency current sensor chip. This current sensing approach reduces the size of current measurement component. These high and low frequency components are separately sensed from the capacitor and the output line and then added together to produce the inductor current. For each phase only one comparator and a PWM generator are

needed to produce the switching signals. Since all the controller parts are located inside the DSP chip the propagation delay is very short for this control method.

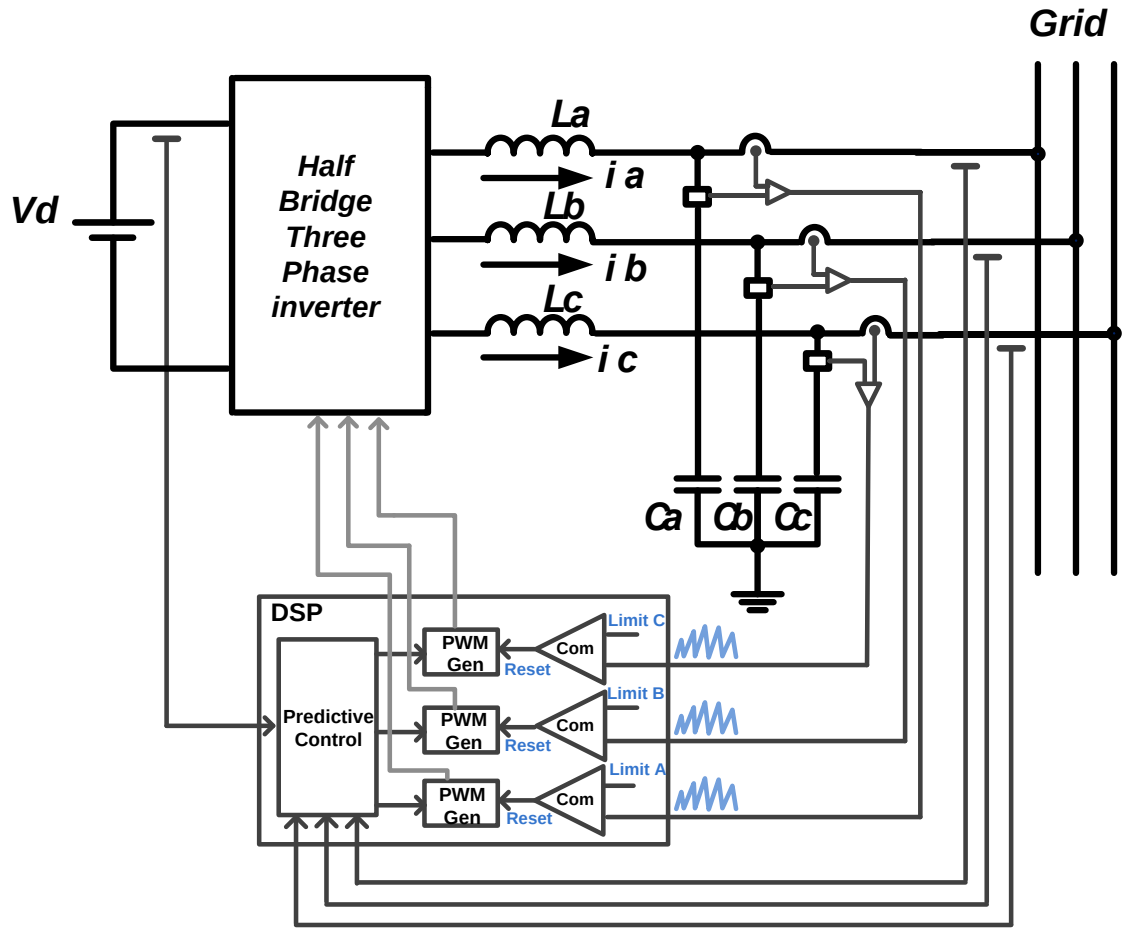

Figure 2-12: DSP implementation of hybrid ZVS BCM current control

2.4 Practical Implementation: Problems and Solutions

In practical implementation of hybrid BCM current control, there is a difference between the points which the actual current reaches and the required boundaries. Delay in the comparator,

driver circuits, and switches and non-ideality of the switches is the main reason of this difference. In order to minimize the effect of this non-ideality on the current waveform, same-shape hardware reset for positive and negative half cycle is desired. Therefore, the lower limit is set as the hardware reset for positive half cycle and for the negative half cycle the upper limit is the hardware reset. Figure 2-13 shows the hardware reset of the inductor current. The comparator value is changed between lower limit and upper limit according to the positive and negative half cycle of the reference current.

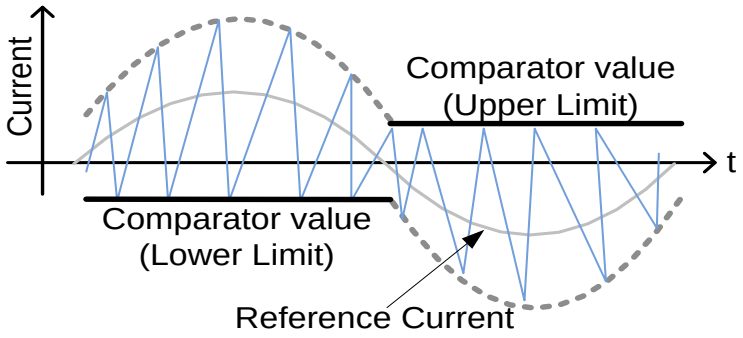

Figure 2-13: Practical hardware reset of hybrid BCM current control

2.5 Predictive Control: Dead-time and Duty Cycle Calculation

In order to achieve zero voltage switching for the proposed current control method some required design consideration should be applied. One of which is the dead-time duration. The dead-time should be long enough for the reverse current to discharge the output capacitor of the MOSFETs. The time to fully discharge the energy stored in the MOSFET output capacitor can be calculated

according to equation (2-9) and for zero voltage switching operation, dead-time should be set more than the time duration t_d.

$$t_d = 2CV_{dc} / B_0 \tag{2-9}$$

Since dead-time duration is very short compared to the duty cycle duration and switching period, the voltage-second balance across the inductor La can be used to derive the expression of turn-on/off time and switching frequency of the inverter. Turn-on time is defined as the time required to keep the upper switch on and to make the inductor current reach from the lower limit to the upper limit. T-on is calculated according to equation (2-10).

$$T_{on} = L \frac{i_{upper} - i_{lower}}{\frac{1}{2}V_{dc} - V_o} \tag{2-10}$$

Turn-off time is defined as the required time which lower switch should stay on to make the inductor current reach from the upper limit to the lower limit. T-off is calculated according to equation (2-11).

$$T_{off} = L \frac{i_{upper} - i_{lower}}{\frac{1}{2}V_{dc} + V_o} \tag{2-11}$$

BCM ZVS current control has a variable switching frequency. It is derived using the T-on and T-off expressions according to equation (2-12).

$$F_{swt} = \frac{(V_{dc}/2)^2 - V_o^{\,2}}{LV_{dc}(i_{upper} - i_{Lower})} \tag{2-12}$$

Predictive control unit of hybrid BCM current control calculates the duty cycle for each switching cycle using equation (2-10) for positive half cycle and (2-11) for negative one.

2.6 Three-phase Micro-inverter Design Consideration

Inductor value:

Inductor value selection of output LC filter is typically an important step in the inverter design procedure. It generally has significant effects on the efficiency, control stability, and operation mode of the inverters. However, for the hybrid current control three-phase micro-inverter this process is very simple. Since the upper and lower limit of inductor current is controlled by the controller; the only consideration for inductor value selection is maximizing the efficiency. In order to maximize the efficiency, the lowest possible switching frequency is desired since it decreases the inductor core losses, turn-off switching losses and AC conduction losses. The lowest switching frequency considered in three-phase micro-inverter design is 20KHz which is the maximum audible frequency.

For hybrid current control inverter the minimum switching frequency happens at full load and at the peak of the inductor current. Using equation (2-12) and considering the lowest switching frequency as 20KHz the value of the inductor can be calculated as 270 uH.

Capacitor value:

Since in the previous step the inductor value was chosen based on the efficiency optimization, the capacitor value selection should meet the filter design and closed loop stability requirements. The primary goal in our design is decreasing the component cost of the micro-inverter; therefore, the lowest possible capacitor value is desired. Considering the lowest switching frequency component in the inductor current as 20KHz and a 270 µH inductor value, the capacitor value of 1 µF (10KHz cut-off frequency of the LC filter) is chosen. The designed LC filter can remove the high frequency components of the injected current to the grid.

B0 value:

The value of B0 should be large enough to ensure that the reverse current is sufficient to discharge the output capacitor of the MOSFETs. B0 selection can be considered a trade-off between the current distortion and conduction losses. Figure 2-14 shows conduction loss and required dead-time for the rated power of the three-phase micro-inverter versus the value of B0. According to this figure by increasing the value of B0, lower dead-time can be chosen. Although lower dead-time decreases the current distortion but larger B0 increases the conduction losses. The value of B0 is chosen as 1A and the dead-time is 800nSec for the 400W micro-inverter. In order to have a theoretical optimization of B0 accurate modeling of the parasitic capacitor of the MOSFETs is required and is outside the scope of this dissertation.

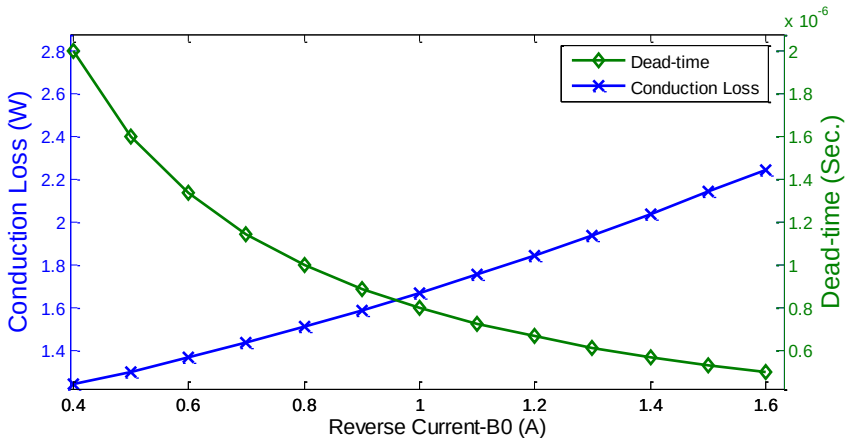

Figure 2-14: Dead-time and conduction loss for a 400W hybrid control three-phase micro-inverter versus different value of reverse current-B0

EMI filter:

It is a general assumption that designing an EMI filter for a fixed switching frequency converter is easier than designing one for a variable switching frequency converter, while the opposite is actually true. All soft switching converter schemes using a variable switching frequency spread the conducted and radiated emissions over a broader range of frequency. As a result, the average spectral power density (SPD) of the broadband noise can thus be significantly reduced; such that it reduces the average EMI and allows the average noise to fall below the legal electromagnetic compatibility (EMC) standards [52],[53].

Magnetics cores:

Physical size of an inductor magnetic core is a function of the energy that has to be stored in it. The higher the energy to be stored, the larger the size of the core will be. Even though the peak of inductor current in BCM soft switching control is higher than the CCM micro-inverters, the

required stored energy in the inductor is much lower than CCM due to the much smaller inductance.

The following comparison between two micro-inverters with CCM and BCM ZVS current control can be useful.

A typical CCM 230W 230V single phase micro-inverter might have up to a 14mH inductor. Considering the RMS current as 1A, the stored energy inside the core can be calculated using equation (2-13) as 0.01391j.

$$E = E_L = \frac{1}{2} Li^2 \tag{2-13}$$

For the three-phase BCM soft switching micro-inverter the designed inductor value is 270µH. Considering the RMS current as 1A, the peak current using equation (2-8) can be calculated as 3.82A. Using equation (2-13) the stored energy inside the core is 0.001969J. The results of this comparison confirm that BCM soft switching current control decreases the size of the inductor core considerably.

Nominal Power:

BCM soft switching current control is suitable for low power applications where switching losses are dominant. Switching and conduction losses of a three-phase micro-inverter for different rated powers with ZVS BCM current control is shown in Figure 2-15. One characteristic that should be noted is that for a three-phase micro-inverter with rated power more than 750W, the conduction losses are more than switching losses and implementing the BCM

soft switching current control might not be able to achieve high efficiency. In Figure 2-15 the modeled source of conduction losses are the MOSFET on-resistance and inductor winding resistance.

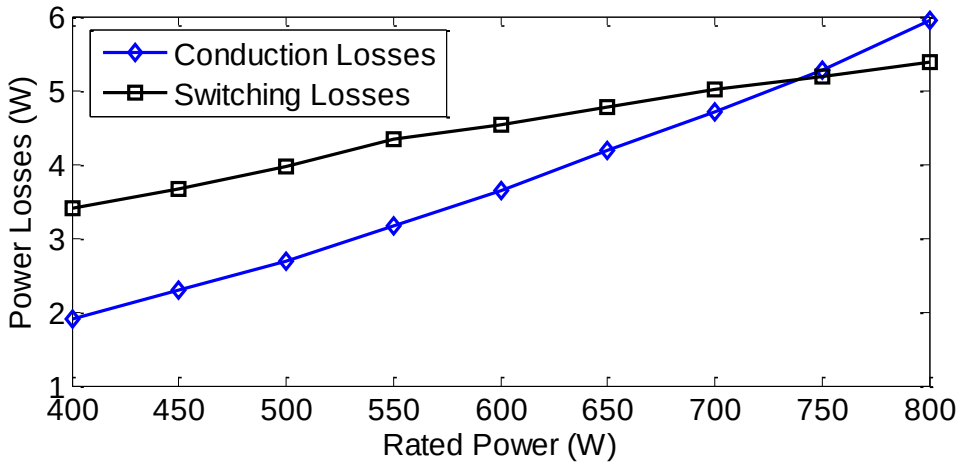

Figure 2-15: Switching and conduction losses of hybrid BCM current control versus different rated power

2.7 Experimental Results

To prove the viability and merits of the proposed three-phase micro-inverter with hybrid BCM current control, a 400W, 208VAC half-bridge inverter system in standalone and grid tied operations was designed and tested. The power circuit structure of the prototype is the same as in Figure 2-1, and the current control scheme applied is shown in Figure 2-12. The system controller and PWM generation are conducted by Microchip floating point DSP dsPIC33FJ6GS504.

The MOSFET is selected as FCB20N60 with on-resistance 150mΩ. Parameters of the circuit system are set as below: Input: 400Vdc, Output: 208VAC, 60Hz, Rated power: 400W; Switching frequency: 20kHz~180kHz; $L_a=L_b=L_c=270\mu H$, $R_{La}=R_{Lb}=R_{Lc}=0.2\Omega$, $C_a=C_b=C_c=1\mu F$. The current of PWM hardware reset is set for B0=1A.

Output and inductor current waveforms for the phase A of three-phase micro-inverter are shown in Figure 2-16. Figure 2-17 depicts the current of the inductor La, the main switch S2 driver signal and its drain to source voltage. It can be clearly seen in this figure that the drain to source voltage across the corresponding MOSFET has already reached zero before the arrival of the turn-on driver signal. These waveforms verify that the proposed controller can realize ZVS during turn-on transitions.

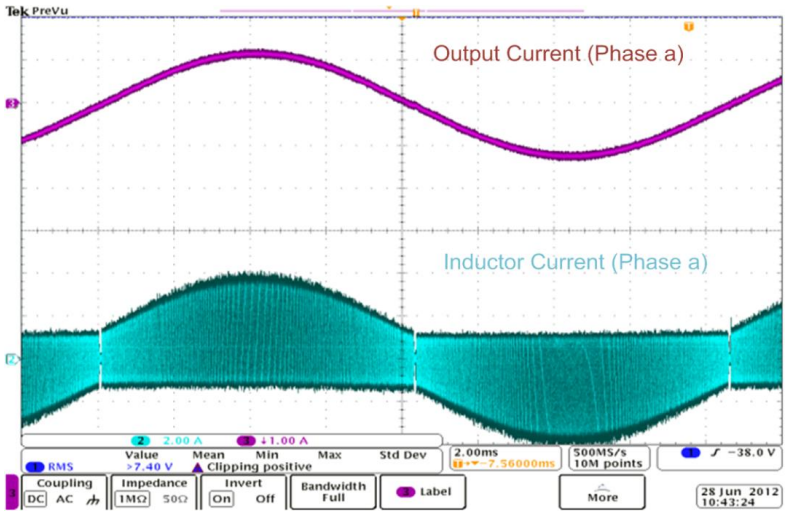

Figure 2-16: Output and inductor current of phase A of three-phase micro-inverter with hybrid BCM current control

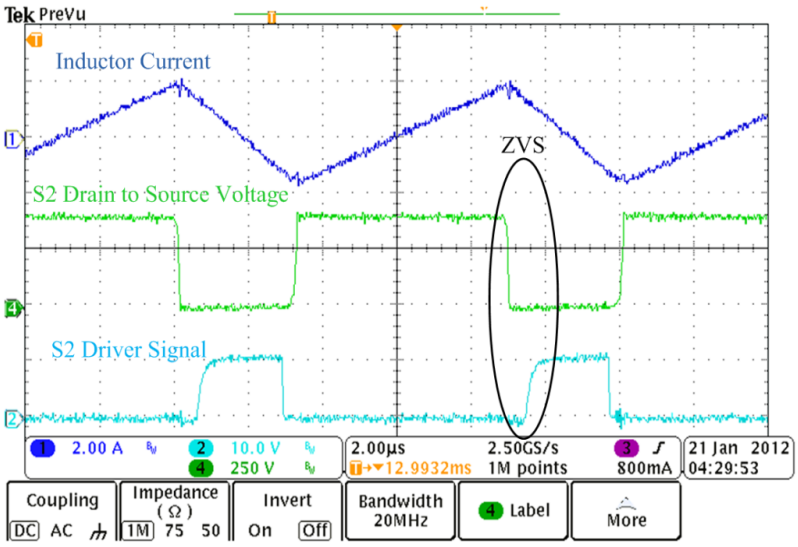

Figure 2-17: Zero voltage switching of hybrid BCM current control, Inductor current, Drain to source voltage and gate signal of switch S2

Figure 2-18 and Figure 2-19 demonstrate the switching loss for switch S2 close to the peak and zero crossing point of the inductor current. Switching loss has been calculated using the product of MOSFET drain current and drain to source voltage. These figures confirm that the turn-on loss over the full range of switching frequency is zero.

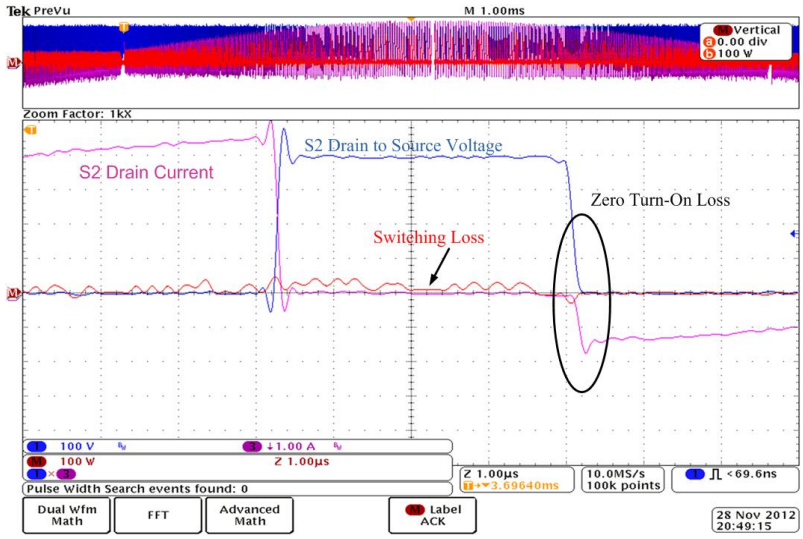

Figure 2-18: Current, voltage and switching loss waveforms of switch S2 at the peak of the inductor current

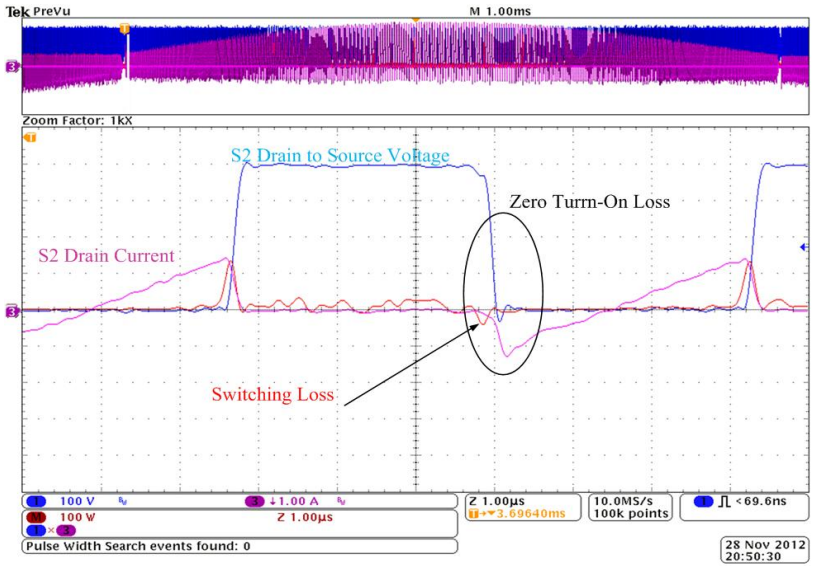

Figure 2-19: Current, voltage and switching loss waveforms of switch S2, close to the zero crossing point of inductor current

Figure 2-20 shows the three-phase inductor current and Figure 2-21depicts the output current of the three-phase micro-inverter. Although the inductor current in Figure 2-20 has high frequency ripple, the THD of the output current is less than 2.5% and meets the IEEE 1547 and UL 1741 5% THD requirements.

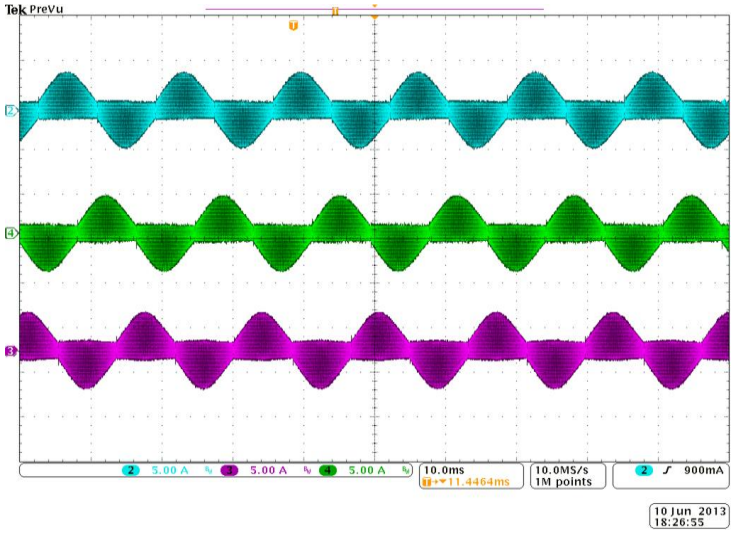

Figure 2-20: Three-phase inductor current for hybrid BCM current control micro-inverter

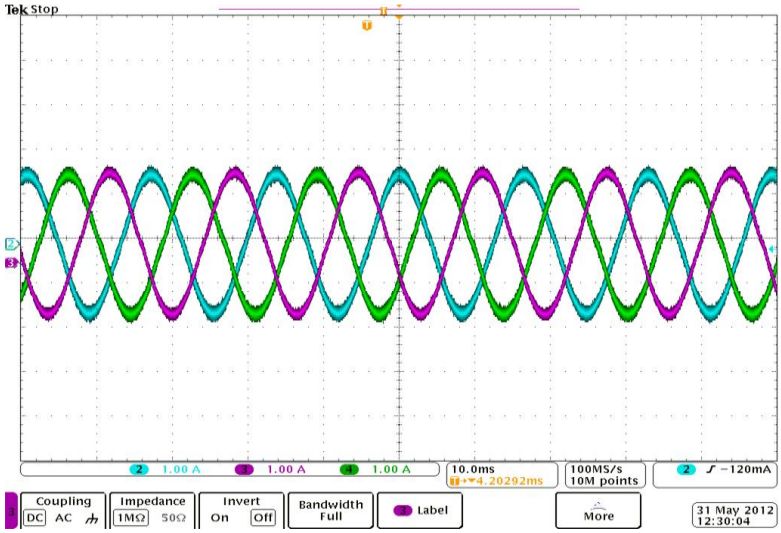

Figure 2-21: Three-phase output current of hybrid BCM current control micro-inverter

In order to study the robustness and performance of the hybrid BCM current control micro-inverter in case of grid disturbances, a step change of the grid voltage is considered. Figure 2-22 shows the dynamic response of the micro-inverter output current to the step change in the grid

voltage from 120Vrms to 80Vrms. Dynamic response to the 100% increase in the current injected to the grid is also shown in Figure 2-23.

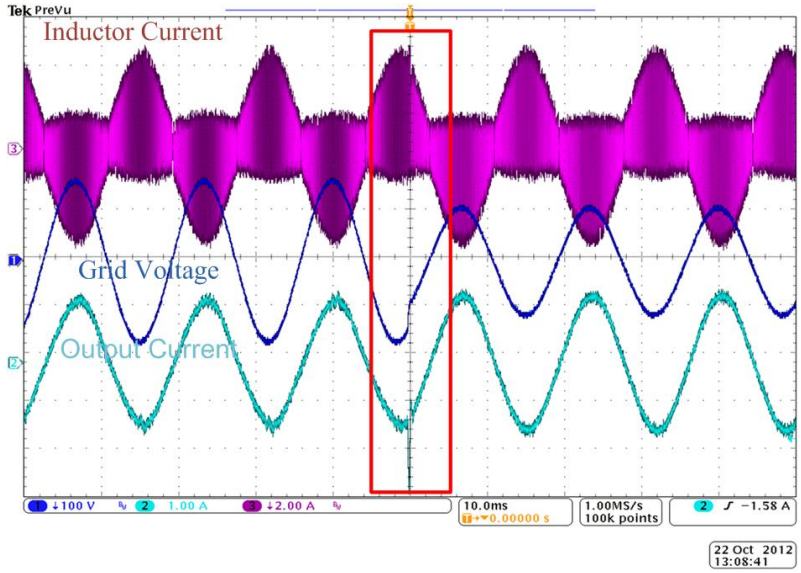

(a)

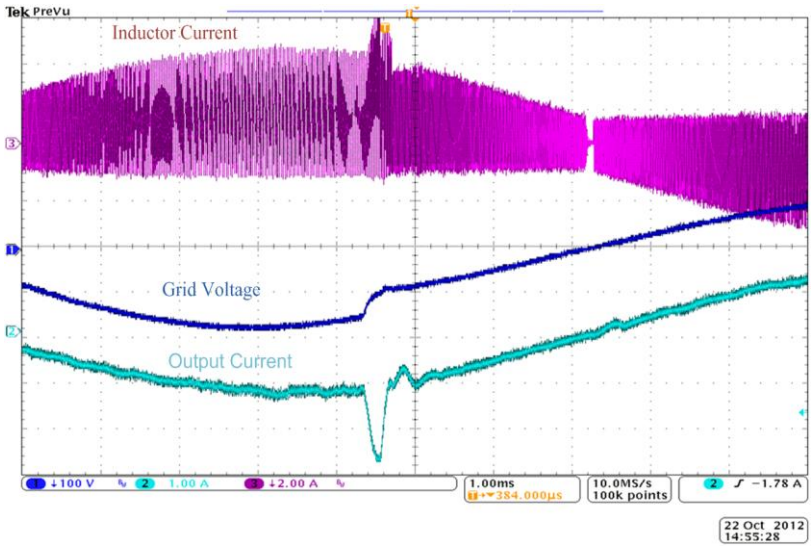

(b)

Figure 2-22: Dynamic response to the step change in the grid voltage from 120V to 80V

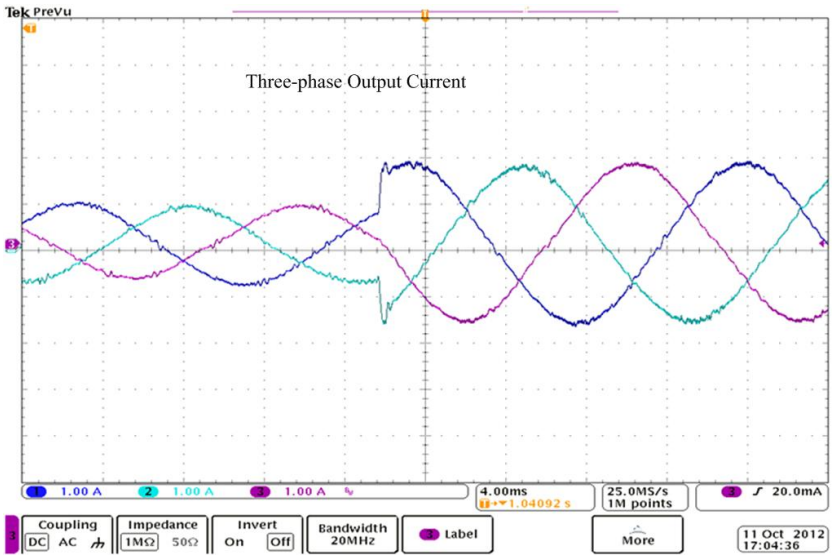

Figure 2-23: Dynamic response to 100% increase in the injected current to the grid

A simple current closed loop was implemented for the three-phase micro-inverter to verify its performance under closed loop operation. The closed loop control performs active and reactive power control and corrects the error of injected current to the grid. Figure 2-24 shows one phase of the three-phase micro-inverter under open and closed loop operations. In this figure the reference of active and reactive power are set for P= 340W and Q=0Var.

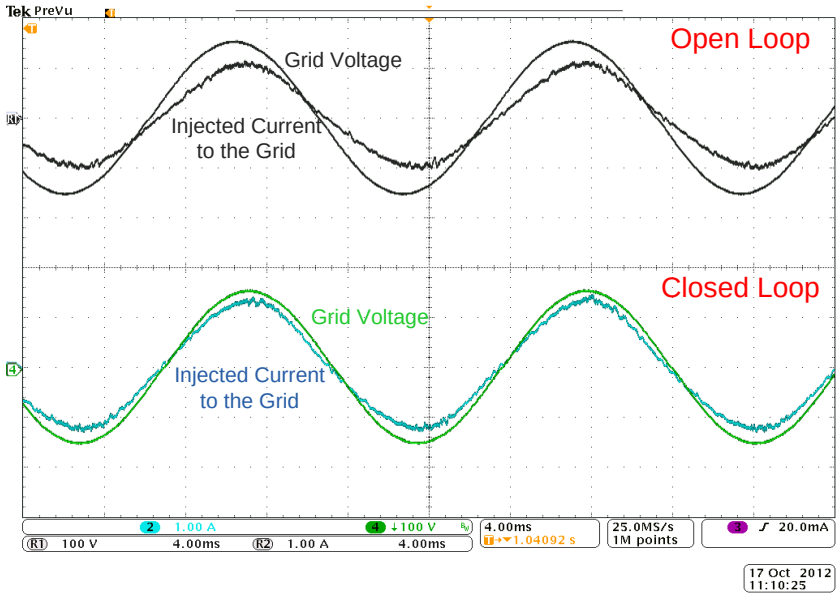

Figure 2-24: Closed loop control of hybrid BCM current control

Figure 2-25 shows the converter efficiency versus output power. The power MOSFETs used in the prototype for efficiency measurement are FCB20N60. The efficiency measurement was performed through light load until full load condition. It can be seen that the peak efficiency of 98.4% is achieved with the hybrid BCM current control with no additional cost. All the efficiency measurements were performed using a Yokogawa PZ4000 power analyzer. The measured efficiency does not include driving power losses.

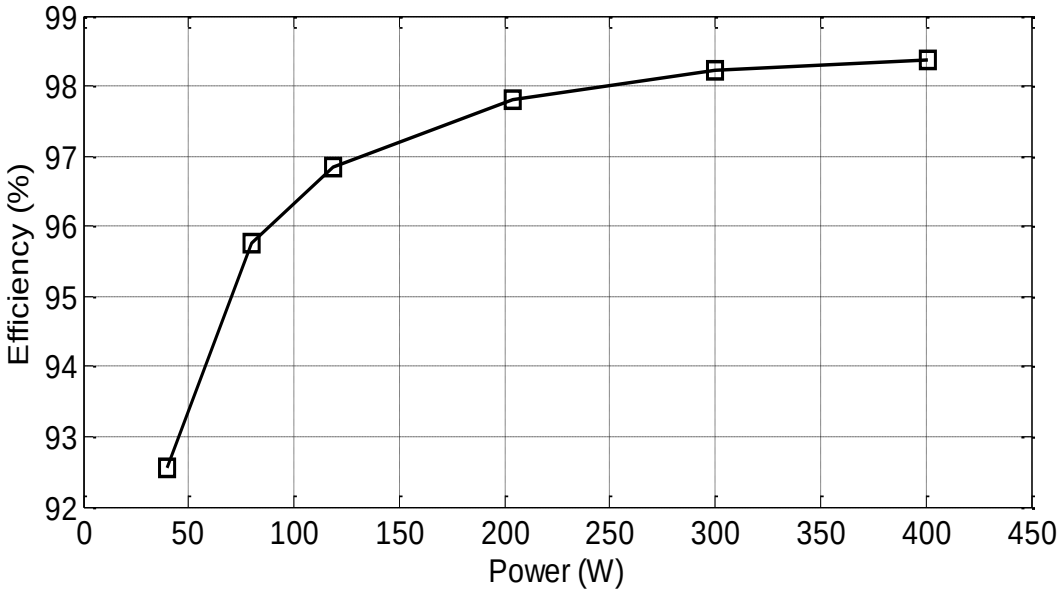

Figure 2-25: Efficiency of three-phase micro-inverter with hybrid BCM current control

2.8 Power Device Selection

Hybrid BCM current control scheme eliminates the turn-on switching losses; therefore, turn-off loss and conduction loss remain as the main source of power dissipation in the power devices. MOSFET selection for the proposed control method is a compromise between conduction loss and turn-off switching loss. Conduction loss of a MOSFET can be evaluated by its on resistance while its turn-off switching loss depends on the parasitic input (Ciss) and output capacitors (Coss). Lower Ciss makes the switch turn off voltage and current waveforms sharper and by decreasing the overlap between them it reduces the switching loss. Higher Coss acts as a snubber capacitor parallel with the MOSFET and it also reduces the turn off loss.

Different MOSFETs were tested in the prototype and their body temperature was measured. The one that has the lowest temperature has the lowest power dissipation and can give us the best efficiency. Table 2-1 shows the body temperature of different MOSFETs after running the prototype for half an hour. For the results in Table 2-1 only internal ground plane of the PCB board has served as a heat sink for the MOSFETs. It can be found from this table that FCB20N60 has the lowest body temperature and therefore lowest power dissipation. This is due to the fact that its on-resistance and input parasitic capacitor (Ciss) are acceptable compared to the other MOSFETs but its large output parasitic capacitor (Coss) acts as a snubber and decreases the turn-off loss significantly.

STB42N65M5 has half the on resistance as the FCB20N60, and it was expected to have the lowest temperature and power dissipation, but since its Coss is low and Ciss is high, switching losses increased significantly. The temperature of this power device is comparable to the FCB20N60 which confirms that switching losses has a significant impact on the power dissipation.

In order to decrease the power dissipation further, it might be an interesting idea to attach an external capacitor in parallel with STB42N65M5 as a snubber and measure its temperature, but since the price of this MOSFET is almost double compared to the FCB20N60, it is not a cost-effective choice for micro-inverter production.

Table 2-1: Power Switch Selection for the Hybrid BCM Current Control

Manufacturer Part Number	Vdds (V)	Id (A)	Rds-ON (Ω)	Ciss (pF)	Coss (pF)	Crss (pF)	Rg (Ω)	Temp (°C)
STB42N65M5	650	33	0.070	4650	110	3.2	1.1	66.6
STB30N65M5	650	22	0.125	2880	68	5	1.6	67
STB21N65M5	650	17	0.150	1950	46	3	2.5	65.7
STB16N65M5	650	12	0.230	1250	30	3	2	67
STD12N65M5	650	8.5	0.390	900	22	2	2.5	72.6
STB11NM60FD	600	11	0.400	900	350	35	3	70
FCB20N60	600	20	0.150	2370	1280	95	NA	65
IPD65R600C6	650	18	0.540	440	30	NA	17.5	82.6
IPW65R280C6	650	13	0.250	950	60	NA	12.5	69.7

2.9 Summary

A new zero voltage switching method and its digital implementation have been proposed for the three-phase micro-inverter application. The new hybrid control method is a combination of peak current control and predictive control and has the merits of low cost, high reliability, and high efficiency. Hybrid current control was implemented for the standard half bridge topology and it does not add to the component count of the micro-inverter or complexity of the control circuit.

Design consideration of a three-phase micro-inverter with hybrid current control is presented in this chapter. It was observed that the proposed current control method is suitable for low power inverter application where switching losses are dominant.

To prove the effectiveness of the proposed hybrid current control scheme, a three-phase micro-inverter with 400W, 208Vac output capability has been designed and tested. By presenting experimental results, the viability and advantages of the proposed soft switching micro-inverter was validated. The peak efficiency of 98.4% for the three-phase micro-inverter was achieved.

CHAPTER 3. DEAD-TIME COMPENSATION FOR ZVS BCM CURRENT CONTROL

3.1 Introduction

Hybrid boundary conduction mode current control soft switching micro-inverter features high efficiency and high power density. Due to easy digital implementation and no requirement of additional components this control method is very promising for low power applications such as three-phase micro-inverters. However some practical aspects of its implementation such as dead-time insertion can degrade the performance of the micro-inverter. This chapter presents a dead-time compensation method that improves the performance of hybrid BCM current control by decreasing the output current THD and reducing zero crossing distortion [54].

It is a requirement to insert a switching delay time between the turn off and turn on of the power devices in each leg of the voltage source inverters [55]. This delay is to avoid the shoot through due to the conduction overlap of the devices and it causes serious output current and voltage distortions [56], [57]. Significant research has been conducted on the control of inverters to compensate the dead-time effects [58], [59]. Dead-time compensation methods are conventionally based on altering either the reference voltage or switching instructions [60],[61]. However, one can see that conventional methods cannot be applied for BCM current control. The first reason is that BCM current control has a variable switching frequency. Most of the conventional methods are for the fixed switching frequency. The second reason is MOSFETs parasitic capacitance has been ignored for all the conventional dead-time analysis methods. In

case of BCM ZVS current control the MOSFETs parasitic capacitor has a significant effect on the current waveform during the dead-time duration.

3.2 Dead-time Effect Analysis

Non-ideal practical implementation factors such as dead-time effect has negative influence on the hybrid BCM current control performance. In this part the transition from switch S2 to switch S1 of one phase leg of the inverter will be studied with considering the dead-time and parasitic output capacitance of the MOSFETs. Figure 3-1 shows the current and voltage waveforms during the dead-time interval for the switch S2 and S1. It can be seen in this figure that the inductor current ia goes beyond the desired limit B_0 due to the dead-time application and it causes massive distortion in the output current. The detailed analysis is given as follows.

Stage 1:

(t1-t3) Switch S2 is on and switch S1 is off. As shown in Figure 3-1 the inductor current is linearly decreasing until it crosses the zero point (at t2) and after that it increases in the opposite direction. Current increases in value until it reaches the lower limit B_0 and PWM is reset using the internal comparator of the DSP.

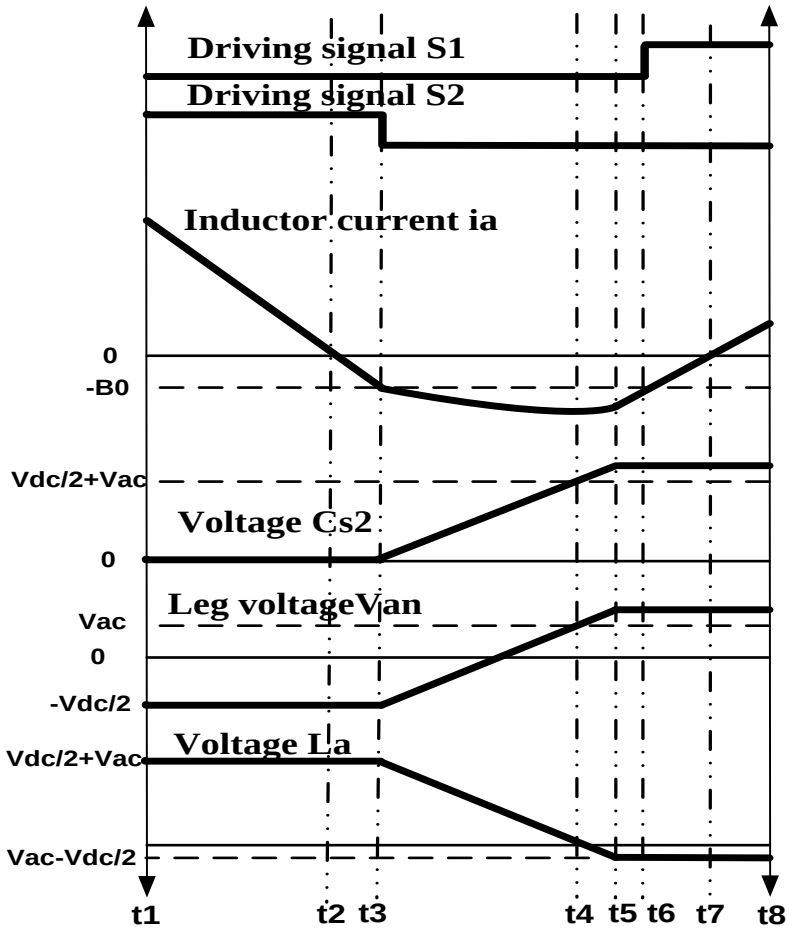

Figure 3-1: Current and voltage waveforms for dead-time interval of switch S2 and S1

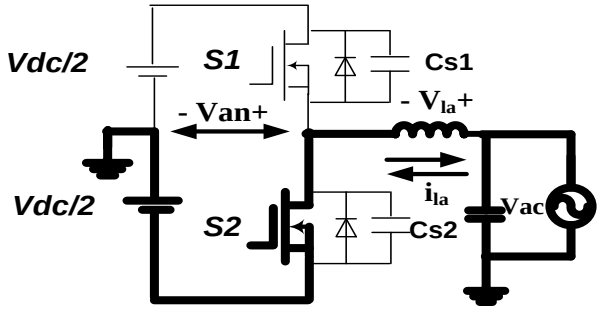

(t1-t3)

Figure 3-2: Stage one of dead-time analysis for switch S2 and S1

Stage 2:

This stage is divided into two time intervals:

A. (t3-t4) As the switch S2 is turned off the parasitic capacitor of the MOSFET S1 is being discharged and parasitic capacitor of the MOSFET S2 is being charged by the inductor current La. Leg voltage V_{an} starts rising from –Vdc/2. The current of inductor keeps increasing until the voltage across the inductor is zero, meaning the voltage V_{an} reaches the same value of the output voltage V_{ac}.

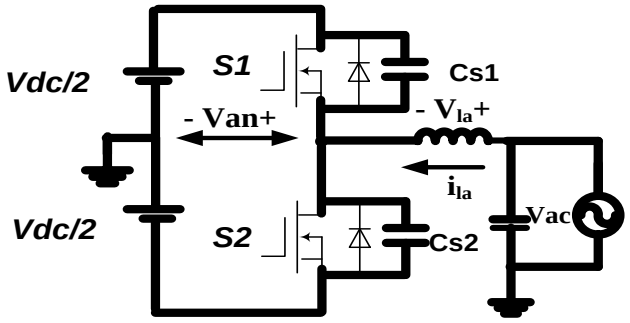

(t3-t5)

Figure 3-3: Stage two of dead-time analysis for switch S2 and S1

For the proposed dead-time compensation method, the equivalent parasitic capacitance of the MOSFETs is assumed to be Ce. Capacitor Ce is equal to the MOSFETs output capacitance value that can be extracted from the datasheet. The value of Ce is assumed to be constant for the sake of the analysis, which means it is not a function of the voltage across the MOSFETs. Considering this assumption voltage across the capacitors of switch S1 and S2 changes in a linear fashion [62]. The time duration of this stage can be approximated using equation (3-1) and inductor voltage during this time can be calculated using equation (3-2).

$$\Delta t_p = t4 - t3 = C_e \frac{V_{dc}/2 + V_{ac}}{i_{la}/2} \tag{3-1}$$

$$v_{la}(t) = V_{dc}/2 + V_{ac} - (\frac{V_{dc}/2 + V_{ac}}{\Delta t_p})t \tag{3-2}$$

Using equation (3-2) inductor current can be found as equation (3-3).

$$i_{la}(t) = \frac{1}{la}\int v_{la}(t)\,dt + i_0 \tag{3-3}$$

B. (t4-t5) During this time interval as it is shown in Figure 3-1 inductor current starts slightly decreasing in value as the leg voltage V_{an} rises above the value of the output voltage V_{ac}.

Stage 3:

(t5-t6) The body diode of the switch S1 is forward biased and the inductor current starts ramping up. Power circuit of this stage is shown in Figure 3-4.

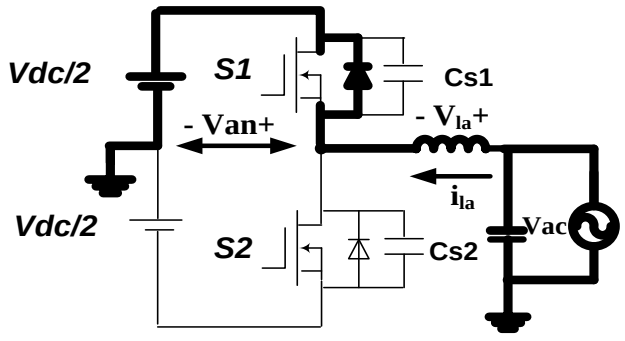

(t5-t6)

Figure 3-4: Stage three of dead-time analysis for switch S2 and S1

Stage 4:

(t6-t8) Beginning at this stage switch S1 turns on at zero voltage. Inductor current keeps decreasing linearly until it reaches a zero value. After crossing the zero point, it increases in the opposite direction. Figure 3-5 shows the power circuit of this stage.

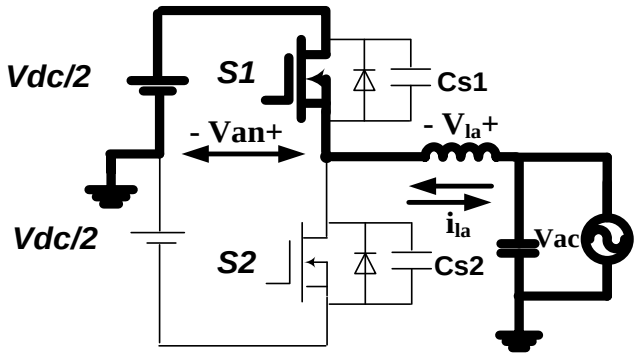

Figure 3-5: Stage four of dead-time analysis for switch S2 and S1

3.3 Dead-time Compensation

There is a dead-time in the switch control method of hybrid BCM micro-inverter to avoid shoot-through of the power source. The analysis of the dead-time effect in the previous part shows that the current of the inductor goes beyond the desired limit. Figure 3-6 shows the inductor current waveform before implementing the dead-time compensation method. This shape of inductor current causes output current to have high THD and zero crossing distortion. In order to solve this problem some modifications in the hardware reset process are performed. The value of extra

current that goes beyond the desired current limit and should be compensated is referred to as Δi_{comp} in this chapter.

Δi_{comp} is calculated as equation (3-4) which results from substituting equations (3-1) and (3-2) in equation (3-3).

$$\Delta i_{Comp} = \frac{C_e}{2l_a} \frac{(V_{dc}/2 + V_{ac})^2}{B_0} \tag{3-4}$$

For the dead-time compensation method the lower limit that is set for the comparator value is considered to be B_0 minus the compensated value Δi_{comp}. Current waveform using this dead-time compensation method is shown in Figure 3-7.

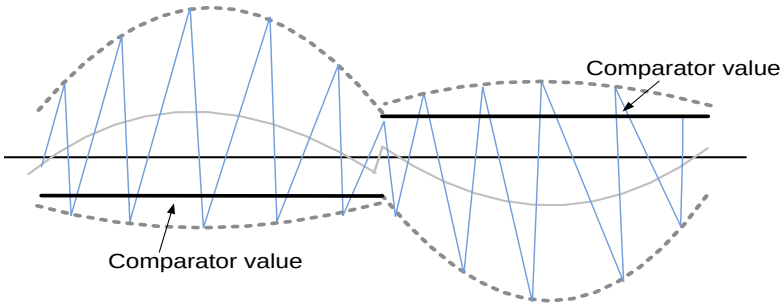

Figure 3-6: Dead-time effect on the inductor current before implementing the dead-time compensation scheme

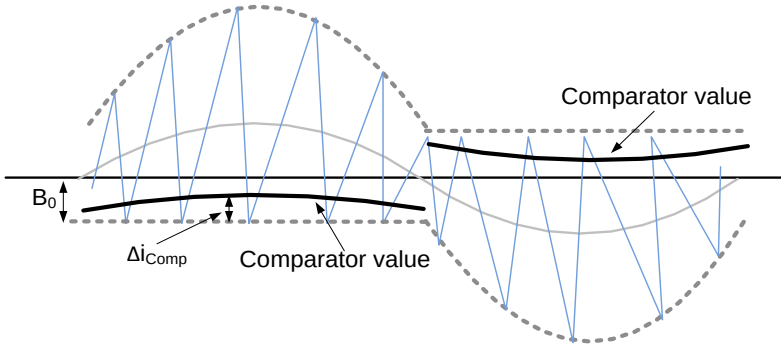

Figure 3-7: Inductor current after implementing dead-time compensation

3.4 Simulation Results

In order to verify the proposed hybrid current control with dead-time compensation technique, the simulation was carried out using LTspice simulation software. The key circuit parameters for this simulation are: DC Voltage-480V, AC grid voltage-208V, power rating-400W, switching frequency range-50-100kHz, filter inductor-200uH, filter capacitor-2uF, dead-time-800ns and Ce-500pf. Figure 3-8 shows the output and inductor current of the inverter with hybrid BCM current control without using any dead-time compensation techniques. The inductor current does not have the desired shape (hardware reset part of the inductor current is not flat and it goes beyond the boundaries) and output current THD is 4.1%. Output and inductor current of hybrid BCM current control with the proposed dead-time compensation method is shown in Figure 3-9. The output current THD with the proposed method decreases to 1.8%.

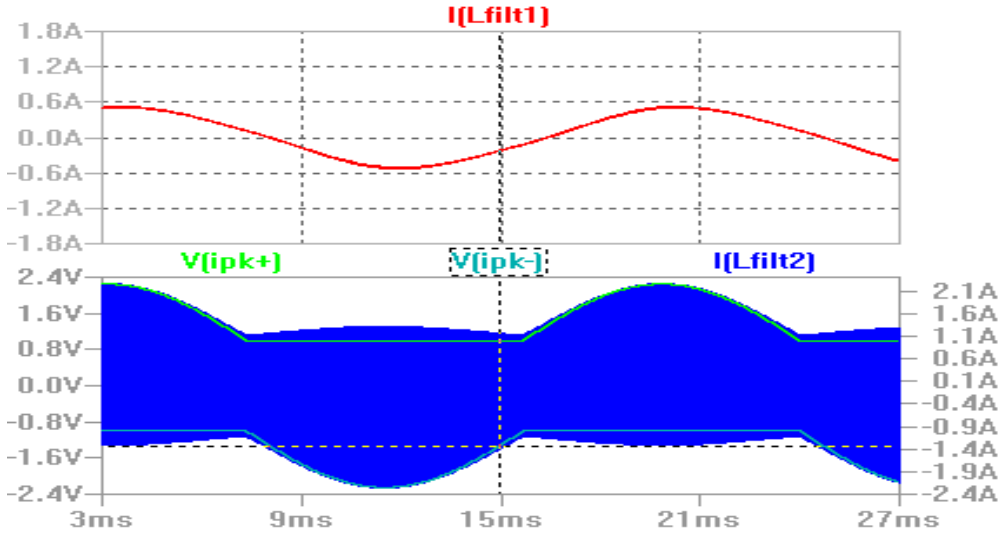

Figure 3-8: Output and inductor current waveforms of hybrid BCM current control without dead-time compensation, Output current THD is 4.1%

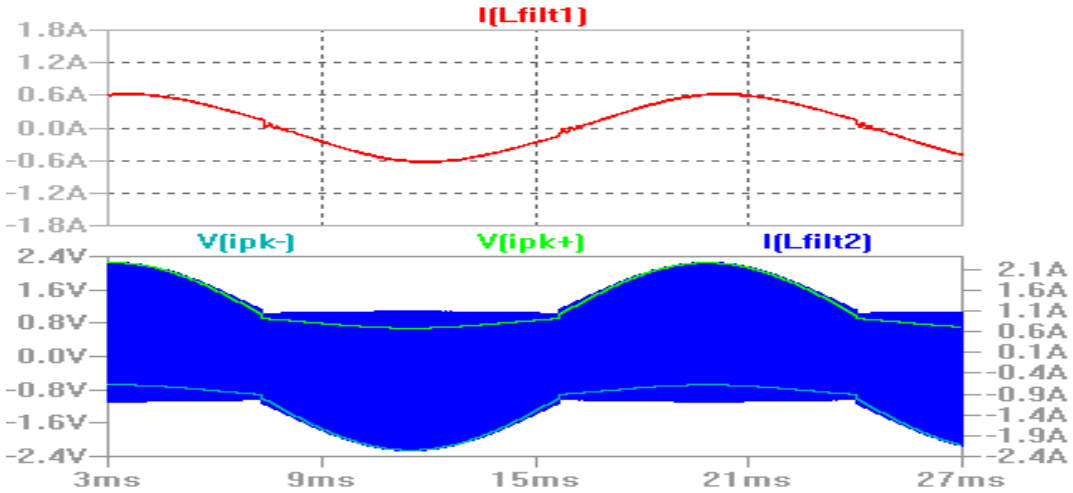

Figure 3-9: Output and inductor current waveforms of hybrid BCM current control with the proposed dead-time compensation method, Output current THD is 1.8%

3.5 Experimental Results

The proposed dead-time compensation technique is designed and implemented for a 400W three-phase micro-inverter with dsPIC33F from Microchip being used to execute the Hybrid BCM and dead-time compensation algorithms. The power MOSFET is FCB20N60. Parameters of the circuit system are set as below: Input: 480Vdc, Output: 208VAC RMS, Rated power: 400W, 60Hz; $L_a=L_b=L_c=200\mu H$, $R_{La}=R_{Lb}=R_{Lc}=0.2\Omega$, $C_a=C_b=C_c=2\mu F$. The current of PWM hardware reset and dead-time are set for B0=1A and 800n seconds respectively.

Figure 3-10 shows the output and inductor current waveforms without dead-time compensation for one phase of the three-phase micro-inverter with hybrid BCM current control. Current waveforms for different loads are shown in this figure. It can clearly be seen that the output current has significant zero crossing distortion.

Output and inductor current of the three-phase micro-inverter with dead-time compensation and for different loads is shown in Figure 3-11. Current waveforms in this figure have desired shape and the distortion has been reduced significantly compared to the state without implementing any dead-time compensation method. The output three-phase current is shown in Figure 3-12 and its THD is less than 2.5%.

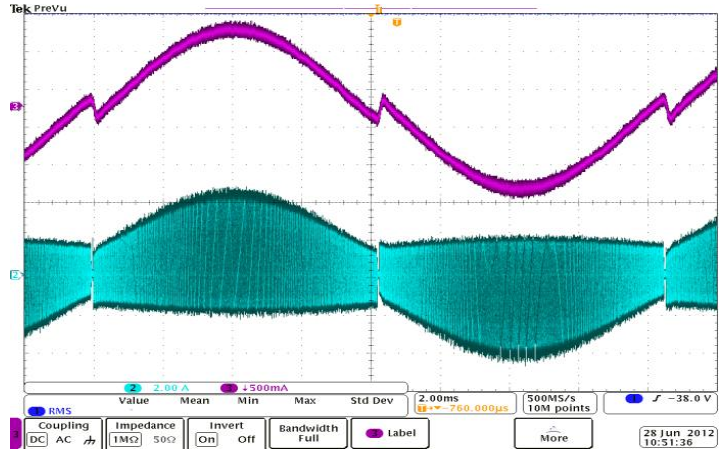

(a)

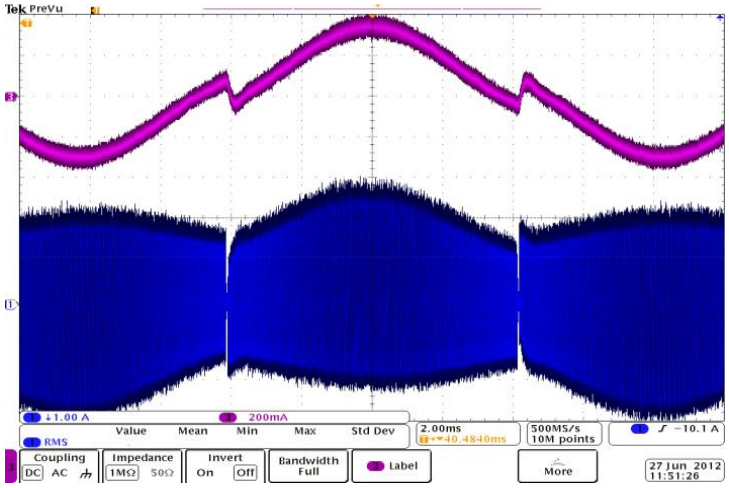

(b)

Figure 3-10: Output and inductor current of hybrid BCM current control without dead-time compensation, (a) 700mA output current, (b) 250mA output current

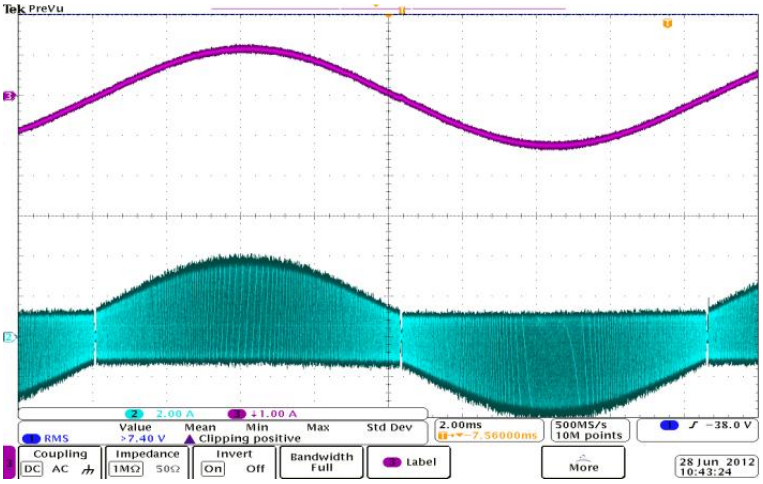

(a)

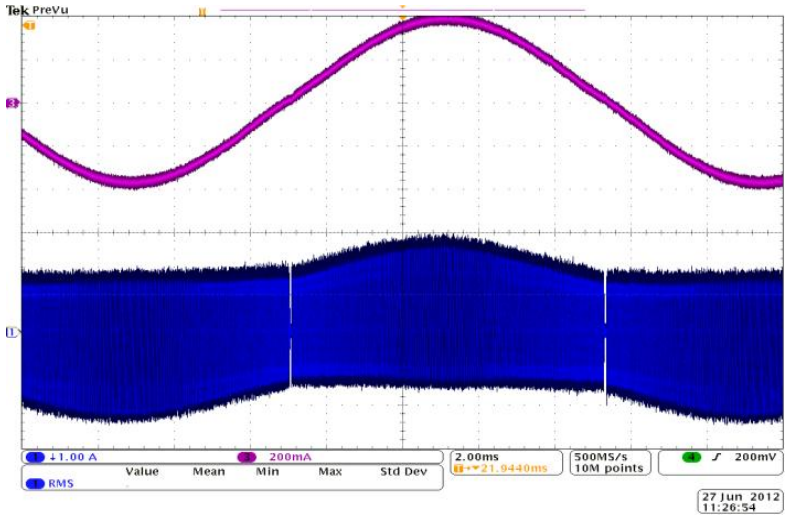

(b)

Figure 3-11: Output and inductor current of hybrid BCM current control with dead-time compensation, (a) 700mA output current, (b) 250mA output current

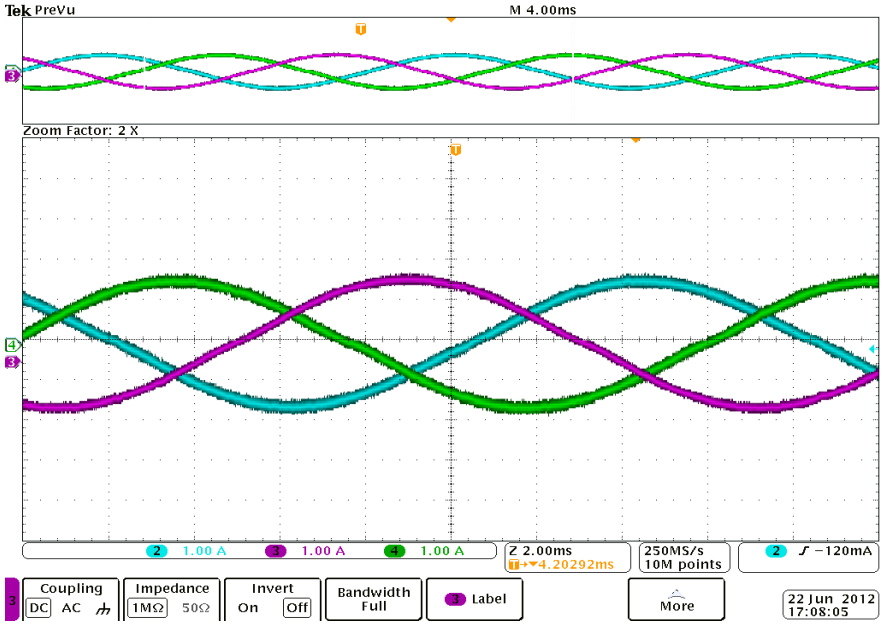

Figure 3-12: Output current of three-phase micro-inverter with hybrid BCM current control and dead-time compensation

3.6 Summary

This chapter proposed a dead-time compensation technique for hybrid BCM current control three-phase inverter to compensate for the zero crossing distortion and improve output current THD. Hybrid BCM current control performance was analyzed in details considering the effects of dead-time and output parasitic capacitance of the MOSFETs.

To prove the feasibility and effectiveness of the proposed dead-time compensation technique, the algorithm was implemented for a 400W three-phase micro-inverter with hybrid BCM current control. Experimental results indicate that using the proposed dead-time compensation method reduces zero crossing distortion to a great extent at different loads. THD measurement of the

output current shows an average 2% improvement by using the dead-time compensation algorithm.

The high efficiency of hybrid BCM control and low output current THD makes this current control method suitable for micro-inverter applications.

CHAPTER 4. CURRENT MODULATION SCHEMES FOR HYBRID BCM CURRENT CONTROL

4.1 Introduction

ZVS BCM current control is a promising soft switching technique for micro-inverter applications due to its high reliability, low cost, high power density, and high efficiency. The digital implementation of this soft switching approach has been verified in Chapter Two of this dissertation. In this chapter three different current modulation schemes will be introduced for this current control approach. They are referred to as Fixed Reverse Current Modulation (FRCM), Variable Reverse Current Modulation (VRCM), and Constant Bandwidth Current Modulation (CBCM). Break-down power loss analysis of these three current modulation schemes is presented and used in order to optimize the efficiency of the micro-inverter. This chapter also provides a detailed comparison of these three current modulation schemes with respect to the switching frequency range and output current quality.

Compared to continuous conduction mode (CCM) current control, BCM ZVS current control decreases MOSFET switching losses and filter inductor conduction losses but increases MOSFET conduction losses and inductor core losses. Based on the loss analysis of BCM ZVS current control a dual-mode current modulation scheme is proposed in the final part of this chapter to improve the efficiency of the micro-inverter. The proposed current modulation reduces the conduction loss and the current stress on the components with combining ZVS and zero current switching (ZCS) schemes. The experimental results verify that by implementing this

proposed current modulation scheme 0.5 percent higher efficiency can be achieved with no additional cost for a 400W three-phase micro-inverter [63].

4.2 Fixed Reverse Current Modulation Scheme

Implementation of the ZVS BCM current control requires setting the upper and lower boundaries (limits) of the inductor current. Depending on the boundary shape of the current limits, different current modulation schemes for achieving ZVS operation can be derived. They can have some advantages over each other, but designing a current modulation scheme for hybrid BCM current control can be considered as a multi objective optimization. The main goal of designing a current modulation scheme for the micro-inverter is efficiency optimization, but other characteristics such as the output current quality, switching frequency and current stress on the components are also important.

Boundary of fixed reverse current modulation for one cycle of the reference current is shown in Figure 4-1. For the positive half cycle the upper limit is set to ensure that the average current during each switching cycle is equal to the reference current whereas the lower boundary is set to ensure that the reverse current is sufficient to discharge the output capacitor of the MOSFETs and achieve ZVS operation. During the negative half cycle the situation is opposite and the upper boundary ensures the soft switching and the lower boundary is calculated from the reference current.

Upper and lower limits of fixed reverse current modulation are calculated from equation (4-1). In this equation B_0 is the reverse current required to achieve zero voltage switching and iref sin(ωt) is the reference current.

$$\begin{cases} i_{upper} = 2i_{ref}\sin(\omega t) + B_0 \\ i_{lower} = -B_0 \end{cases} \quad if\ i_{ref}\sin(wt) \geq 0$$
$$\begin{cases} i_{upper} = B_0 \\ i_{lower} = 2i_{ref}\sin(\omega t) - B_0 \end{cases} \quad if\ i_{ref}\sin(wt) < 0 \qquad (4\text{-}1)$$

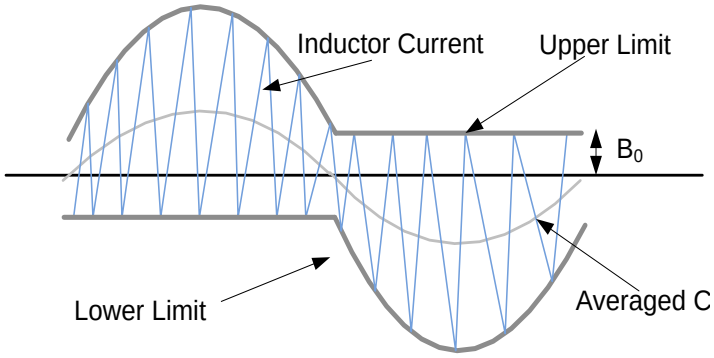

Figure 4-1: Fixed reverse current modulation

Switching Frequency

Figure 4-2 shows the switching frequency and load range variation for fixed reverse current modulation. Wide switching frequency range and high change in the switching frequency versus load are the characteristic of this current modulation. Figure 4-2 illustrates that switching frequency changes from 20KHz to 180KHz during a half cycle of output current for the full load condition. Maximum switching frequency is always fixed and does not change with load

variations, while minimum switching frequency increases from 20KHz to 40KHz from full load to light load conditions.

Since the micro-inverter output LC filter and the EMI filter are designed for full load condition, changing the switching frequency range slightly will not be an issue due to broadband performance of these filters.

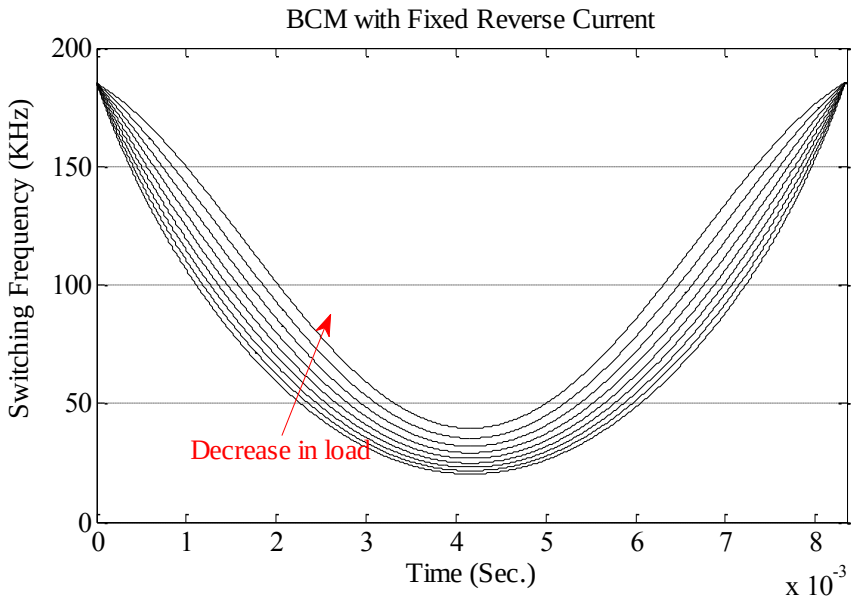

Figure 4-2: Switching frequency and load range variation of fixed reverse current modulation for the half cycle of output current

Power loss break-down

In order to have a comparative power loss analysis of different current modulations presented in this chapter, all the design parameters are considered to be the same. The maximum difference between upper and lower limits in all the current modulations is considered to be 5A and the full

load reference current is defined as 1.1A. The lowest reverse current over the half cycle of inductor current is considered to be 1A, since this is the ZVS condition desired.

Figure 4-3 shows the calculated loss distribution of a 400W three-phase micro-inverter with fixed reverse current modulation scheme. This figure depicts the power losses under 100%, 50% and 10% rated output power of the micro-inverter. The break-down power losses consist of the conduction and turn-off switching losses of the MOSFETs, core and copper losses of the inductors, and anti-parallel diode losses. Increase in the micro-inverter output power does not make any significant change in the turn-off switching losses and core losses for this current modulation scheme, while MOSFETs and inductors conduction losses and anti-parallel diode losses are directly a function of load and by increasing micro-inverter output power they increase significantly.

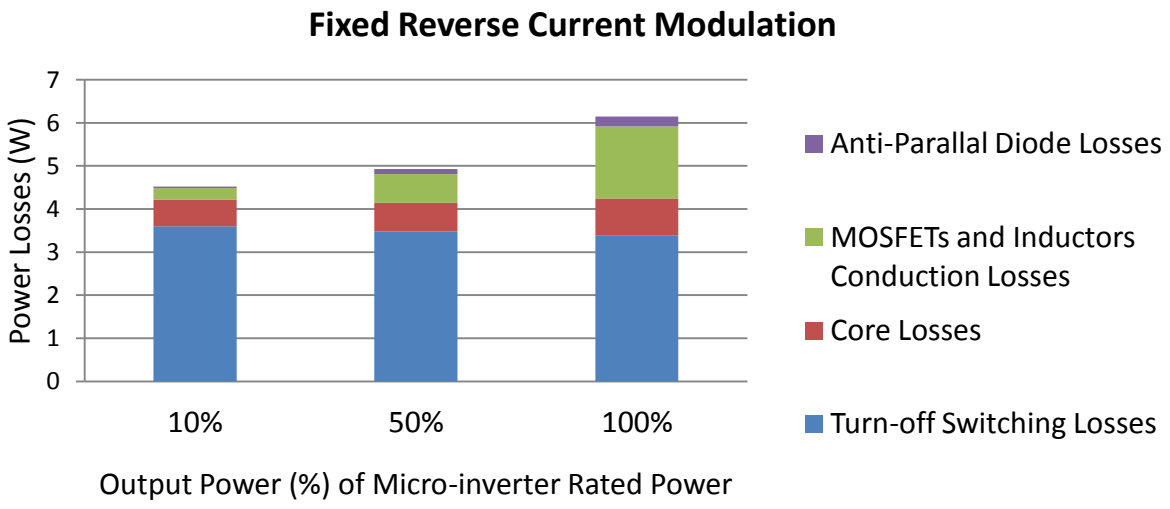

Figure 4-3: Power losses break-down for ZVS BCM current control with fixed reverse current modulation scheme at 10%, 50% and 100% of micro-inverter rated power

4.3 Variable Reverse Current Modulation Scheme

Upper and lower boundaries of variable reverse current modulation for one cycle of the reference current is shown in Figure 4-4. As can be seen in this figure the current reaches variable values in each switching cycle. The upper and lower limits for positive and negative half cycles can be expressed by equation (4-2). In this equation, B_0 is the maximum of reverse current and iref sin(ωt) is the reference current.

$$\begin{cases} i_{upper} = \frac{3}{2} i_{ref} \sin(\omega t) + B_0 \\ i_{lower} = \frac{1}{2} i_{ref} \sin(\omega t) - B_0 \end{cases} \quad if\ i_{ref} \sin(wt) \geq 0$$

$$\begin{cases} i_{upper} = \frac{1}{2} i_{ref} \sin(\omega t) + B_0 \\ i_{lower} = \frac{3}{2} i_{ref} \sin(\omega t) - B_0 \end{cases} \quad if\ i_{ref} \sin(wt) < 0 \qquad (4\text{-}2)$$

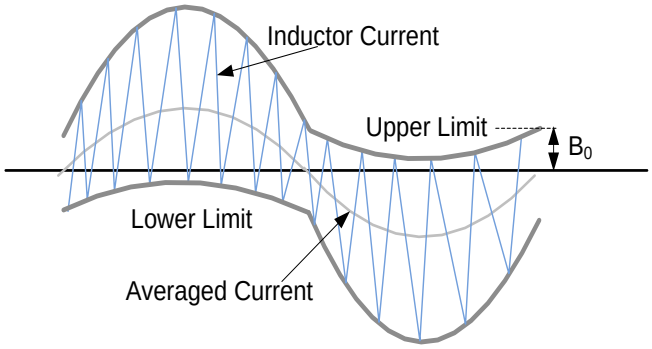

Figure 4-4: Variable reverse current modulation

Switching Frequency

The switching frequency and load range variation for variable reverse current modulation is shown in Figure 4-5. Switching frequency range is decreased compared to the fixed reverse current modulation. Switching frequency of this current modulation changes from 20KHz to 103KHz during a half cycle of output current for the full load condition. Change in the switching frequency versus load is also smaller compared to the fixed reverse current modulation. Maximum switching frequency is always fixed and does not change with load variations, while minimum switching frequency increases from 20KHz to 27KHz from full load to light load conditions.

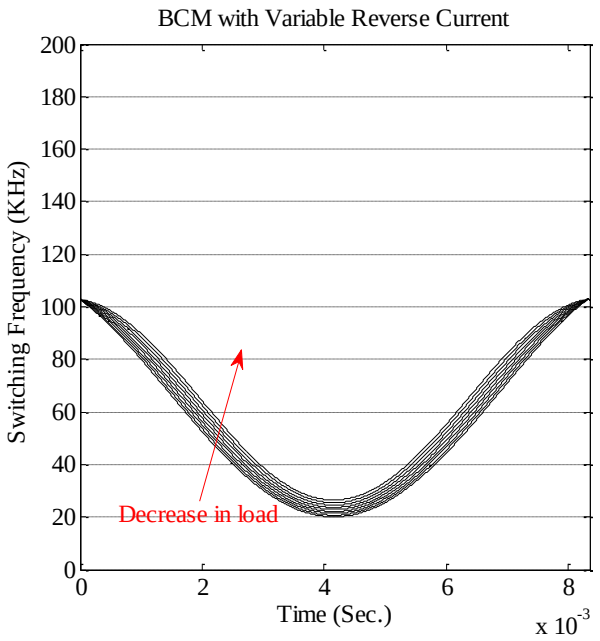

Figure 4-5: Switching frequency and load range variation of variable reverse current modulation for the half cycle of output current

Power loss break-down

Figure 4-6 shows the calculated loss distribution of a 400W three-phase micro-inverter with variable reverse current modulation scheme. This figure depicts the power losses under 100%, 50% and 10% rated power of the micro-inverter. The break-down power losses consist of the conduction and turn-off switching losses of the MOSFETs, core and copper losses of the inductors, and anti-parallel diode losses. Compared to the fixed reverse current modulation scheme, power losses increase on average by 15% for variable reverse current modulation. For this current modulation as shown in Figure 4-6 by increase in the load all four sources of power dissipation show higher values.

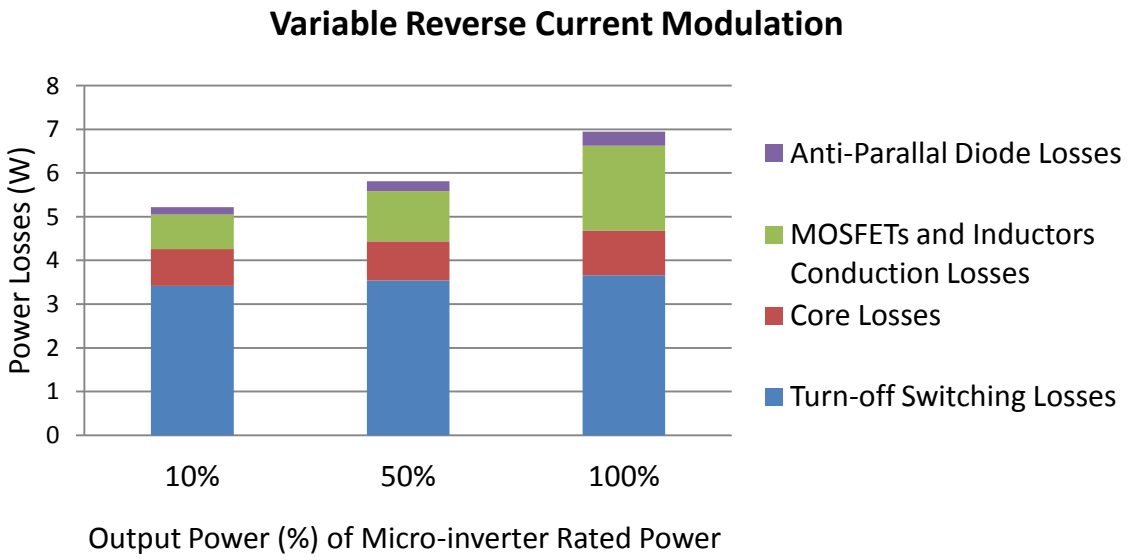

Figure 4-6: Power losses break-down for ZVS BCM current control with variable reverse current modulation scheme at 10%, 50% and 100% of micro-inverter rated power

4.4 Fixed Bandwidth Current Modulation Scheme

Upper and lower boundaries can be found from equation (4-3) for the fixed bandwidth current modulation scheme. In this equation, B_0 is the maximum of the reverse current and iref sin(ωt) is the reference current. Boundaries of this current modulation are shown in Figure 4-7 for one cycle of the reference current.

$$\begin{cases} i_{upper} = i_{ref} \sin(\omega t) + B_0 \\ i_{lower} = i_{ref} \sin(\omega t) - B_0 \end{cases} \quad (4\text{-}3)$$

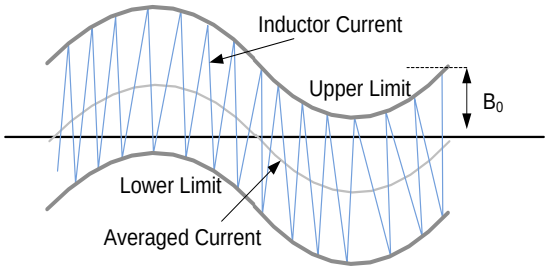

Figure 4-7: Fixed bandwidth current modulation

Switching Frequency

The switching frequency and load range variation for fixed bandwidth current modulation is shown in Figure 4-8. BCM with fixed bandwidth current modulation has the narrowest switching frequency range compared to the fixed reverse and variable reverse current modulation schemes. Switching frequency of this current modulation changes from 20KHz to 72KHz during a half

cycle of output current. This current modulation scheme also exhibits no change in the switching frequency versus load.

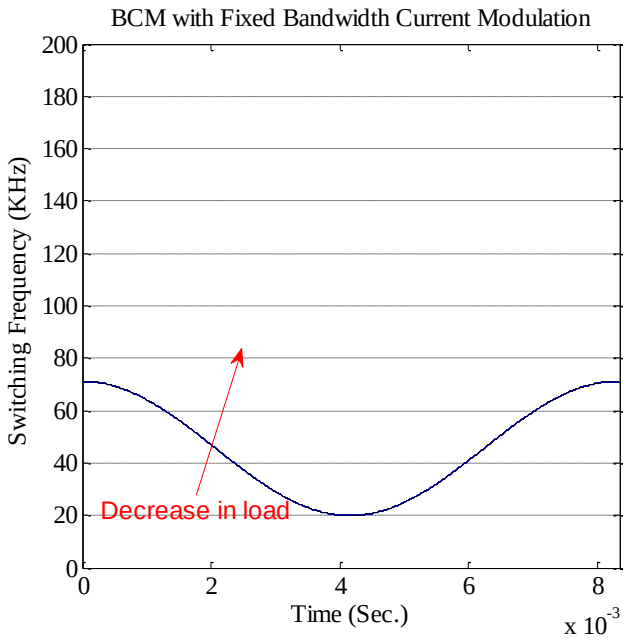

Figure 4-8: Switching frequency and load range variation of fixed bandwidth current modulation scheme for the half cycle of output current

Power loss break-down

The calculated loss distribution of a 400W three-phase micro-inverter with fixed bandwidth current modulation scheme is shown in Figure 4-9. This figure demonstrates the power losses under 100%, 50% and 10% rated power of the micro-inverter. The break-down power losses consist of the conduction and turn-off switching losses of the MOSFETs, core and copper losses of the inductors, and anti-parallel diode losses. Compared to the fixed reverse current modulation scheme, power losses increase on average by 40% for light load and 20% for full load.

Compared to the reverse current modulation scheme, power losses increase on average by 25% for light load and 8% for full load. Fixed bandwidth current modulation has higher power losses compared to the other modulation schemes extensively under light load conditions.

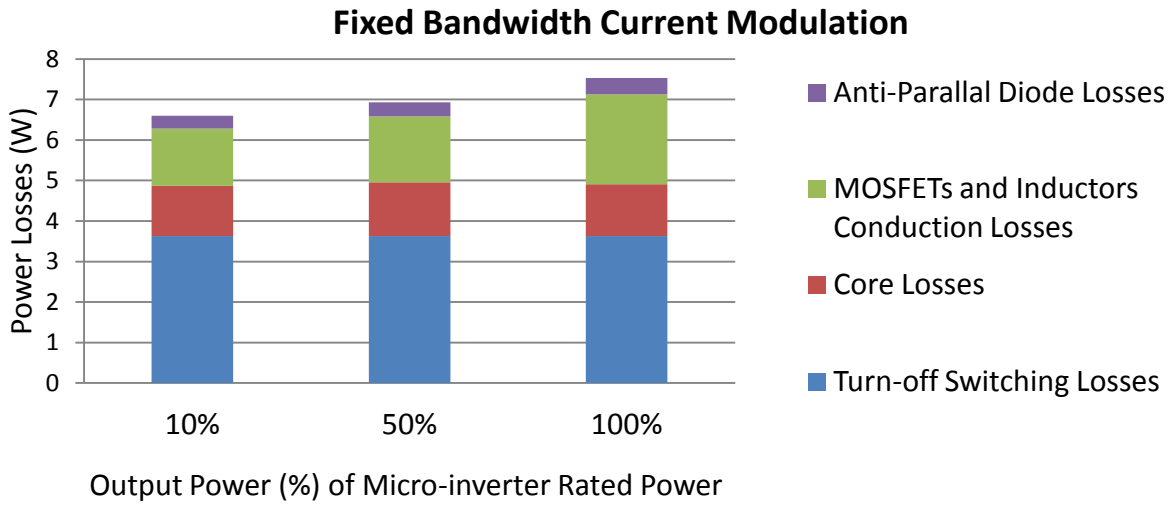

Figure 4-9: Power losses break-down for ZVS BCM current control with fixed bandwidth current modulation scheme at 10%, 50% and 100% of micro-inverter rated power

4.5 Dual Mode ZVS ZCS Current Modulation Scheme

In order to further improve the efficiency and reduce the current stress on the power components, a dual-mode ZVS ZCS current modulation scheme is proposed. In this current modulation scheme switching between ZVS and ZCS operation is used during each line half cycle. Using ZVS around the line zero crossing point reduces the switching frequency and switching losses. Using ZCS at the peak of the current during each line half cycle reduces the high frequency RMS current thus reducing conduction losses. The proposed current modulation scheme is shown in

Figure 4-10. The idea here is to combine the ZVS and ZCS BCM current modulation schemes alternatively according to the different value of the current during each line half cycle so that the dominant losses can be optimized and higher efficiency is achieved.

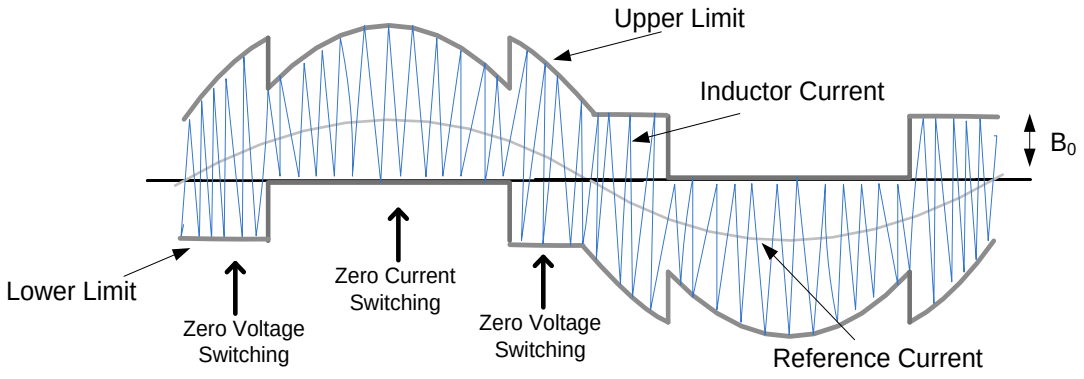

Figure 4-10: Dual mode ZVS ZCS current modulation scheme

The upper and lower boundaries of the dual mode ZVS ZCS current modulation scheme are calculated using equation (4-4).

$$\begin{cases} i_{upper} = 2i_{ref}\sin(\omega t) + B_0 \\ i_{lower} = -B_0 \end{cases} \quad if\ (\sin(wt) \geq 0\ \&\ \sin(wt) \leq I_B)$$
$$\begin{cases} i_{upper} = 2i_{ref}\sin(\omega t) \\ i_{lower} = 0 \end{cases} \quad if\ (\sin(wt) \geq 0\ \&\ \sin(wt) > I_B)$$
$$\begin{cases} i_{upper} = B_0 \\ i_{lower} = 2i_{ref}\sin(\omega t) - B_0 \end{cases} \quad if\ (\sin(wt) < 0\ \&\ \sin(wt) \geq -I_B) \qquad (4\text{-}4)$$
$$\begin{cases} i_{upper} = 0 \\ i_{lower} = 2i_{ref}\sin(\omega t) \end{cases} \quad if\ (\sin(wt) < 0\ \&\ \sin(wt) < -I_B)$$

Where i_{ref} sin(ωt) is the reference current and B_0 is the reverse current required to achieve ZVS. In equation (4-4) the boundary point between the ZVS and ZCS operation modes is defined based on the sin(ωt) and I_B. More details about I_B selection is given in the next part of this chapter.

4.6 Variable Boundary Dual Mode Current Modulation Scheme

In equation (4-4) the boundary point between the ZVS and ZCS operation has been defined based on the sin(ωt) and I_B. Sin(ωt) is generated using the PLL algorithm inside the three-phase micro-inverter program. I_B is considered to be a function of the reference current. The basic idea here is to have a variable boundary between the ZVS and ZCS operations to further improve the efficiency of BCM ZVS current control. As shown in Figure 4-11 decreasing the reference current (i_{ref}) will move this boundary point toward the peak of the current during a line half cycle and it will reduce the maximum of the switching frequency range and therefore switching losses at light loads. Increasing the reference current (i_{ref}) will move this boundary point toward the zero crossing of the reference current and it will reduce the conduction losses further at heavier loads [64]. Figure 4-12 shows the boundary point between ZVS and ZCS operations at heavy load.

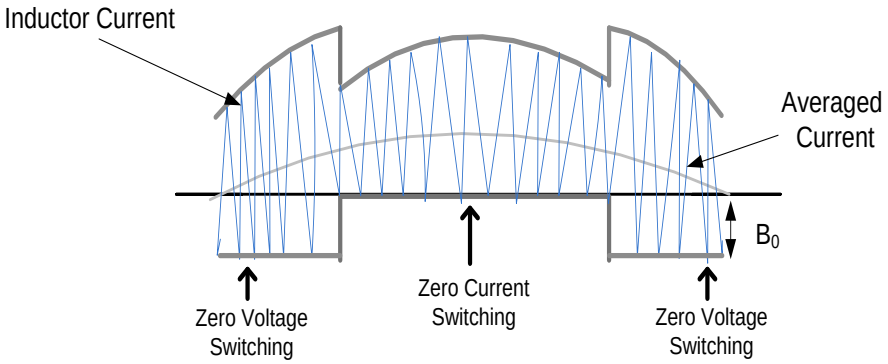

Figure 4-11: Lower reference current moves the ZVS and ZCS boundary point toward the peak of the reference current

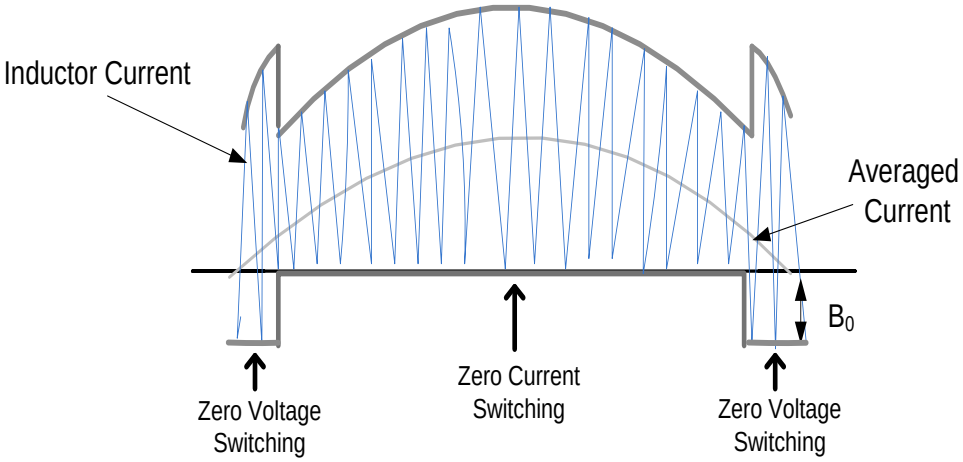

Figure 4-12: Higher reference current moves the ZVS and ZCS boundary point toward the zero crossing of the reference current

I_B is defined using equation (4-5). A simple optimization was conducted to determine the value of α and β in order to minimize the RMS value of the inductor current while maximum switching frequency is considered as a design constraint.

$$I_B = \alpha - I_{ref} \times \beta \tag{4-5}$$

Figure 4-13 shows the variable boundary dual mode current modulation scheme implementation.

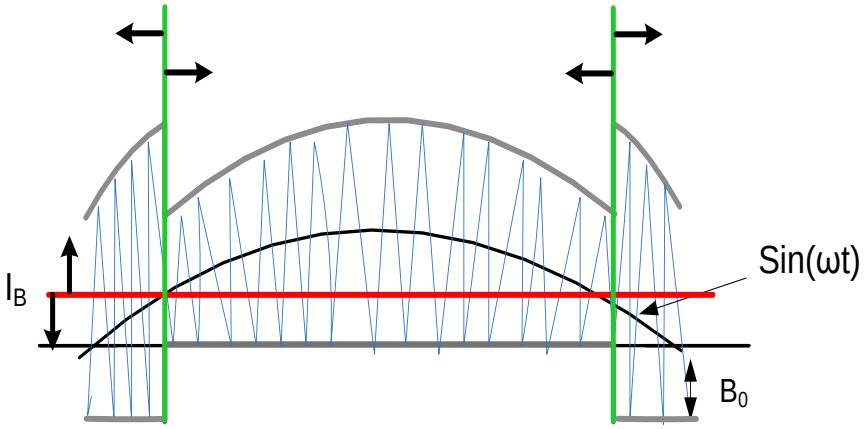

Figure 4-13: Variable boundary point between ZVS and ZCS operations

Switching Frequency and RMS Value of Inductor Current

Figure 4-14 shows the switching frequency and load range variation for dual mode current modulation with fixed boundary point between ZVS and ZCS operations. In order to keep the maximum of switching frequency range less than 200KHz under different load conditions, the boundary point is considered to be close to the peak of the reference current during a line half cycle. The RMS value (High frequency and 60 Hz) of inductor current for this current modulation scheme versus output current variation is shown in Figure 4-16. As seen in this figure this current modulation compared to the fixed reverse current modulation scheme can reduce the RMS value of inductor current and therefore the conduction and core losses.

Switching frequency and load range variation for dual mode current modulation with variable boundary point between the ZVS and ZCS operations is shown in Figure 4-15. As shown in

Figure 4-16 the RMS value of inductor current can be reduced considerably using the variable boundary point dual mode current modulation scheme.

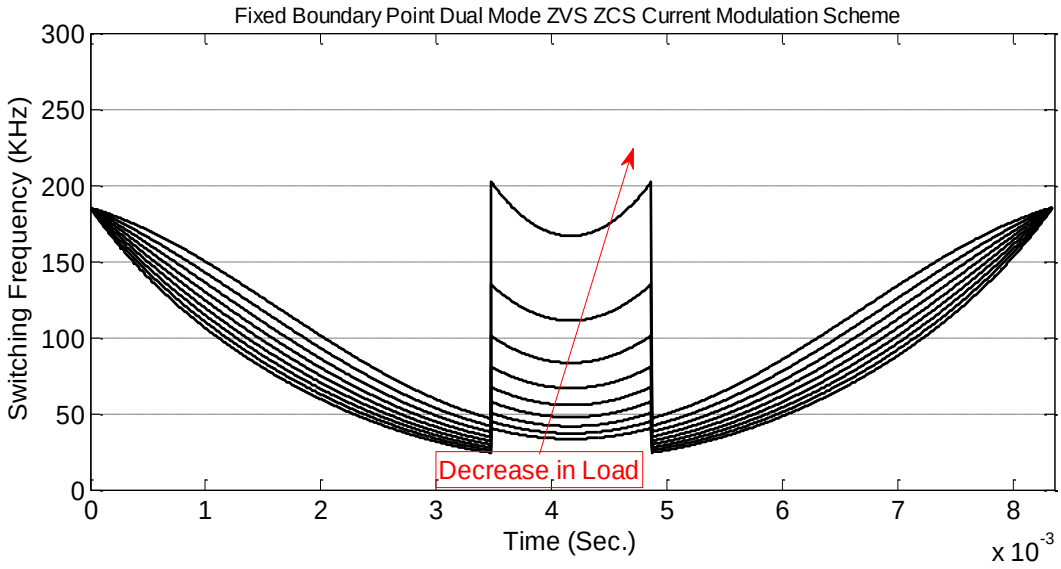

Figure 4-14: Switching frequency and load range variation of dual mode current modulation scheme for the half cycle of output current, fixed ZVS ZCS boundary point, load variation from 100% to 10%

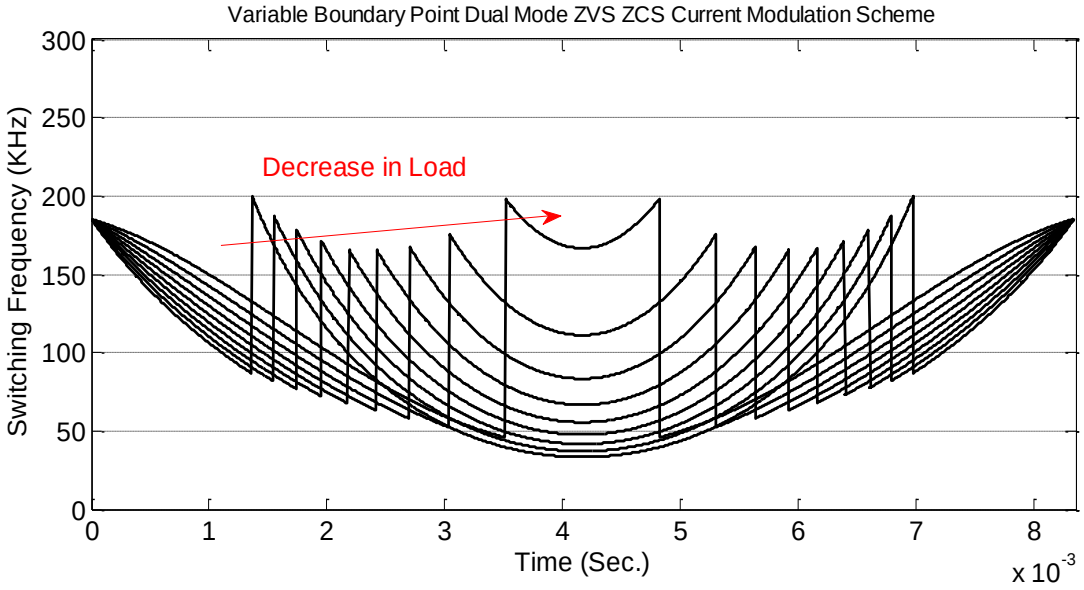

Figure 4-15: Switching frequency and load range variation of dual mode current modulation scheme for the half cycle of output current, variable ZVS ZCS boundary point, load variation from 100% to 10%

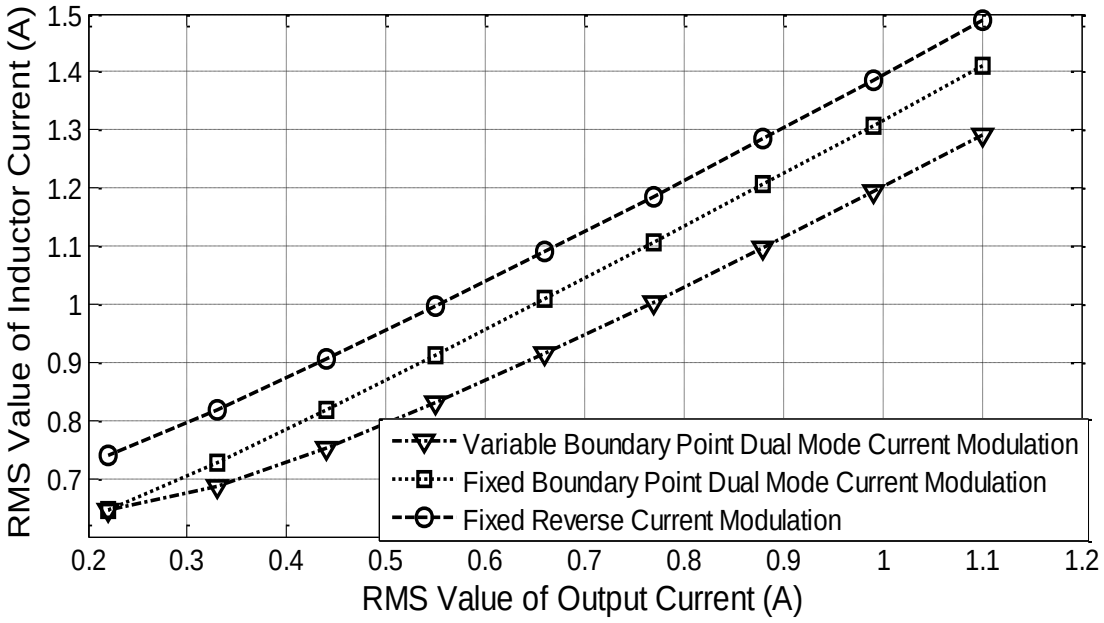

Figure 4-16: RMS value of inductor current (RMS value of high frequency and 60 Hz) versus RMS value of output current

Power loss break-down

Figure 4-17 shows the calculated loss distribution of a 400W three-phase micro-inverter with dual mode ZVS ZCS current modulation scheme. This figure demonstrates the power losses under 100%, 50% and 10% rated power of the three-phase micro-inverter. The break-down power losses consist of the conduction and turn-off switching losses of the MOSFETs, core and copper losses of the inductors, and anti-parallel diode losses. Compared to the three previously studied current modulation schemes power losses decrease significantly over full range of load variations.

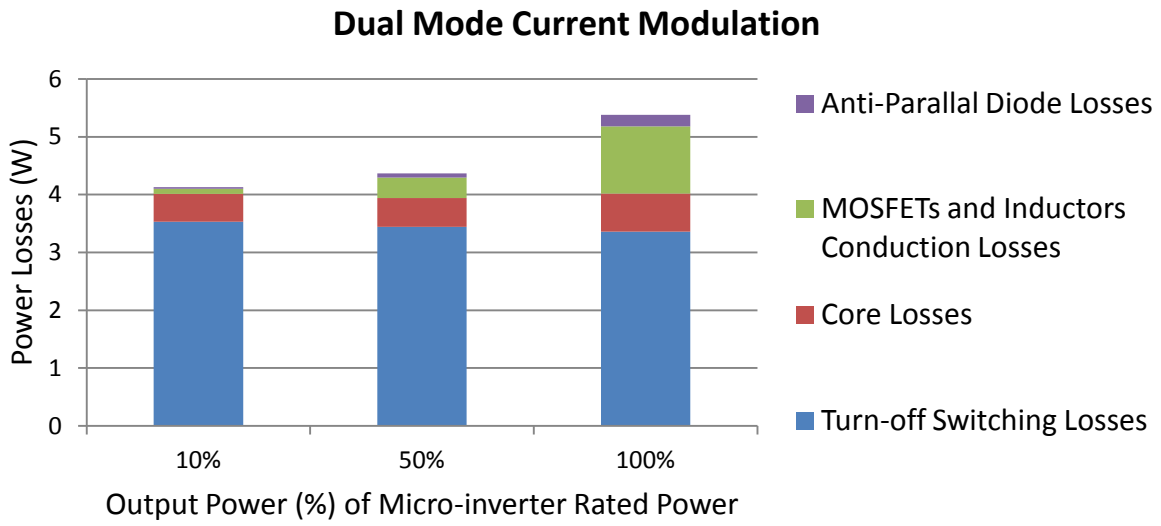

Figure 4-17: Power losses break-down for ZVS BCM current control with dual mode current modulation scheme at 10%, 50% and 100% of micro-inverter rated power

4.7 BCM ZVS Current Modulation Schemes Comparison

In order to fairly compare the four different current modulation methods in this part, all of the micro-inverter parameters are considered to be the same. The lowest reverse current over a line half cycle is set to 1A in ZVS BCM operation, since this is the desired ZVS condition.

The switching frequency range comparison of different current modulation schemes at micro-inverter rated power is shown in Figure 4-18. This figure depicts the switching frequency variation during each half cycle of line frequency. Constant Bandwidth current modulation scheme exhibits the narrowest switching frequency range. The proposed dual mode current modulation scheme reduces the switching frequency range compared to that in the fixed reverse current modulation.

Power loss comparison of different current modulation schemes for a 400W three-phase micro-inverter is given in Figure 4-19. This figure presents the comparison for 10%, 50% and 100% load. The three-phase micro-inverter power losses can be reduced significantly under different load conditions using the proposed dual mode ZVS ZCS current modulation scheme.

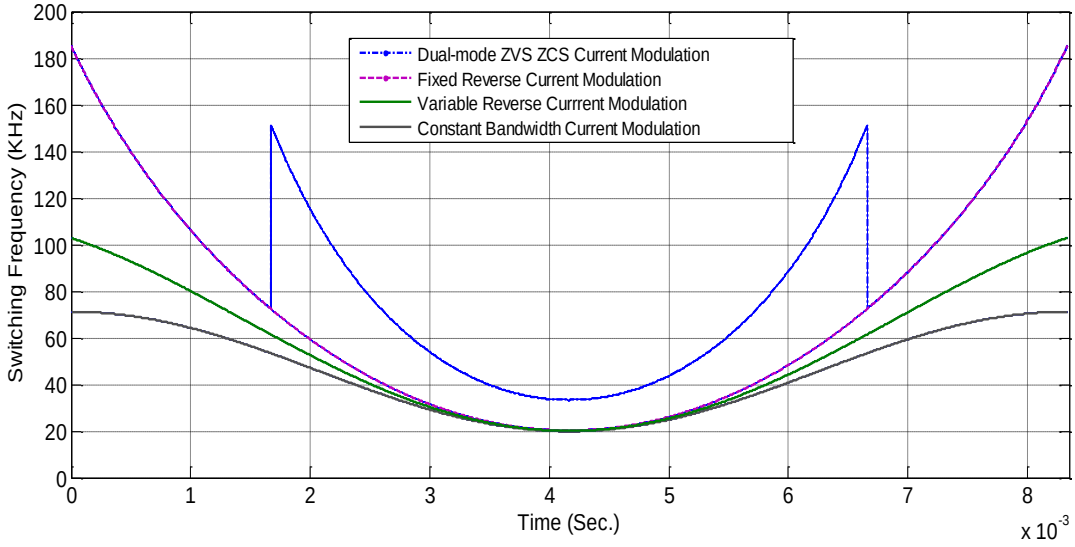

Figure 4-18: Switching frequency variation of four different current modulation schemes for half cycle of line frequency at rated power of micro-inverter

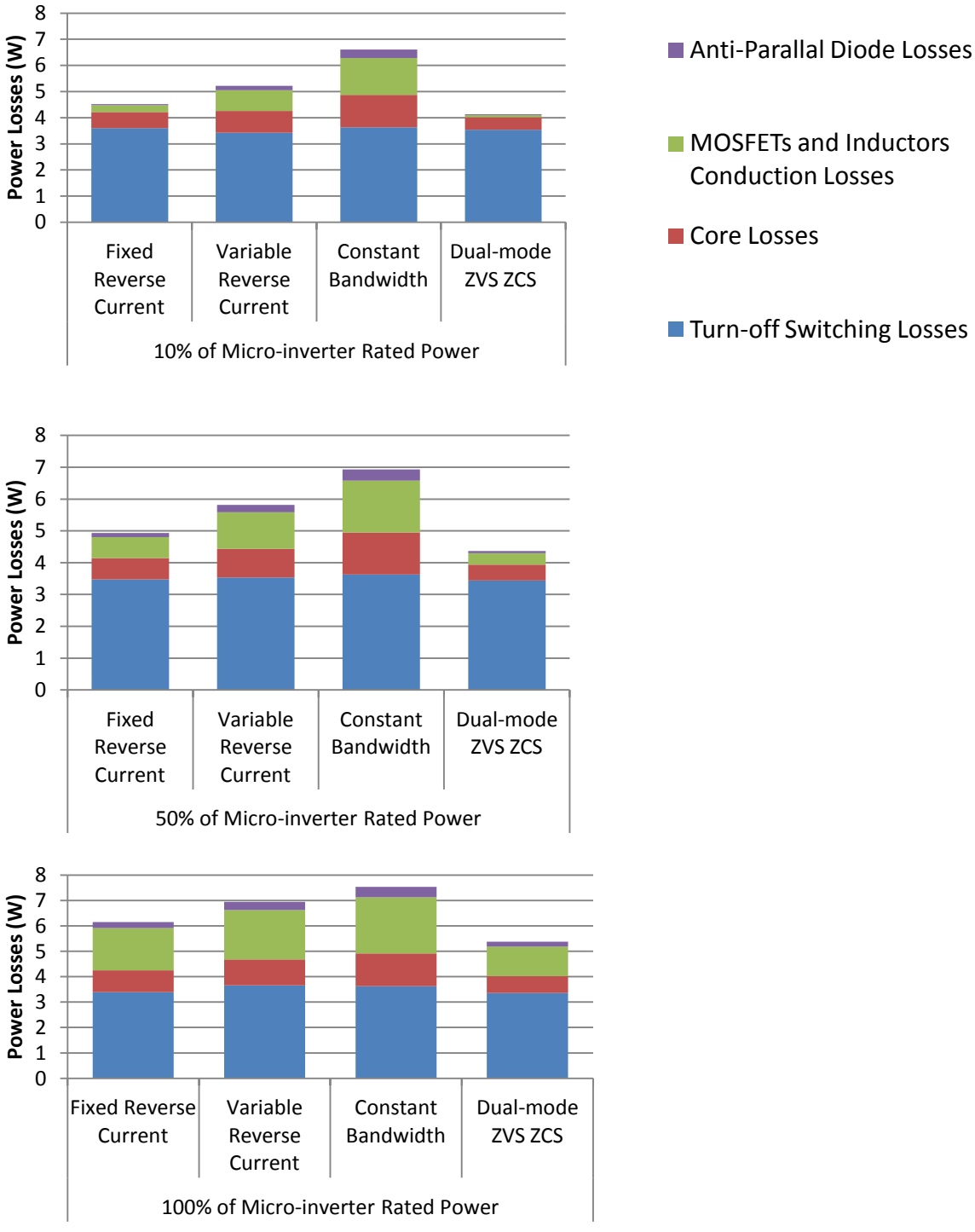

Figure 4-19: Power losses comparison of different ZVS BCM current modulation schemes at 10%, 50% and 100% of micro-inverter rated power

4.8 Comparative Experimental Results

To experimentally compare different current modulation schemes and to prove the merits of the proposed dual mode current modulation method a 400W three-phase micro-inverter prototype was designed and built. The inverter specifications are as follows: input voltage: Vdc=400V; Grid voltage: Vac=208V; Grid frequency: F=60Hz; and the major components used in the power stage are as follows: inductor filter: La=270uH; capacitor filter: 1uF. The MOSFET is selected as FCB20N60. The BCM ZVS controller and different current modulation methods are conducted by a microchip DSP dsPIC33F.

Experimental results of three-phase micro-inverter with different current modulation schemes are shown in Figure 4-20 to Figure 4-23. Figure 4-20 shows the three-phase inductor current of dual mode ZVS ZCS current modulation scheme. Inductor current of fixed reverse current modulation scheme is shown in Figure 4-21. Figure 4-22 depicts the variable reverse current modulation scheme. Three-phase inductor current of fixed bandwidth current modulation scheme is shown in Figure 4-23.

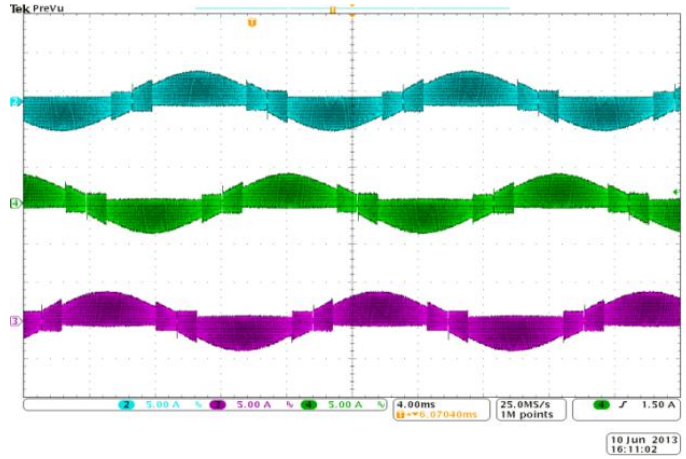

Figure 4-20: Dual mode ZVS ZCS current modulation scheme, inductor current

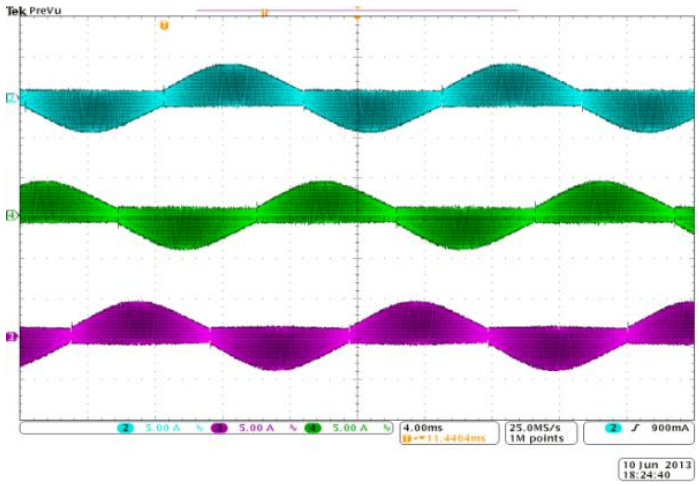

Figure 4-21: Fixed reverse current modulation scheme, inductor current

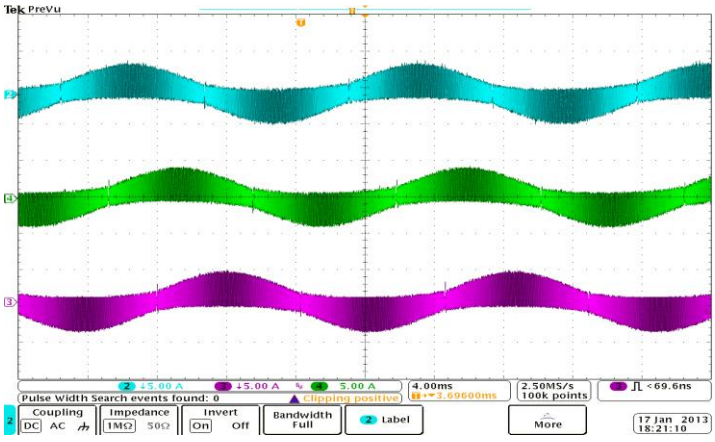

Figure 4-22: Variable reverse current modulation scheme, inductor current

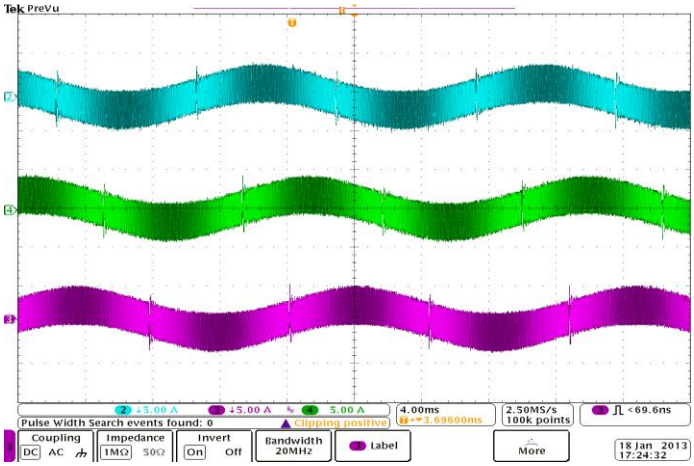

Figure 4-23: Fixed bandwidth current modulation scheme, inductor current

Inductor current and output current of one phase of a three-phase micro-inverter with dual mode current modulation method is shown in Figure 4-24. The output current THD is less than 2.5% and meets the IEEE 1547 and UL 1741, 5% THD requirements. Three-phase output current of the micro-inverter with dual mode current modulation method is shown in Figure 4-25.

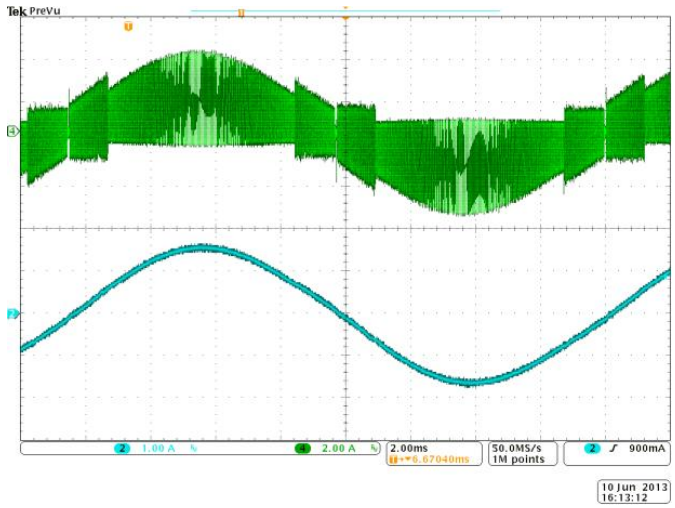

Figure 4-24: Inductor current and output current of one phase of three-phase micro-inverter with dual mode current modulation scheme

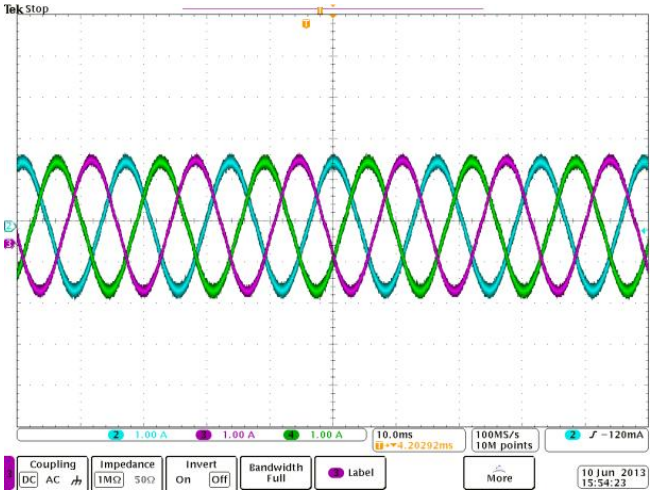

Figure 4-25: Three-phase output current of micro-inverter with dual mode current modulation scheme

Comparison of the inductor current RMS value and output current THD of different current modulation schemes is given in Table 4-1. The RMS value in this table includes both high frequency and 60 Hz current components. Please notice that the inductor current RMS value of dual mode ZVS ZCS current modulation scheme is considerably less than the other three current modulation schemes. This leads to reduction in conduction losses and thus, higher efficiency of micro- inverter can be achieved.

Table 4-1: Inductor Current RMS Value and Output Current THD Comparison of Different Current Modulation Schemes

	dual mode Current Modulation	Fixed Reverse Current Modulation	Variable Reverse Current Modulation	Fixed Bandwidth Current Modulation
THD (%)	2.5%	2.5%	1.6%	0.7%
Inductor Current (RMS value)	1.33A	1.52A	1.68A	1.81A

Efficiency of a 400W three-phase micro-inverter with different current modulation schemes was measured experimentally and is shown in Figure 4-26. Using dual mode current modulation scheme, higher efficiency can be achieved without any additional cost. All the efficiency measurements have been conducted using a Yokogawa PZ4000 power analyzer. The efficiency curves in Figure 4-26 do not include auxiliary circuit power consumption.

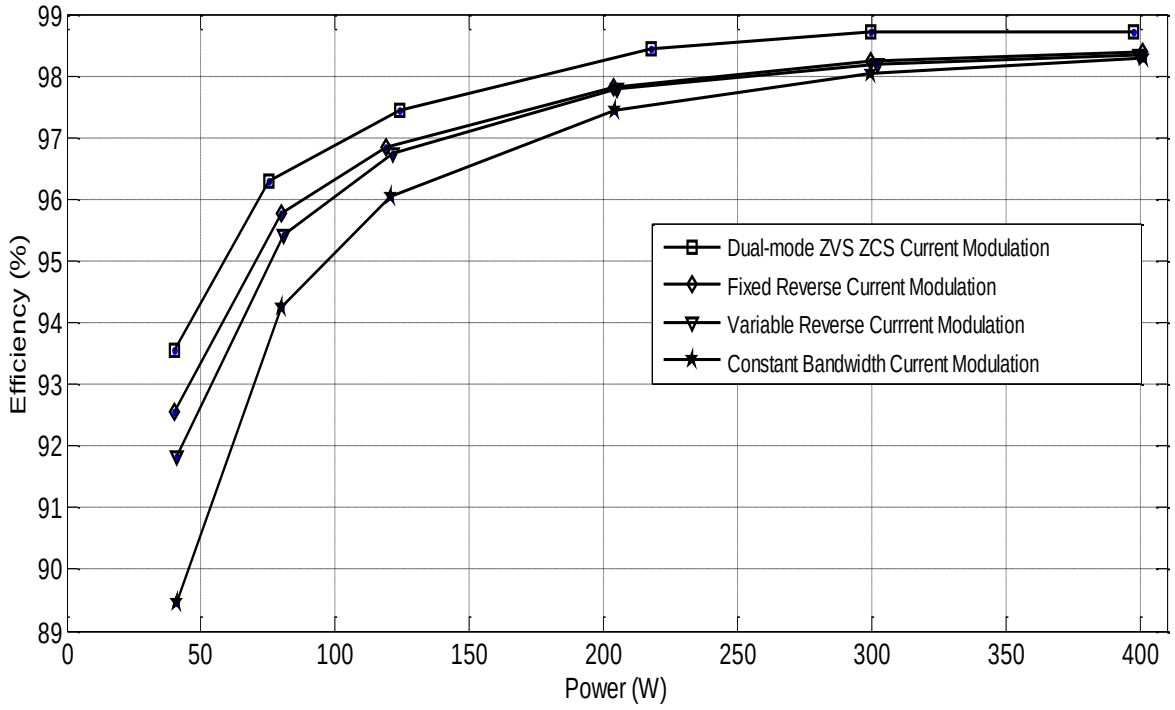

Figure 4-26: Three-phase micro-inverter efficiency versus output power for different current modulation schemes

4.9 Summary

Three different current modulation schemes of BCM ZVS current control three-phase micro-inverter were studied analytically. A comparative analysis of power loss distribution, efficiency, switching frequency, and output current THD was presented in this chapter. It was observed that BCM with fixed reverse current modulation scheme has the highest efficiency and output current THD. BCM with fixed bandwidth current modulation scheme has the lowest efficiency and output current THD and it also has the narrowest switching frequency range.

In order to further improve the efficiency of fixed reverse current modulation scheme and reduce the current stress on the components a new dual mode ZVS ZCS current modulation scheme was proposed. This current modulation scheme improves the efficiency of the micro-inverter by reducing the RMS value of the inductor current resulting in reduction of conduction and core losses.

To prove the efficiency improvement using dual mode current modulation scheme, a 400W three-phase micro-inverter was designed and tested. The comparative experimental results for all different current modulation schemes were presented in this chapter and the advantages of the dual mode current modulation scheme were validated. It was observed that using this current modulation scheme, higher efficiency of 0.5 percentage point for a 400W three-phase micro-inverter can be achieved with no additional cost.

CHAPTER 5. THREE-PHASE MICRO-INVERTER LIGHT LOAD EFFICIENCY ENHANCEMENT: PHASE SKIPPING CONTROL

5.1 Introduction

Efficiency improvement of micro-inverters plays a significant role in gaining economical benefits, higher power density, and reliability [65],[66]. Due to the intermittent feature of the PV generation, it is impossible for micro-inverter to always operate at its rated power. It usually operates at light or half load conditions [67], [68]. Therefore, European and CEC weighted-efficiency are mostly used to evaluate overall efficiency of these devices [69], [70].

Soft switching techniques can be employed to maintain a high conversion efficiency and low EMI. ZVS BCM current control proposed in Chapter Two is an interesting soft switching candidate for micro-inverter applications due to its low cost, high power density, and high efficiency. Different current modulation schemes of this control approach and their loss analysis were presented in Chapter Four. Although they can enhance the efficiency of the three-phase micro-inverter, they still suffer from light load efficiency drop.

This chapter presents a method of maintaining high power-conversion efficiency across the entire load range of a three-phase micro-inverter. The proposed method guarantees a flatter conversion efficiency curve at light load for the PV system [71].

5.2 Three-phase Micro-Inverter Light Load Efficiency Drop

Typically, a power converter has higher efficiency at heavier loads and poorer efficiency at lighter loads [72]. The power losses in a converter can be broken down into two main components; load dependent losses which vary directly as a function of load current and load independent losses which remain constant regardless of the value of load current [73],[74]. Losses like conduction losses in power semiconductor devices, conduction losses in body diode and inductor copper losses fall under the category of load dependent losses whereas losses like switching losses and gate drive losses fall under the category of load independent losses [75],[76].

Figure 5-1 shows the calculated loss distribution of the 400W three-phase micro-inverter with fixed reverse current modulation scheme. This figure illustrates the power losses under different load conditions. The power losses break-down includes the conduction and turn-off switching loss of the MOSFETs, core and copper loss of the inductors, and anti-parallel diode losses.

It can be clearly seen in Figure 5-1 that turn-off switching losses and core losses of magnetic components are almost independent of the load. These fixed sources of power losses as shown in Figure 5-2 cause micro-inverter efficiency curve as a function of the load to exhibit a steep fall off at light loads.

In this chapter a new control method of reducing the variation of power conversion efficiency with fluctuations of the PV module's output power is presented.

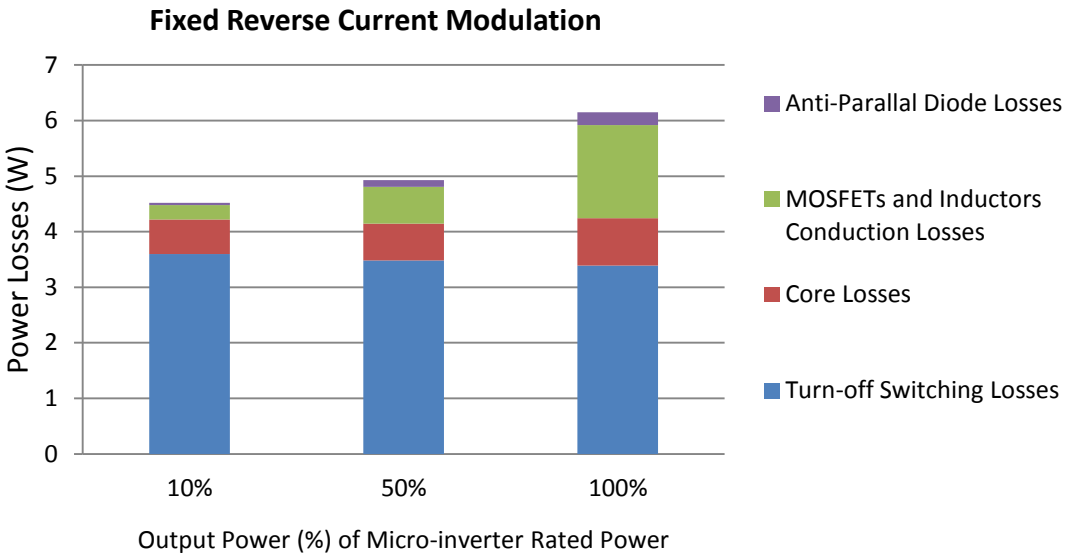

Figure 5-1: Power losses break-down for ZVS BCM current control three-phase micro-inverter at 10%, 50% and 100% of micro-inverter rated power

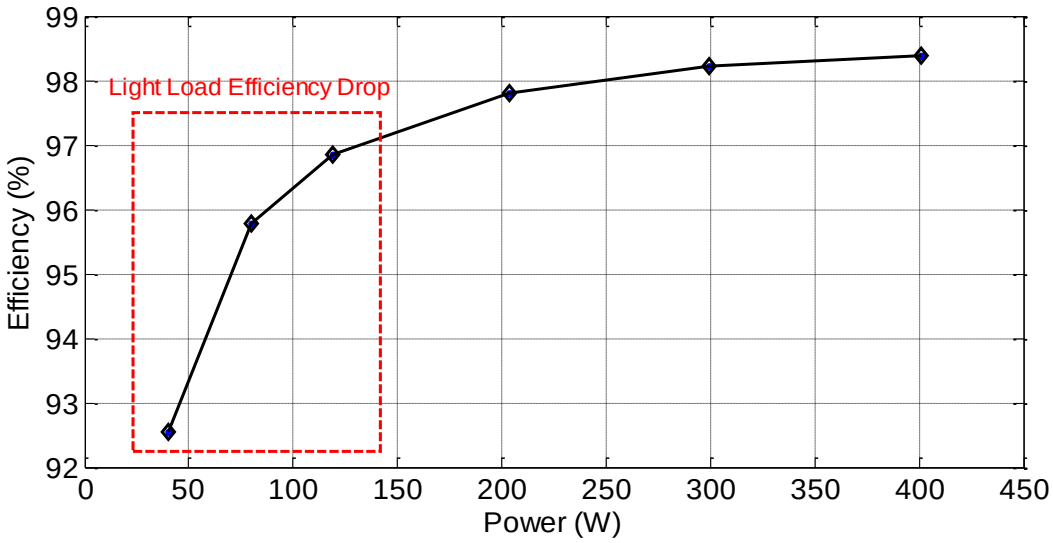

Figure 5-2: Light load efficiency drop of three-phase micro-inverter

5.3 Light Load Efficiency Enhancement: Phase Skipping Control

The proposed method of light-load efficiency optimization is based on a simple observation that the maximum efficiency occurs when each phase of the three-phase micro-inverter is operated close to full load.

Due to independent operation of each phase in the hybrid BCM current control micro-inverter, it is capable of disabling two phases at light loads thereby improving light load efficiency. Through a MPPT algorithm, available PV module's power can be determined. Once the available power falls below the preset light load point, two phases are turned off. Similarly, when available power increases above the light load point, the disabled phases will be enabled. Figure 5-3(a) shows a two-stage micro-inverter under normal operation and Figure 5-3(b) shows the two-stage micro-inverter under phase skipping control mode.

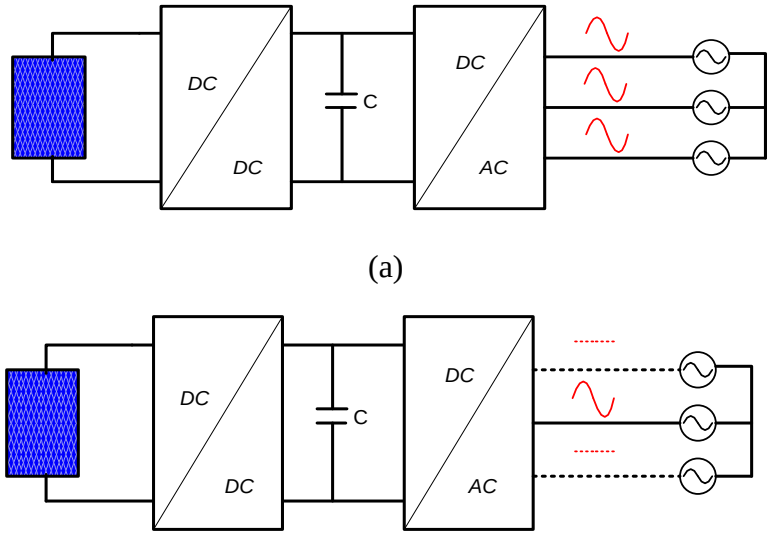

Figure 5-3: Light load efficiency enhancement for a two-stage three-phase micro-inverter, (a) normal operation, (b) phase skipping mode operation

The DC/AC stage part of the three-phase micro-inverter under normal and phase skipping control is shown in Figure 5-4.

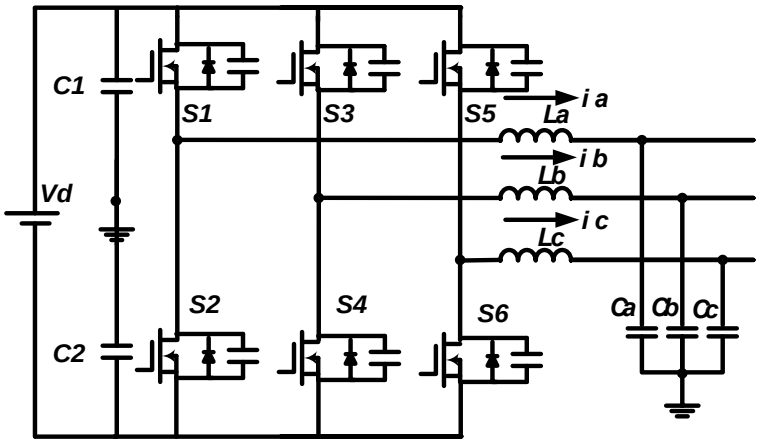

(a)

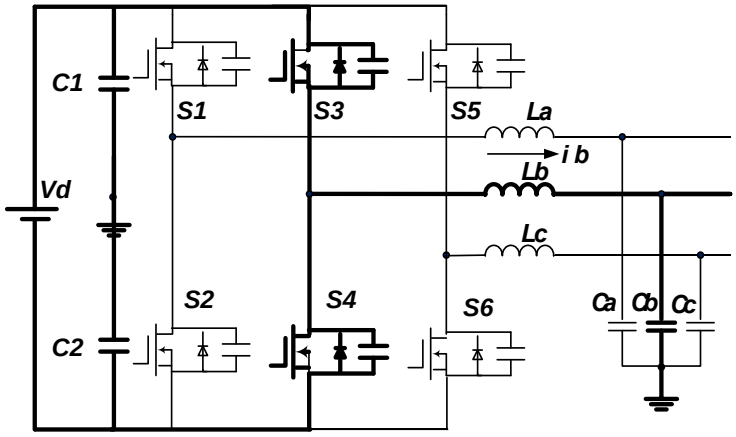

(b)

Figure 5-4: DC/AC stage of three-phase micro-inverter, (a) normal operation, (b) phase skipping mode

The idea here is to combine the advantages of three-phase systems and single-phase systems by employing phase skipping technology in order to optimize efficiency over a wide load range.

5.4 Size Calculation of DC-link Capacitor under Phase Skipping Control

The transition from three-phase to single-phase happens in power levels less than 30% of the rated power of the micro-inverter. At these low power levels the voltage transient response and steady state ripples of the DC link capacitor do not cause any over or under voltage problems. For a single phase micro-inverter the size of the decoupling capacitor can be determined using equation (5-1) knowing that the power into the DC link is constant and that the power drawn from the DC link follows a $\sin^2(\omega t)$ waveform.

$$C_{DC} = \frac{P_{DC}}{2 \cdot \omega \cdot U_{DC} \cdot \hat{u}_{DC}} \tag{5-1}$$

Where P_{DC} is the average DC link power, ω is the grid frequency, U_{DC} is the average DC link voltage and is the amplitude of the ripple voltage. The grid current cannot be controlled if the DC link voltage is lower than the peak grid voltage plus the voltage drop across the power semiconductor devices and output filter. Therefore, the minimum DC link voltage at 10% over-voltage in the grid for the micro-inverter is calculated as 375V. Considering that U_{DC} is 400V, DC link capacitor is calculated by equation (5-1) as 17µF at 130W.

Size calculation of the decoupling capacitor for the three-phase micro-inverter has been carried on in [77]. Considering grid voltage dips and surges, and disturbance response time it is determined as 35.3µF which meets the requirements of phase skipping operation mode.

5.5 DC/DC Stage of the Micro-Inverter

LLC topology has been chosen for the front-end DC/DC stage of the three-phase micro-inverter. This topology features both high efficiency and power density due to its natural zero voltage switching operation [78]. Considerable research has been done at Florida Power Electronics Center on the LLC topology, its modeling and optimization to accommodate the wide input voltage range of PV applications (The DC output voltage of the PV panels) while maintaining a high efficiency [79],[80], [81]. LLC resonant converter topology is shown in Figure 5-5.

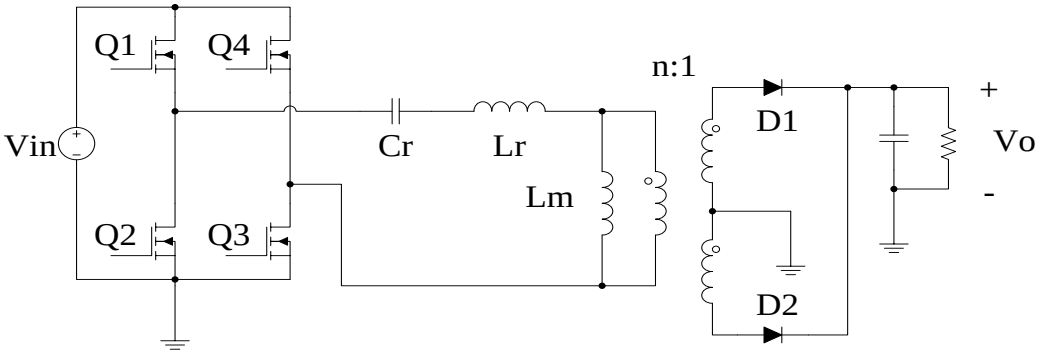

Figure 5-5: Front-end DC/DC stage of the three-phase micro-inverter; LLC resonant topology

5.6 Solar Farm Architecture based on Three-phase Micro-Inverter

The PV solar farm architecture based on three-phase micro-inverters is shown in Figure 5-6. In this architecture the outputs of each micro-inverter are directly connected to a low voltage three-phase grid and then through a medium voltage transformer to the high voltage at power

transmission line. Each micro-inverter operates independently regardless of failure of the other micro-inverters and carries out communication and MPPT functions.

Each micro-inverter comprises a node on a communication network and can exchange information with other micro-inverters on the network as well as a system level controller. This communication is an integral part of system maintenance and monitoring. ZigBee devices are often used in mesh network form to transmit data over longer distances, passing data through intermediate devices to reach more distant ones.

Each micro-inverter operates in normal control mode. Under light load conditions, it attempts to change its operating mode to phase skipping control but it is not allowed to until it finds two other micro-inverters in a similar state. After discovering each other, they build a three member cluster and then change their operating mode to phase skipping control simultaneously. Once they are in phase skipping mode, each one of them selects a unique phase. The idea here is to combine three different three-phase systems and create a new three-phase system out of three micro-inverters operating in single phase mode.

When one micro-inverter exits single phase operating mode, it commands the other two micro-inverters in its cluster to exit single phase mode regardless of their power output. It is important to remember that the default operating mode of each micro-inverter is three-phase at all power levels and that phase skipping is strictly a method of improving the efficiency at low power.

It should be noted that each micro-inverter of a cluster operates below 30% of its rated power. At this low power any difference at their output power causes negligible imbalance in the grid.

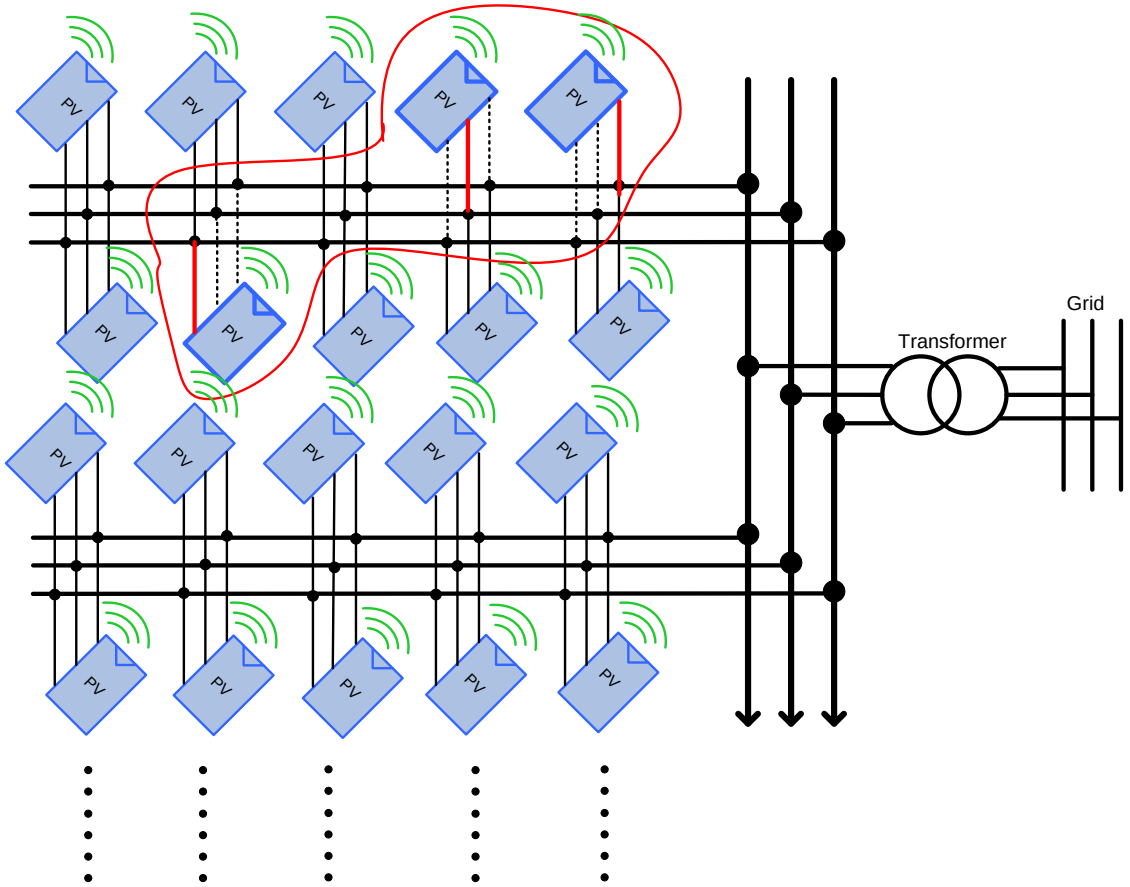

Figure 5-6: Solar farm architecture based on three-phase micro-inverter, three micro-inverters are operating in phase skipping mode

5.7 Experimental Results

To verify the light load efficiency enhancement using the proposed phase skipping control method a 400W three-phase micro-inverter prototype was built. The specifications are as follows: input voltage: Vdc=400V; Grid voltage: Vac=208V; Grid frequency: F=60Hz; and the major components used in the power stage are as follows: inductor filter: La=270uH; capacitor filter: 1uF; MOSFETs: FCB20N60. The controller was implemented using a microchip DSP dsPIC33F.

Figure 5-7 illustrates the three-phase output current of the micro-inverter under normal operation. The output power of the micro-inverter is 130W. Figure 5-8 shows the output of the three-phase micro-inverter with the same power under the phase skipping control. The output current THD is less than 2.5% and meets the industrial requirements.

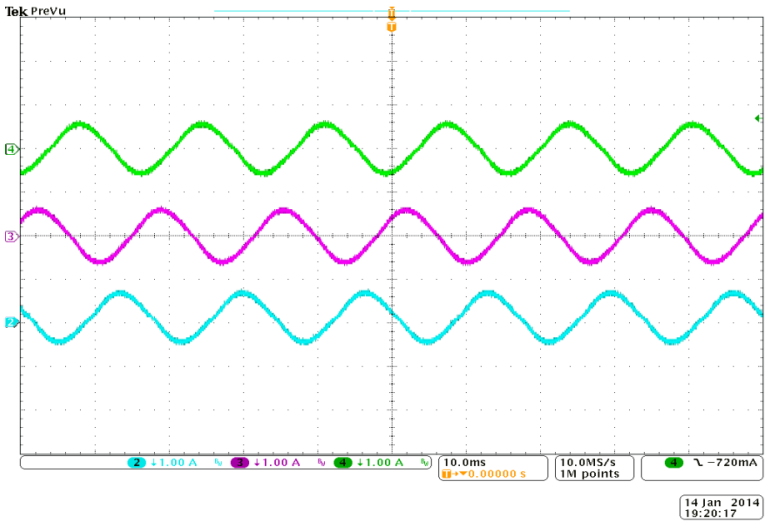

Figure 5-7: Output current of the three-phase micro-inverter under normal operation with 130W output power

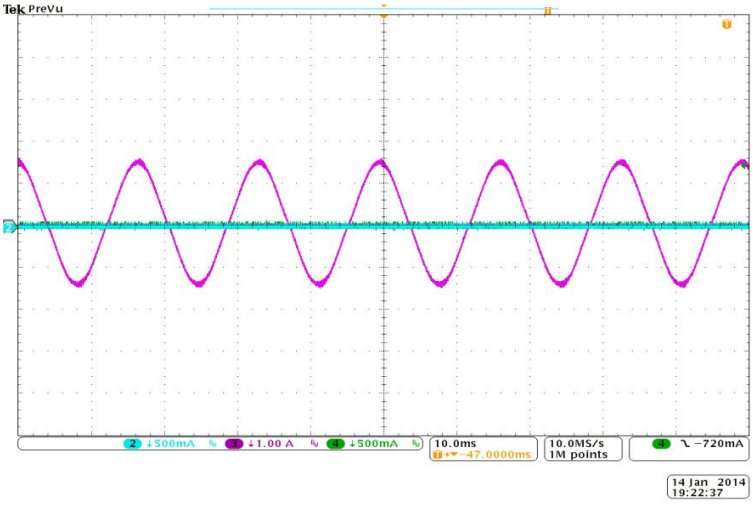

Figure 5-8: Output current of the three-phase micro-inverter under phase skipping mode with 130W output power

Transition from normal operation mode to phase skipping mode is given in Figure 5-9. Notice that the transition is very smooth and voltage ripple in the DC link capacitor meets the design requirements.

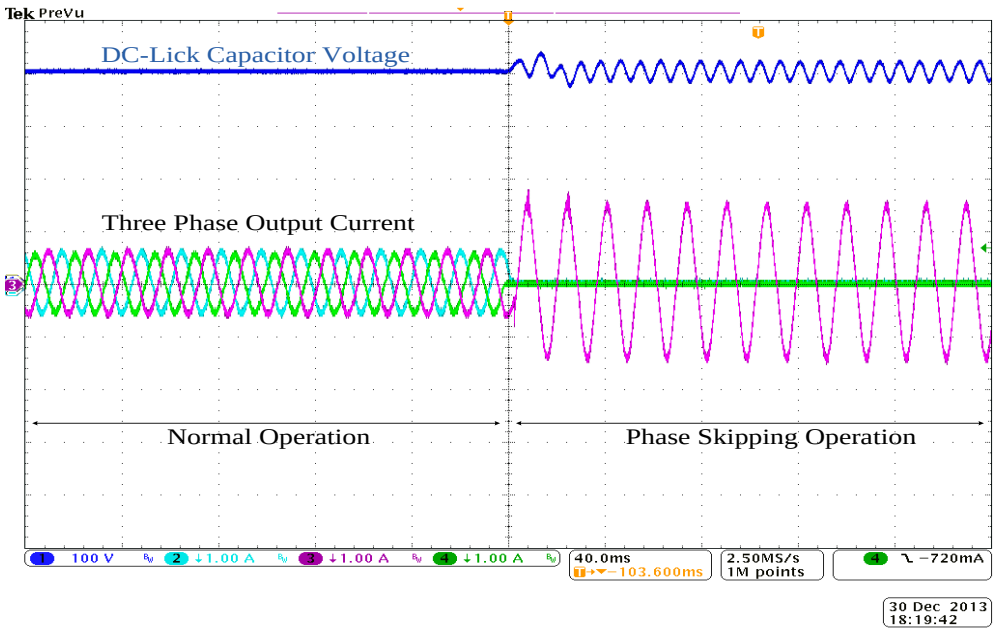

Figure 5-9: Transition from normal control mode to phase skipping control

Figure 5-10 shows a comparison of the three-phase micro-inverter DC/AC stage measured efficiency for original hybrid BCM current control and the one with phase skipping control. Figure 5-11 depicts the same comparison for total system (DC/DC and DC/AC stages) efficiency. Owing to phase skipping control, higher efficiency can be achieved at light load without additional cost. All the efficiency measurements were performed using a Yokogawa PZ4000 power analyzer. The measured efficiency does not include auxiliary circuit power consumption.

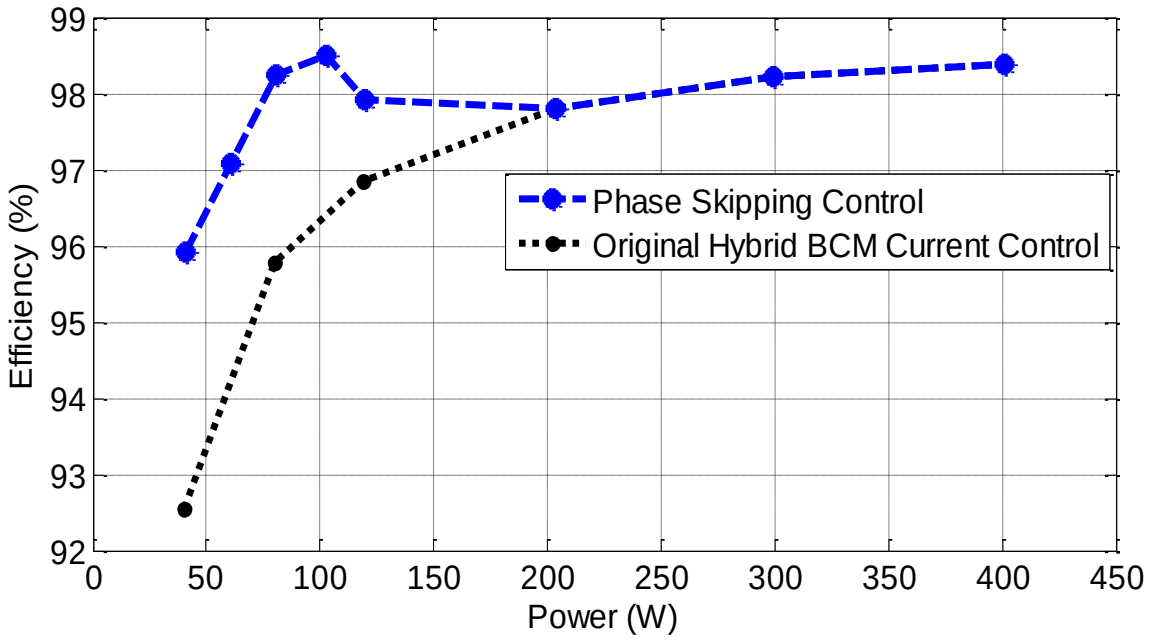

Figure 5-10: DC/AC stage efficiency versus output power

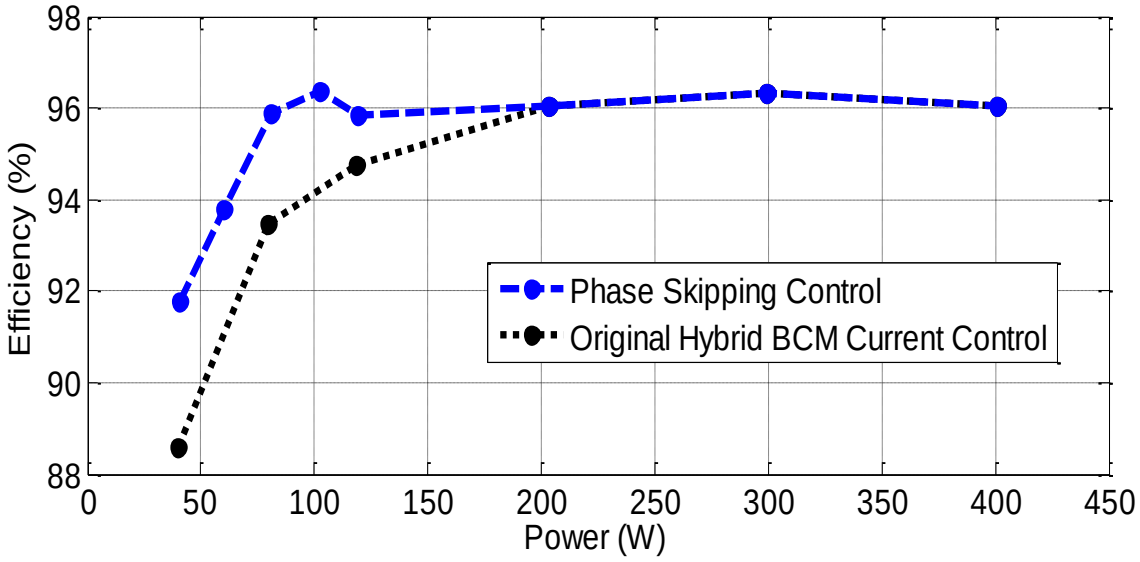

Figure 5-11: Total system efficiency versus output power

5.8 Summary

In this chapter, a new control strategy for efficiency enhancement of solar farms based on three-phase micro-inverter was proposed. Three-phase micro-inverters with the proposed control method have flat efficiency curve throughout all load range which contribute in increasing the CEC weighted efficiency. In phase skipping control, switching and driving losses of semiconductor devices, as well as core losses of magnetic components are minimized by turning off two phases of the three-phase micro-inverter.

To reduce the effect of phase skipping control on the utility grid, three three-phase micro-inverters under light load conditions create a new three-phase system with each micro-inverter feeding a different phase.

To prove the light load efficiency improvement using phase skipping control, a 400W three-phase micro-inverter was designed and tested. The comparative experimental results for normal and phase skipping operations were presented in this chapter and the advantages of the new control method were validated. The experimental results verified that with the phase skipping control method the efficiency is improved more than 2% under light-load condition.

CHAPTER 6. CONCLUSIONS AND FUTURE WORK

6.1 Conclusion

With energy demand constantly increasing, along with the need for clean energy sources, solar energy will certainly be an essential part of the future energy mix. In the field of solar energy the grid-tied PV micro-inverter structure has become more interesting due to its advantages such as enhanced reliability, safety, and energy production. Micro-inverters are small, compact, low-power modules with power level ranging from 150 to 400W directly attached to the back of the solar panels. Increasing the switching frequency may be the best way to reduce cost of the micro-inverter by shrinking the size of reactive components and heat-sinks. However, this approach could cause conversion efficiency to drop dramatically. To maintain high efficiency while increasing the switching frequency a new zero voltage switching method and its digital implementation have been proposed for the three-phase micro-inverter applications. The new hybrid control method is a combination of peak current control and predictive control and has the merits of low cost, high reliability, and high efficiency. Hybrid current control was implemented for the standard half bridge topology and it does not add to the component counts of the micro-inverter or complexity of the control circuit. The proposed current control method is suitable for low power inverter application where switching losses are dominant. By presenting experimental results the viability and advantages of the proposed soft switching micro-inverter was validated.

The performance of the proposed hybrid BCM current control was analyzed in detail considering the effects of dead-time and output parasitic capacitance of the MOSFETs. A dead-time compensation technique for the hybrid current controlled three-phase micro-inverter was presented in Chapter Three. The proposed method compensates for zero crossing distortion and improves the output current THD. Experimental results indicate that using the proposed dead-time compensation method reduces the zero-crossing distortion to a great extent at different loads. THD measurement of the three-phase micro-inverter output current shows an average 2% improvement by using the dead-time compensation algorithm. The high efficiency of hybrid BCM current control and low output current THD makes this current control method suitable for micro-inverter applications.

In Chapter Four three different current modulation schemes of BCM ZVS current controlled three-phase micro-inverter were studied analytically. A comparative analysis of power loss distribution, efficiency, switching frequency, and output current THD was presented in this chapter. It was observed that BCM with fixed reverse current modulation scheme has the highest efficiency and output current THD. BCM with fixed bandwidth current modulation scheme has the lowest efficiency and output current THD and it also has the narrowest switching frequency range. In order to further improve the efficiency of the fixed reverse current modulation scheme and reduce the current stress on the components a new dual mode ZVS ZCS current modulation scheme was proposed. This current modulation scheme improves the efficiency of the micro-inverter by reducing the RMS value of the inductor current resulting in reduction of conduction and core losses. The comparative experimental results for all different current modulation schemes were presented in Chapter Four.

It is impossible for a micro-inverter to always operate at its rated power due to the intermittent feature of the PV generation. Usually, it operates at light or half load conditions. Considerable research has been conducted on soft switching control method and different current modulation schemes to improve the efficiency of the micro-inverter in Chapters Two and Four. Although they can enhance the efficiency of the micro-inverter, they still suffer from poor light load efficiency. In Chapter Five a new control method of reducing the variation of power conversion efficiency with fluctuations of the PV module's output power was presented. A three-phase micro-inverter employing the proposed control method has a flat efficiency curve throughout its entire load range which improves its CEC weighted efficiency. In phase skipping control, switching losses of semiconductor devices, as well as core losses of magnetic components are minimized by disabling two of the three phases. To reduce the effect of phase skipping control on the utility grid, three three-phase micro-inverters under light load conditions are combined to create a new three-phase system with each micro-inverter feeding a different phase.

6.2 Future Works

Four different current modulation schemes of BCM ZVS current controlled three-phase micro-inverter were studied analytically in this dissertation. More research can be done in order to propose other current modulation schemes with lower maximum switching frequency and higher efficiency. To further improve the performance of the micro-inverter, switching between different current modulation schemes can be considered as another research topic. At heavy loads dual mode current modulation scheme can reduce the conduction losses and improve the inverter

efficiency while at lighter loads, fixed reverse current modulation scheme can be used to reduce the maximum switching frequency.

For the proposed dead-time compensation method in Chapter Three, the equivalent parasitic capacitance of the MOSFETs is assumed to be constant for the sake of the analysis, which means it is not a function of the voltage across the MOSFETs. More research can be done in order to obtain a model for the parasitic capacitance of the MOSFETs based on its voltage.

It would be advantageous to do more research about the power rating of the three-phase micro-inverter. By increasing the power level of the micro-inverter from 400W to 750W and use it as an AC module for three 250W panels in series, it would be possible to improve reliability by effectively reducing the number of components per watt and reduce in dollars per watt since one inverter (albeit more expensive) is now amortized over three panels as opposed to one.

6.3 Publications

- **A. Amirahmadi**, U. Somani, L. Chen, N. Kutkut, I. Batarseh "Light Load Efficiency Enhancement of Three-phase ZVS Micro-Inverter" Submitted to IEEE Transactions on Power Electronics, 2014
- **A. Amirahmadi**, L. Chen, U. Somani, N. Kutkut, I. Batarseh "High Efficiency Dual Mode Current Modulation Method for Low Power DC/AC Inverters" IEEE Transactions on Power Electronics, vol. 29, no. 6, pp. 2638-2642, June 2014.

- **A. Amirahmadi**, H. Hu, A. Grishina, Q. Zhang, L. Chen, U. Somani, I. Batarseh "Hybrid ZVS BCM Current Controlled Three-Phase Micro-inverter" IEEE Transactions on Power Electronics, vol. 29, no. 4, pp. 2124-2134, 2014.
- L. Chen, **A. Amirahmadi**, Q. Zhang, N. Kutkut, I. Batarseh "Design and Implementation of Three-phase Two-stage Grid-connected Module Integrated Converter" Published in IEEE Transactions on Power Electronics, 2014
- L. Chen, H. Hu, Q. Zhang, **A. Amirahmadi**, I. Batarseh "Boundary Mode Forward-Flyback Converter with Efficient Active LC Snubber Circuit" IEEE Transactions on Power Electronics, vol. 29, no. 6, pp. 2944-2958, June 2014
- Q. Zhang, C. Hu, L. Chen, **A. Amirahmadi**, N. Kutkut, I. Batarseh "A Center Point Iteration MPPT Method With Application on the Frequency-Modulated LLC Microinverter" IEEE Transactions on Power Electronics, vol. 29, no. 3, pp. 1262-1274, 2014
- **A. Amirahmadi** , H. Hu, A. Grishina, L. Chen, J. Shen, I. Batarseh, " Improving Output Current Distortion in Hybrid BCM Current Controlled Three-phase Micro-inverter" IEEE Energy Conversion Congress and Exposition (ECCE 2013), pp.1319-1323, 2013
- **A. Amirahmadi**, H. Hu, A. Grishina, L. Chen, J. Shen, I. Batarseh "Hybrid Control of BCM Soft-switching Three Phase Micro-inverter" IEEE Energy Conversion Congress and Exposition (ECCE 2012) pp. 4690-4695, 2012
- X. Fang, H. Hu, L. Chen, **A. Amirahmadi**, J. Shen, I. Batarseh "Operation Analysis and Numerical Approximation for the LLC DC-DC Converter", IEEE Applied Power Electronics Conference and Exposition (APEC2012), pp. 870-876, 2012

- D. Zhang, Q. Zhang , A. Grishina, **A. Amirahmadi** , J. Shen, I. Batarseh "A Comparison of Soft and Hard-switching Losses in Three Phase Micro-inverters" ECCE 2011, pp 1076-1082, Arizona, US, 2011
- A. Grishina, H. Hu, D. Zhang, **A. Amirahmadi** , J. Shen, I. Batarseh " A New Quasi Resonant DC Link for Single Phase Micro-inverter" IEEE Energy Conversion Congress and Exposition (ECCE 2012), pp 3221-3225, 2012
- F. Chen, Q. Zhang, **A. Amirahmadi**, I. Batarseh, "Design and implementation of three-phase gridconnedted two-stage module integrated converter" IEEE 14th Workshop on Control and Modeling for Power Electronics (COMPEL), pp. 1-8, 2013
- C. Hu, L. Chen, Q. Zhang, J. Shen, **A. Amirahmadi**, I. Batarseh, D. Xu "Current Dual-loop control for RPI with LCL filter in Micro-inverter" IEEE Applied Power Electronics Conf.(APEC), pp. 2907-2912, 2013
- **A. Amirahmadi**, U. somani, L. Chen, N. Kutkut, I. Batarseh"Variable Boundary Dual Mode Current Modulation Scheme for Three-phase Micro-inverter", Accepted at IEEE Applied Power Electronics Conference and Exposition 2014
- L. Chen, Q. Zhang, **A. Amirahmadi**, I. Batarseh"Modeling and Analysis of DC-Link voltage for Three-phase Four-Wire Two-Stage Micro-inverter", Accepted at IEEE Applied Power Electronics Conference and Exposition 2014
- U. somani, C. Jourdan, **A. Amirahmadi**, A. Grishina, H. Hu, I. Batarseh"Phase Skipping Control to Improve Light Load Efficiency of Three Phase Micro-Inverters", Accepted at IEEE Applied Power Electronics Conference and Exposition 2014

6.4 Patents Pending

- **A. Amirahmadi**, H. Hu, I. Batarseh, Soft Switching Current Control for High Efficiency Power Inverters
- U. Somani, **A. Amirahmadi**, C. Jourdan, I. Batarseh, Phase Skipping Control to Improve Light Load Efficiency of Three-phase Grid tied Micro-inverter
- H. Hu, I. Batarseh, **A. Amirahmadi**, A New PV System Architecture Based on Three-phase Micro Inverter for PV Solar Farm and Commercial Applications

REFERENCES

[1] F. Blaabjerg, Z. Chen, S.B. Kjaer, "Power Electronics as Efficient Interface in Dispersed Power Generation Systems," IEEE Transactions on Power Electronics, vol. 19, no. 5, pp. 1184-1194, Sep. 2004.

[2] "Technology Roadmap - Solar Photovoltaic Energy". [Online]. Available: www.iea.org

[3] "EPIA, Global Market Outlook for Photovoltaics Until 2015". [Online]. http://www.epia.org/

[4] J. M. Carrasco, L. G. Franquelo, J. T. Bialasiewicz, E. Galvan, R. C. P. Guisado, "Power-electronic Systems for the Grid Integration of Renewable Energy Sources: a Survey," IEEE Transactions on Industrial Electronics,vol. 53, no. 4, pp. 1002-1016, June 2006.

[5] Q. Zhang, C. Hu, L. Chen, A. Amirahmadi, N. Kutkut, I. Batarseh , "A Center Point Iteration MPPT Method With Application on the Frequency-Modulated LLC Microinverter," IEEE Transactions on Power Electronics, vol. 29, no. 3, pp. 1262-1274, 2014.

[6] S. B. Kjaer, J. H. Pedersen, F. Blaabjerg, "A Review of Single-Phase Grid-connected Inverters for Photovoltaic Modules.," IEEE Transactions on Industry Application. Vol.41 no.5, pp.1292-1306, Sept. 2005.

[7] C. Zheng, R. Chen, H. Ma, B. Chen, C. Chen, W. Yu, J. Lai, E. Faraci, "An Optimization Design for 5-kW Centralized PV Inverter to Achieve 99% Efficiency," , in Proc.

Applied Power Electronics Conference and Exposition (APEC) 2013, pp. 2967-2970.

[8] E. Roman, R. Alonso, P. Ibanez, S. Elorduizapatarietxe, and D. Goitia, "Intelligent PV Module for Grid-Connected PV Systems," IEEE Transactions on Industrial Electronics, vol. 53, no.4, pp. 1066-1073, June 2006.

[9] Tigo Energy: Solar Optimizer and PV Monitoring. [Online]. Available: http://www.tigoenergy.com/

[10] H. Hu, W. Al-Hoor, N. H. Kutkut, I. Batarseh, and Z. J. Shen, "Efficiency Improvement of Grid-Tied Inverters at Low Input Power Using Pulse-Skipping Control Strategy," IEEE Transactions on Power Electronics, Vol. 25, No.12, pp. 3129-3138, Dec. 2010.

[11] H. Hu, I. Batarseh, A. Amirahmadi, "A New PV-System Architecture Based on Three-phase Micro-inverter for PV Solar Farm and Commercial Applications," , US Patent (Pending).

[12] W. Dong, "Analysis and Evaluation of Soft Switching Inverter Techniques in Electric Vehicle Application," PhD Dissertation, Virginia Polytechnic Institute and State University 2003.

[13] D. M. Divan, "The Resonant DC-link Converter; a New Concept in Static Power Conversion," , in Proc. IEEE-IAS Annu. Meeting, 1986, pp. 648-656.

[14] Y. Li, , "Unified Zero Current Transition Techniques for High Power Three Phase PWM

Inverter," PhD Dissertation, Virginia Polytechnic Institute and State University 2002.

[15] D. M. Divan and G. Skibinski, "Zero Switching Loss Inverters for High Power Applications," , in Proc. IEEE-IAS Annual Meeting, 1987, pp. 627-634.

[16] S. Chen and T. A. Lipo, "A Passively Clamped Quasi Resonant DC Link Inverter," , in Proc. IEEE-IAS Annual Meeting, 1994, pp. 841-848.

[17] R. Li, Z. Ma, D. Xu, "A ZVS Grid-connected Three-phase InverteR," IEEE Transactions on Power Electronics, Vol. 27, No. 8, pp. 3595-3604, August 2012.

[18] R. Gurunathan, A. K. S. Bhat, "Zero-voltage Switching DC Link Single-phase Pulsewidth-modulated Voltage Source Inverter," IEEE Transactions on Power Electronics, Vol. 22, No. 5, pp. 1610-1618, Sept. 2007.

[19] K. Wang, Y. Jiang, S. Dubovsky, G. Hua, D. Boroyevich, F. C. Lee, "Novel DC-Rail Soft-switched Three-phase Voltage-source Inverters," IEEE Transactions on Industry Applications, Vol. 33, No. 2, March/April 1997.

[20] M. ZhengFeng and Z. MengChu, "Impact of Zero-voltage Notches on Outputs of Soft-switching Pulsewidth Modulation Converters," IEEE Transactions on Industrial Electronics, Vol. 58, No.6, pp. 2345-2354, 2011.

[21] A. Grishina, H. Hu, D. Zhang, A. Amirahmadi , J. Shen, I. Batarseh , "A New Quasi Resonant DC Link for Single Phase Micro-inverter," IEEE Energy Conversion

Congress and Exposition (ECCE 2012), pp 3221-3225, 2012.

[22] J. He and N. Mohan, "Parallel Resonant DC-link Circuit- a Novel Zero Switching Loss Topology with Minimum Voltage Stresses," , in Proc. IEEE-PESC, 1989, pp. 1006-1012.

[23] J. Cho, H. Kim, and G. Cho, "Novel Soft-switching PWM Converter Using a Parallel Resonant DC-link," , in Proc. IEEE-PESC, 1991, pp. 241-247.

[24] L. Malesani, P. Tenti, P. Tomasin, and V. Toigo, "High Efficiency Quasi Resonant DC-link Converter for Full-range PWM," , in Proc. IEEE-APEC, 1992, pp. 472-478.

[25] Y. Chen, "A New Quasi-parallel Resonant DC Link for Soft-switching PWM Inverters," IEEE Transactions on Power Electronics, Vol. 13, No. 3, pp. 427-435. May/June, 1998.

[26] J. J. Jafar and B. G. Fernandes, "A New Quasi-resonant DC-link PWM Inverter Using Single Switch for Soft Switching," IEEE Transactions on Power Electronics, Vol. 17, No. 6, pp. 1010-1016, Nov. 2002.

[27] M. R. Amini, H. Farzanehfard, "Three-phase Soft-switching Inverter with Minimum Components," IEEE Transactions on Industrial Electronics, Vol. 58, No.6, pp. 2258-2264, 2011.

[28] S. Mandrek, P. J. Chrzan, "Quasi-resonant dc-link Inverter with a Reduced Number of Active Elements," IEEE Transactions on Industrial Electronics, Vol. 54, No. 4, pp.

2088–2094, Aug. 2007.

[29] W. McMurray, "Resonant Snubbers with Auxiliary Switches," IEEE Transactions on Industry Applications, Vol. 29, No.2, pp. 355-362, March/April, 1993.

[30] R. W. DeDonker, J.P. Lyons, "The Auxiliary Resonant Commutated Pole Converter," , in Proc. IEEE-IAS Annual Meeting, 1990, pp. 1228-1235.

[31] S. Frame, D. Katsis, D. H. Lee, D. Boroyevich, F. C. Lee, "A Three-phase Zero Voltage-transition Inverter with Inductor Feedback," , in Proc. VPEC Seminar, 1996, pp.189-193.

[32] X. Yuan and I.Barbi, "Analysis, Designing, and Experimentation of a Transformer-assisted PWM Zero-voltage Switching Pole Inverter," IEEE Transactions on Power Electronics, Vol. 15, No. 1, pp. 72-82, Jan. 2000.

[33] J. Choi, D. Boroyevich, and F. C. Lee, "A Novel ZVT Inverter with Simplified Auxiliary Circuit," , in Proc. IEEE-APEC, 2001, pp. 1151-1157.

[34] H.G. Eckel, L. Sack and K. Rascher, "FPGA Based Control of an ARCP Inverter without Additional Sensors," , in Proc. IEE-EPE, 1997, pp. 4385-4390.

[35] W. Dong, J. Choi, Y. Li, H. Yu, J. S. Lai, D. Boroyevich, and F. C. Lee, "Efficiency Consideration of Load Side Soft-switching Inverters for Electric Vehicle Applications," , in Proc. IEEE-APEC, 2000, pp. 1049-1056.

[36] C. M. Wang, C. H. Su, M. C. Jiang, and Y. C. Lin, "A ZVS-PWM Single Phase Inverter Using a Simple ZVS-PWM Commutation Cell," , IEEE Transactions on Industrial Electronics, Vol. 55, No. 2, pp. 758-766, Feb. 2008.

[37] R. C. Beltrame, J. R. R. Zientarski, M. L. S. Martins, J. R. Pinheiro, H. L. Hey, "Simplified Zero-voltage-transition Circuits Applied to Bidirectional Poles: Concept and Synthesis Methodology," IEEE Transactions on Power Electronics, Vol. 26, No. 6, pp. 17.

[38] G. Hua, E. Yang, Y. Jiang, and F. C. Lee, "Novel Zero-current-transition PWM Converters," , in IEEE PESC Conference, 1996, pp. 438-442.

[39] H. Mao, F. C. Lee, X. Zhou, and D. Boroyevich, "Improved Zero-current-transition Converters for High Power Applications," , in Proc. IEEE-IAS Annual Meeting, 1996, pp.1145-1152.

[40] Y. Li, F. C. Lee, and D. Boroyevich, "A Three-phase Soft-transition Inverter with a Novel Control Strategy for Zero-current and Near Zero-voltage Switching," IEEE Transactions on Power Electronics, Vol. 16, No. 5, pp. 710-723, Sep. 2001.

[41] Y. P. Li, F. C. Lee, D. Boroyevich, "A Simplified Three-phase Zero-current-transition Inverter with Three Auxiliary Switches," IEEE Transactions on Power Electronics, Vol. 18, No.3, pp. 802-813, May 2003.

[42] P. Sun, C. Liu, J. Lai, C. Chen, N. Kees, "Three-phase Dual-buck Inverter with Unified Pulsewidth Modulation," IEEE Transactions on Power Electronics, Vol. 27, No. 3,

pp.1159-1167 March 2012.

[43] B. Gu, J. Dominic, J. Lai, C. Chen, T. LaBella, B. Chen, "High Reliability and Efficiency Single-Phase Transformerless Inverter for Grid-Connected Photovoltaic Systems," IEEE Transactions on Power Electronics, Vol. 28, No. 5, pp. 2235-2245, May 2013.

[44] D. Zhang, Q. Zhang, A. Grishina, A. Amirahmadi, H. Hu, J. shen, I. Batarseh, "A Comparison of Soft and Hard-switching Losses in Three phase Micro-inverters," , in Proc. Energy conversion congress and exposition (ECCE) 2011, pp. 1076-1082.

[45] A. C. Nanakos, E. C. Tatakis, N. P. Papanikolaou, "A Weighted-Efficiency-Oriented Design Methodology of Flyback Inverter for AC Photovoltaic Modules," IEEE Transactions on Power Electronics, Vol. 27, No. 7, pp. 3221-3233, July 2012.

[46] P. Geng, W. Wu, M. Huang, F. Blaabjerg, "Efficiency Analysis on a Two-Level Three-Phase Quasi-Soft-Switching Inverter," in Proc. Applied Power Electronics Conference and Exposition (APEC) 2013, pp. 1206-1212.

[47] A. Trubitsyn, B. J. Pierquet, A. K. Hayman, G. E. Gamache, C. R. Sullivan, D. J. Perreault, "High-Efficiency Inverter for Photovoltaic Applications," in Proc. Energy conversion congress and exposition (ECCE) 2010, pp. 2803-2810.

[48] Q. Zhang, H. Hu, D. Zhang, X. Fang, J. Shen, I. Bartarseh, "A Controlled-type ZVS Technique without Auxiliary Components for the Low Power DC/AC Inverter," IEEE Transactions on Power Electronics, Vol. 28, No. 7, pp. 3287-3296, 2013.

[49] A. Amirahmadi , H. Hu, A. Grishina, Q. Zhang, L. Chen, U. Somani, I. Batarseh , "Hybrid ZVS BCM Current Controlled Three-Phase Micro-inverter," IEEE Transactions on Power Electronics, vol. 29, no. 4, pp. 2124-2134, 2014.

[50] A. Amirahmadi, H. Hu, I. Batarseh, "Soft Switching Current Control for High Efficiency Power Inverters," US Patent (Pending) 2014.

[51] A. Amirahmadi, H. Hu, A. Grishina, L. Chen, J. Shen, I. Batarseh, "Hybrid Control of BCM Soft-switching Three Phase Micro-inverter," IEEE Energy Conversion Congress and Exposition (ECCE 2012) pp. 4690-4695, 2012.

[52] O. Trescases, G. Wei, A. Prodic, W. Tung Ng, "An EMI Reduction Technique for Digitally Controlled SMPS," IEEE Transactions On Power Electronics, Vol. 22, No. 4, pp.1560-1565, July 2007.

[53] J. Balcells, A. Santolaria, A. Orlandi, D. Gonzalez, and J. Gajo, "EMI Reduction in Switched Power Converters Using Frequency Modulation Techniques," IEEE Transaction on Electromagnetic Compatibility, Vol. 47, No. 3, pp. 569-576, Aug. 2005.

[54] A. Amirahmadi , H. Hu, A. Grishina, L. Chen, J. Shen, I. Batarseh, "Improving Output Current Distortion in Hybrid BCM Current Controlled Three-phase Micro-inverter," IEEE Energy Conversion Congress and Exposition (ECCE 2013), pp.1319-1323, 2013.

[55] T. J. Summers, R. E. Betz, "Dead-Time Issues in Predictive Current Control," IEEE Transactions on Industry Applications, Vol. 40, No. 3, PP. 835-844, June 2004.

[56] Y. Wang, Q. Gao, X. Cai, "Mixed PWM for Dead-Time Elimination and Compensation in a Grid-Tied Inverter," IEEE Transactions on Industrial Electronics, Vol. 58, No. 10, PP. 4797-4803, OCT. 2011.

[57] H. Wang, X. Pei,Y. Chen,Y. Kang, X. Yue, "An Adaptive Dead-time Compensation Method for Sinusoidal PWM-controlled Voltage Source Inverter with Output LC Filter," , 26th Annual IEEE Applied Power Electronics Conference and Exposition (APEC), 2011, PP.778-785.

[58] Y. Lin, Y. Lai, "Dead-Time Elimination of PWM-Controlled Inverter/Converter Without Separate Power Sources for Current Polarity Detection Circuit," IEEE Transactions on Industrial Electronics, Vol. 56, No. 6, PP. 2121-2127, June 2009.

[59] S. Han, T. Jo, J. Park, H. Kim, T. Chun, E. Nho, "Dead Time Compensation for Grid-connected PWM Inverter," , 8th International Conference on Power Electronics - ECCE Asia- 2011,Korea, pp.876-881.

[60] Z. Jin, and F. Lin Lue, "An Accurate Approach of Dead-time Compensation for Three-phase DC/AC Inverter," , in 4th IEEE Conference on Industrial Electronics and Applications, 2009, pp. 2929-2934.

[61] C. H. da Silva, R. R. Pereira, L.E.B. da Silva, G. Lambert-Torres, J.O.P. Pinto, Se Un Ahn,

"Dead-time Compensation in Shunt Active Power Filters Using Fast Feedback Loop," , in 13th International Conference on Harmonics and Quality of Power, 2008, pp.

[62] K.J. Szwarc, A. Cichowski, J. Nieznanski, P. Szczepankowski, "Modeling the Effect of Parasitic Capacitances on the Dead-Time Distortion in Multilevel NPC Inverters," , in IEEE 2011 International Symposium on Industrial Electronics, 2011, pp. 1869-1874.

[63] A. Amirahmadi, L. Chen, U. Somani, N. Kutkut, I. Batarseh , "High Efficiency Dual Mode Current Modulation Method for Low Power DC/AC Inverters," IEEE Transactions on Power Electronics, vol. 29, no. 6, pp. 2638-2642, June 2014.

[64] A. Amirahmadi, U. somani, L. Chen, N. Kutkut, I. Batarseh, "Variable Boundary Dual Mode Current Modulation Scheme for Three-phase Micro-inverter," Accepted at IEEE Applied Power Electronics Conference and Exposition 2014.

[65] T. Kerekes, R. Teodorescu, P. Rodriguez, G. Vazquez, E. Aldabas, "A New High-Efficiency Single-phase Transformerless PV Inverter Topology," IEEE Transactions on Industrial Electronics, Vol. 58, No. 1, pp. 184-191, Jan. 2011.

[66] W. Yu, J. Lai, H. Qian, C. Hutchens, "High-Efficiency MOSFET Inverter with H6-Type Configuration for Photovoltaic Nonisolated AC-Module Application," IEEE Transactions on Power Electronics, Vol. 26, No. 4, pp. 1253-1260, April 2011.

[67] Z. Zhang, X. He, and Y. Liu, "An Optimal Control Method for Photovoltaic Grid-Tied-Interleaved Flyback Micro-inverters to Achieve High Efficiency in Wide Load

Range," IEEE Transactions on Power Electronics, Vol. 28, No. 11, pp. 5074-5087, Nov. 2013.

[68] B. Min, J. Lee, J. Kim, T. Kim, D. Yoo, and E. Song, "A New Topology With High Efficiency Throughout All Load Range for Photovoltaic PCS," IEEE Transactions on Industrial Electronics, Vol. 56, No. 11, PP.4427-4435, Nov. 2009.

[69] L. Zhang, K. Sun, H. Hu, Y. Xing, "A System-Level Control Strategy of Photovoltaic Grid-tied Generation Systems for European Efficiency Enhancement," Accepted on July 22, 2013 for publication in IEEE Transactions on Power Electronics.

[70] U. somani, C. Jourdan, A. Amirahmadi, A. Grishina, H. Hu, I. Batarseh, "Phase Skipping Control to Improve Light Load Efficiency of Three Phase Micro-Inverters," Accepted at IEEE Applied Power Electronics Conference and Exposition 2014.

[71] U. Somani, A. Amirahmadi, I. Batarseh, C. Jourdan, "Phase and Pulse Skipping Control to Improve Light Load Efficiency of Three-phase Grid Tied Micro-inverter," US Patent (Pending), 2014.

[72] Y. Jang, and M. M. Jovanovi´C, "Light-Load Efficiency Optimization Method," IEEE Transactions on Power Electronics, Vol. 25, No. 1, PP. 67-74, JAN. 2010.

[73] Z. Zhang, M. Chen, M. Gao, Q. Mo, Z. Qian, "An Optimal Control Method for Grid-Connected Photovoltaic Micro-inverter to Improve the Efficiency at Light-load Condition," In Proc. IEEE Energy Conversion Congress and Exposition (ECCE),

2011, PP. 219-224.

[74] Z. Zhang, M. Gao, Q. Mo, M. Chen, Z. Qian, "Loss-Model Based Interleave Technique to Improve the Efficiency of Micro-inverter," 37th Annual Conference on IEEE Industrial Electronics Society, Nov. 2011, PP. 3888-3893.

[75] L. Zhang, H. Hu, L. Feng, Y. Xing, H. Ge, K. Sun, "A Weighted Efficiency Enhancement Control for Modular Grid-tied Photovoltaic Generation System," In Proc. 37th Annual Conference in IEEE Industrial Electronics Society, Nov. 2011, pp. 3093-3098.

[76] H. Li, H. Gan, J. Ying, "High Active Mode Efficiency Switching Mode Power Supply," In Proc. 23rd IEEE Applied Power Electronics Conference and Exposition, 2008. APEC 2008. PP. 715-721.

[77] L. Chen, A. Amirahmadi, Q. Zhang, N. Kutkut, I. Batarseh , "Design and Implementation of Three-phase Two-stage Grid-connected Module Integrated Converter," Published in IEEE Transactions on Power Electronics, 2014.

[78] X. Fang, H. Hu, L. Chen, A. Amirahmadi, J. Shen, I. Batarseh , "Operation Analysis and Numerical Approximation for the LLC DC-DC Converter," IEEE Applied Power Electronics Conference and Exposition (APEC2012), pp. 870-876, 2012.

[79] H. Hu, X. Fang, F. Chen, Z. J. Shen, I. Batarseh, "A Modified High-Efficiency LLC Converter with Two Transformers for Wide Input Voltage Range Applications," IEEE Transactions on Power Electronics, Vol. 28, No. 4, pp. 1946-1960, 2012.

[80] X. Fang, H. Hu, L. Chen, S. Utsav, E. Auadisian, Z.J. Shen, I. Batarseh, "Efficiency Oriented Optimal Design of the LLC Resonant Converter Based on Peak Gain Placement," IEEE Transactions on Power Electronics, Vol. 28, No. 5, pp. 2285-2296, 2012.

[81] X. Fang, H. Hu, Z.J. Shen, I. Batarseh, "Operation Mode Analysis and Peak Gain Approximation of the LLC Resonant Converter," IEEE Transactions on Power Electronics, vol. 27 , no. 4 , pp. 1985 - 1995, 2012.